

MONITORING OF A LONGLEAF PINE ECOSYSTEM RESTORATION SITE USING UAS-BASED  
REMOTE SENSING AND DEEP LEARNING ANALYSIS

by

RYAN CHRISTOPHER PALMER

(Under the Direction of Marguerite Madden)

ABSTRACT

Integrated geospatial techniques, including UAS-Structure from Motion (SfM), UAS-LiDAR, high-accuracy GNSS receivers, and geospatial deep learning, were used to examine tree growth and survival patterns at a young longleaf pine ecosystem restoration site established in 2016 at Wormsloe State Historic Site near Savannah, Georgia. Direct comparison of SfM and LiDAR three-dimensional models showed that LiDAR produced slightly more accurate estimates of tree height. In recent 2023 UAS-SfM data, the neural network Mask R-CNN identified 3,369 longleaf pines with approximately 87% accuracy; median estimated tree height was 5.37 m. Time series results showed that steady pine vertical growth had begun by 2021, five years after planting. Multiple regression analyses with six environmental variables showed that the variables were better predictors of longleaf pine survival ( $R^2 = 0.35$ ) than height ( $R^2 = 0.10$ ). The results demonstrate the utility of advanced remote sensing and image analysis techniques for monitoring longleaf pine forests.

INDEX WORDS: Longleaf Pine, UAS, Structure from Motion, LiDAR, Canopy Height  
Model, Remote Sensing, Ecological Monitoring, Deep Learning,  
Convolutional Neural Network

MONITORING OF A LONGLEAF PINE ECOSYSTEM RESTORATION SITE USING UAS-BASED  
REMOTE SENSING AND DEEP LEARNING ANALYSIS

by

RYAN CHRISTOPHER PALMER

B.S., University of Georgia, 2018

A Thesis Submitted to the Graduate Faculty of The University of Georgia in Partial  
Fulfillment of the Requirements for the Degree

MASTER OF SCIENCE

ATHENS, GEORGIA

2025

© 2025

Ryan Christopher Palmer

All Rights Reserved

MONITORING OF A LONGLEAF PINE ECOSYSTEM RESTORATION SITE USING UAS-BASED  
REMOTE SENSING AND DEEP LEARNING ANALYSIS

by

RYAN CHRISTOPHER PALMER

Major Professor:	Marguerite Madden
Committee:	Sergio Bernardes
	Jon Calabria

Electronic Version Approved:

Ron Walcott  
Vice Provost for Graduate Education and Dean of the Graduate School  
The University of Georgia  
August 2025



## ACKNOWLEDGEMENTS

First and foremost, I have to give a heartfelt thank you to Marguerite Madden for being the best advisor and mentor anyone could ask for. During the past few years, she has given me so much great advice not just about my research, but about my career, and I know for a fact that she has inspired me and many others by always keeping such a positive outlook on life no matter how tough the going gets. From taking her class for the first time as an undergraduate in 2017, to working in the NASA DEVELOP program a few years later, to eventually being encouraged to return to UGA Geography and the Center for Geospatial Research (CGR) for my graduate studies, Marguerite has helped shape and guide my professional path at many turns.

I would also like to thank Sarah Ross, the amazing former director of the Center for Research and Education at Wormsloe (CREW), who along with Marguerite helped recruit me into becoming a Wormsloe Fellow. Sergio Bernardes and Jon Calabria, my committee members, were incredibly helpful with their wealth of knowledge regarding drone-based remote sensing and longleaf pine ecosystems. More than a few long, wide-ranging, and insightful conversations were had in Sergio's office to discuss not just this research, but anything and everything geosciences-related.

I also would like to express my gratitude to the Wormsloe Foundation and the UGA Graduate School for providing my funding as a Wormsloe Fellow, and to Craig and Diana Barrow for giving me full access to their property to conduct research. The Barrows' continued support of the longleaf pine restoration project and many other UGA-led projects at Wormsloe has been instrumental in the site's preservation and protection.

The following people were extremely helpful for their support with field data collection: Charles Perrie, who assisted with tree measurements; Claudia Venherm, who provided some crucial drone imagery datasets of excellent quality; and Tommy Jordan, who measured trees, helped me conduct drone flights, and was a great source of information on drones and photogrammetry at the beginning of this project.

Finally, I would like to thank the UGA Department of Geography's office staff, who have always been so helpful and accommodating to myself and to my fellow graduate students, and 100 other colleagues, friends, and family members (especially my mom and dad) who accommodated me, encouraged me, and (at times) coerced me into seeing this project through to completion even when life kept getting in the way and there seemed to be no end in sight.

## TABLE OF CONTENTS

	Page
ACKNOWLEDGEMENTS.....	iv
LIST OF TABLES .....	viii
LIST OF FIGURES .....	ix
CHAPTER	
1 INTRODUCTION.....	1
Scientific Contribution of Geospatial Analysis to Longleaf Pine Ecosystem	
Restoration .....	4
Research Setting .....	5
Objectives.....	13
2 LITERATURE REVIEW .....	16
A Brief Longleaf Pine-Centered Land Use History of Wormsloe.....	16
Wormsloe’s Significance as a Longleaf Pine Restoration Site .....	19
Brief History of UAS, Structure from Motion, and LiDAR for Forestry and	
Ecological Monitoring .....	22
Technical Overview of UAS-Related Data Acquisition and Processing	
Methods .....	26
Overview of Instance Segmentation with Deep Learning .....	34
3 METHODOLOGY .....	37
UAS Flights.....	37
Ground-Based Data Collection .....	41

Structure from Motion and LiDAR Data Processing .....	44
Deep Learning for Individual Tree Segmentation .....	51
Tree Height Calculation and Comparison to Environmental Variables .....	58
4 RESULTS & DISCUSSION.....	60
Effects of UAS Flight Parameters on SfM Accuracy.....	60
Comparison of SfM and LiDAR-Derived Tree Heights.....	64
Assessment of Deep Learning Results.....	69
2023 Tree Distribution and Height Estimates for the Full Study Area .....	74
Relationships Between Environmental Conditions and Observed Heights and Survival .....	77
Time Series Analysis of Tree Heights .....	86
Recommended Best Practices for Future Data Collections .....	91
5 CONCLUSIONS .....	98
Future Work .....	101
REFERENCES .....	104
APPENDICES	
A 2023 UAS LIDAR-DERIVED DEM FOR THE STUDY AREA.....	117
B RELATIONSHIPS BETWEEN INDIVIDUAL VARIABLES AND LONGLEAF PINE GROWTH AND SURVIVAL .....	118
C UAS SFM TIME SERIES: FULL STUDY AREA .....	121
D MEASURED HEIGHTS AND POSITIONAL DATA OF TREES USED FOR GROUND TRUTH .....	131

## LIST OF TABLES

	Page
Table 1: SfM tree height errors for the five UAS flights of the 50 x 50-m sample plot .....	60
Table 2: 2023 tree height errors for SfM, LiDAR, and the combined SfM-LiDAR dataset .....	65
Table 3: Longleaf pine height regression model results (Model 1).....	79
Table 4: Longleaf pine survival regression model results (Model 2) .....	80
Table 5: For both regression models, the predicted change in the value of the dependent variable based on changes in the value of each independent variable .....	81
Table 6: The estimated relative weight of each independent variable used in multiple regression .....	82
Table 7: UAS flight metadata for all optical imagery collected at the study area.....	93
Table 8: UAS flight metadata for all optical imagery collected for the 50 x 50-m plot.....	94
Table 9: UAS flight metadata for the LiDAR data collected at the study area .....	94
Table 10: Corrected positional data for the permanent GCP markers.....	96

## LIST OF FIGURES

	Page
Figure 1: Extent of the longleaf pine ecosystem in the South prior to European settlement ..	4
Figure 2: Wormsloe’s location on the Isle of Hope between Savannah and the Georgia coast .....	7
Figure 3: Orthomosaic of the longleaf pine field and its surroundings from an April 2018 drone flight .....	9
Figure 4: (A) aerial and (B) ground-level views of longleaf pines in the field .....	12
Figure 5: Resident gopher tortoise in its burrow near the edge of the study area, taken February 2023.....	20
Figure 6: Visualizing Structure from Motion.....	28
Figure 7: An example of a pulse from an airborne LiDAR sensor .....	31
Figure 8: A simple visualization of the Mask R-CNN framework.....	36
Figure 9: Detail map of the longleaf pine field shown using an orthomosaic from September 2022 .....	38
Figure 10: Dr. Thomas Jordan changes UAV batteries for the DJI Phantom 4 Pro in between flights during the September 2022 data collection .....	39
Figure 11: Dr. Sergio Bernardes gets the Freefly Alta X ready for flight during the February 2023 data collection .....	40
Figure 12: The GNSS base station (left) and rover (right) being used to record individual tree coordinates in September 2022.....	42

Figure 13: Charles Perrie assists with measuring tree heights with the telescopic pole in February 2023.....	43
Figure 14: Capped rebar in the southwest corner of the study area .....	44
Figure 15: Visualization of the Emlid Studio interface .....	46
Figure 16: The aligned photos (blue rectangles), GCPs (labelled blue flags), and sparse point cloud visualized in Agisoft Metashape for one of the five flights of the sample plot in September 2022 .....	47
Figure 17: Two versions of the 2023 CHM for part of the field, without gradual selection (left), and with gradual selection (right) .....	48
Figure 18: Nadir view of the point cloud before (left) and after (right) improving the alignment of two overlapping swaths .....	49
Figure 19: The SfM and LiDAR point clouds merged into one in CloudCompare .....	50
Figure 20: A normalized point cloud of the study area created using the R package lidR ....	51
Figure 21: A close-up visualization of all ten bands in the raster dataset used for deep learning model training .....	54
Figure 22: Training/validation and testing zones with completed data annotations in the northwest corner of the field.....	56
Figure 23: Field-measured tree heights plotted against SfM-measured tree heights for the five UAS flights of the sample plot.....	61
Figure 24: Comparing SfM tree height accuracy for the 60-m UAS flight and the 120-m flight . .....	62
Figure 25: Field-measured tree heights plotted against tree height estimates for each UAS-based technique .....	65

Figure 26: Comparing the accuracy of tree height measurements using SfM versus LiDAR ....	
.....	66
Figure 27: Aerial views of vegetation density in the 50 x 50-m plot in September 2022 (left)	
versus February 2023 (right) .....	67
Figure 28: Final learning curve results for the deep learning model .....	70
Figure 29: Screenshot showing model accuracy metrics using the chosen confidence	
threshold of 59% and an IoU threshold of 50% .....	71
Figure 30: Visualizing accuracy by comparing model results (yellow polygons) to annotated	
data from a testing zone (purple circles) .....	72
Figure 31: Final results showing the spatial distribution of 3,369 objects (pink dots) that the	
deep learning model identified as longleaf pines as of February 2023 .....	75
Figure 32: Approximate distribution of longleaf pine heights in the study area in February	
2023 .....	76
Figure 33: Longleaf pine heights compared to heights predicted by multiple regression	
model 1 .....	85
Figure 34: Longleaf pine local survival (defined as percent survival within a 10-meter radius	
of each point) compared to survival values predicted by multiple regression model 2	
.....	86
Figure 35: (A) orthomosaics, (B) CHMs, and (C) oblique LAS point cloud views showing part	
of the west side of the field during three different years .....	87
Figure 36: Longleaf pine changes over time, Plots 1-3 .....	88
Figure 37: Longleaf pine changes over time, Plots 4-6 .....	89
Figure 38: Rebar marking a GCP location that has been damaged and is missing its safety	
cap.....	96



## CHAPTER 1

### INTRODUCTION

Longleaf pine (*Pinus palustris*) is the centerpiece of the longleaf pine ecosystem, a diverse environment found only in the southeastern U.S. that offers habitat to a wide array of rare and endangered plant and animal species. Despite being visually dominated by just a few species, such as wiregrasses, scrub oaks, and the namesake longleaf pines, this ecosystem can contain well over 100 plant species per 1000 m<sup>2</sup> of forest, many of which are specialists that cannot thrive anywhere else. Such plant species richness is not known to exist in any other plant community in temperate North America (Peet & Allard, 1993). The most famous animal residents are the red-cockaded woodpecker (*Picoides borealis*) and gopher tortoise (*Gopherus polyphemus*), both keystone species whose tree cavities and underground burrows, respectively, shape the physical environment and are depended on by dozens of other native species. In addition to these two rather well-known inhabitants, there at least 17 amphibians, 12 other reptiles, 4 other birds, and 3 mammal species who are longleaf pine specialists with ranges mostly confined to this ecosystem, including the eastern indigo snake (*Drymarchon corais*), flatwoods salamander (*Ambystoma cingulatum*), fox squirrel (*Sciurus niger*), and bobwhite quail (*Colinus virginianus*). These are just a few notable examples of the hundreds of vertebrates that can be found in healthy longleaf pine forests (Means, 2006).

A unique aspect of this ecosystem is that the flora and fauna inhabiting it, including the pines themselves, revolve around and even depend on regularly occurring fire. While low to medium-intensity fires such as those started by lightning may kill hardwoods and even

other pine species, they are usually too cool to kill longleaf pines, which are protected by their thick bark (Wang et al., 2016) or, in the case of seedlings, by their densely packed needles (O'Brien et al., 2008). Prescribed burning experiments done by Brethauer et al. (2021) found that even high-intensity fires posed surprisingly little threat to longleaf pine seedlings, with the exception of high-intensity summer fires, which did have some adverse effects on growth and survival. Longleaf pines take advantage of this special relationship with fire by relying on it to germinate their seeds: when a wildfire burns away surrounding vegetation and ground cover, it allows their serotinous seed cones to make direct contact with the earth and sprout (Wade & Lundsford, 1990). Without frequent (one to three-year interval) fires, the pines and other fire-reliant flora and fauna can be outcompeted by less fire-tolerant species and disappear (Brethauer et al., 2021).

Unfortunately, longleaf pine disappearance linked to decades of fire suppression and habitat destruction has been a central theme in southern U.S. land use and land cover trends. The longleaf pine ecosystem has become one of the most endangered in the United States, at one point existing in only 3% of its original range (Frost, 1993). Such magnitude of habitat degradation and destruction exceeds the extent of habitat loss for any other ecosystem in the Southeast – even the region's often-threatened wetland ecosystems have not seen losses so severe (Noss et al., 1995). Besides fire suppression, a primary reason for this decline can be seen in historical trends of the Georgia Lowcountry. After the Civil War, this region of the South saw a decline in agriculture and a surge in industries such as timber and tourism. The Isle of Hope on the coast of Georgia, where this study takes place, never formally became part of the timber industry, but many of the lands surrounding it did, and the nearby city of Savannah was a centerpiece of the quickly growing pulp-paper industry by the mid-twentieth century. Creating the requisite pine plantations often meant clearing

native forest to grow rows of fast-growing slash pine (*Pinus elliottii*) or loblolly pine (*Pinus taeda*), a method which produced large quantities of wood but eliminated longleaf pine forests and was a poor habitat for most native plant and animal species that thrived in the longleaf pine ecosystem (Swanson, 2012). Due to this growth of monoculture timber plantations and in conjunction with fire suppression, urbanization, and agricultural conversion practices, the tree historically found across more than 90 million acres of the southeastern U.S. (and dominant across more than two-thirds of that extent) was only to be found on a mere 3 million acres of mostly poor-quality forest by the 1990s (Frost, 1993; Lord, 2022), seriously imperiling biodiversity and ecosystem functioning (Aschenbach et al., 2010). Longleaf pine conservation and restoration efforts have raised the present-day figure to approximately 5.2 million acres (Lord, 2022), but this acreage still falls far short of the ecosystem's original extent (Figure 1), and the tree itself remains classified as endangered according to the most recent assessment by the International Union for Conservation of Nature (IUCN) (Farjon, 2013).

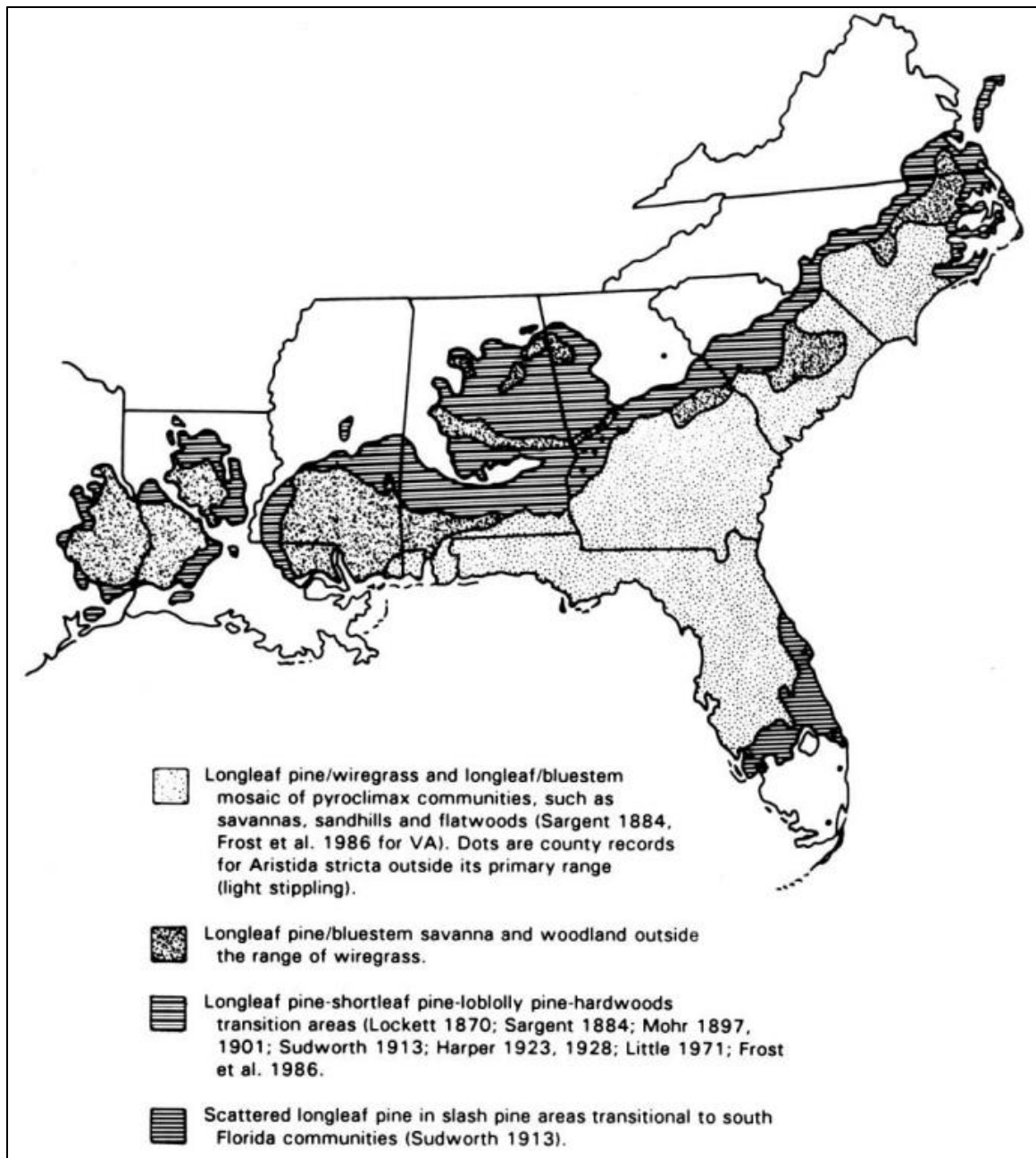


Figure 1. Extent of the longleaf pine ecosystem in the South prior to European settlement. Image credited to Frost (1993).

### **Scientific Contribution of Geospatial Analysis to Longleaf Pine Ecosystem Restoration**

Conservation and restoration initiatives continue working to bring *Pinus palustris* back from the brink. These efforts go beyond restoring the range of a single species, as they

simultaneously offer the chance to replenish habitat for additional threatened and endangered species as well as introduce long-term regional benefits due to the climate change-resilient nature of the longleaf pine ecosystem (Lord, 2022). As these efforts progress, new technological advances in remote sensing data collection and geospatial analysis are providing opportunities to increase the scope and efficiency of longleaf pine ecosystem monitoring projects. With each passing year the capabilities of these technologies (e.g., UAS-based remote sensing, high-accuracy GNSS solutions, and geospatial deep learning tools) increase, and as they develop, they are also becoming cheaper, more widespread, and easier to use. These continued advancements make their application to longleaf pine monitoring ever more warranted. By investigating ways to apply these technologies, this research can inform those who wish to streamline their monitoring efforts, increase knowledge of best practices for longleaf pine restoration and conservation, and simultaneously advise related forestry, land management, and ecological monitoring work. These methods will be assessed by monitoring a small longleaf pine restoration area at a state historic site on the coast of Georgia.

### **Research Setting**

Wormsloe State Historic Site sits in Chatham County, Georgia on the southern end of the Isle of Hope, technically a long peninsula connected to the mainland by a single thin, swampy piece of land. It lies about nine miles southeast of downtown Savannah, Georgia but is directly adjacent to the Savannah suburbs making up much of the north end of the Isle (Figure 2). Though bordered by roads and houses to the north, most of Wormsloe is surrounded by coastal salt marsh, an estuarine maze of water, grass, and mud, teeming with life and constantly changing with the flux of the tides. Beyond the marsh and tidal creeks to the west

lies the mainland, and to the east lie Long Island and Skidaway Island, which provide a buffer between the Isle of Hope and the Atlantic Ocean (Swanson, 2012).

Wormsloe contains an astounding array of historical artifacts in a beautiful natural setting: from the ruins of a colonial tabby fortification, to shell middens left behind by Native Americans, to Civil War-era earthworks, to a slave cabin that offers a stark reminder of the African American experience at Wormsloe during its time as a plantation (Swanson, 2012, foreword by Sutter). It is one of the only places in the country where a visitor can experience nearly the entirety of three centuries of American history, from European colonization through to the present day, in a single setting. Though most of Wormsloe is now owned and operated by the state of Georgia, the early-nineteenth-century plantation house and surrounding land is privately owned by descendants of Noble Jones (one of the original settlers of the Georgia colony), making it the only property in the state to remain in the hands of one family from the founding of the Georgia colony in the 1730s to the present. Furthermore, its natural setting is equally impressive: a patchwork of marshland, forests, and tidal creeks where land, river, and sea blend together into a single cohesive environment. With so many habitats in close proximity to each other, Wormsloe remains a beautiful and biologically diverse landscape in spite of the development that surrounds much of it (Swanson, 2012). It is, in summation, “one of the most significant historical, archaeological, and natural sites in Georgia and the entire Lowcountry” (Swanson, 2012, foreword by Sutter, p. ix).

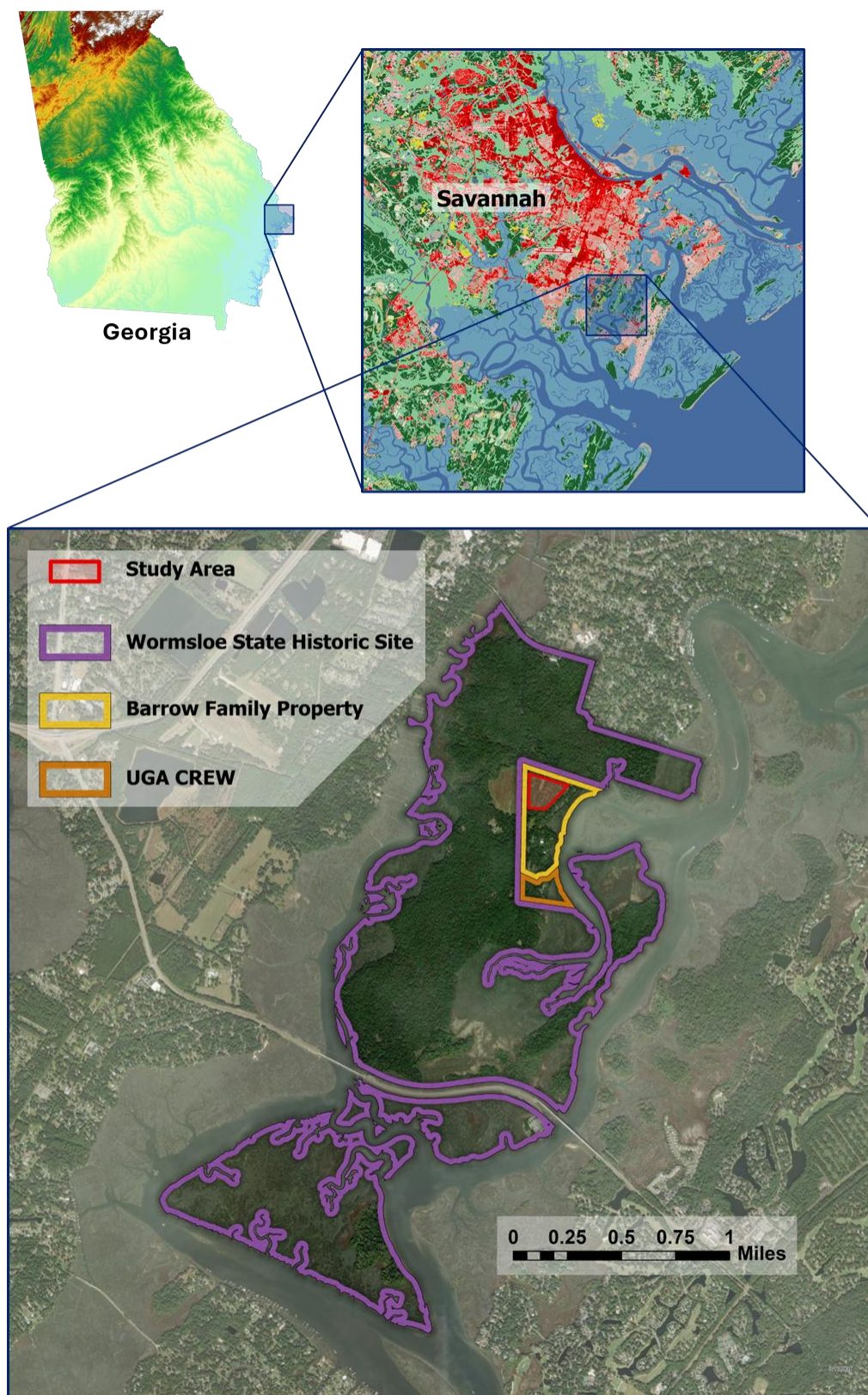


Figure 2. Wormsloe's location on the Isle of Hope between Savannah and the Georgia coast. Map data sourced from Esri (2024), Esri (2025), Hall (2024), and USGS (2024).

### ***The Longleaf Pine Field and the Planting of Seedlings***

Present-day satellite imagery of the Historic Site will reveal a property whose land is nearly entirely forested with the notable exception of three cleared sections that largely lack mature trees. The two easternmost sections are the longleaf pine restoration site, visible in an orthomosaic of unmanned aerial system (UAS) imagery in Figure 3. As the study area for this research, these two areas may be jointly referred to as “the field” (though this “field” is becoming ever more forest-like with each passing year as the pines mature). The field lies on the east side of Wormsloe, close to the marshes bordering the nearby Skidaway River. It is not a part of Wormsloe Historic Site proper; rather, it sits on the northern part of the private property owned by Craig and Diana Barrow. Most of the adjacent land is part of the state-owned historic site, but to the south lies more of the Barrows’ property, where the main house and grounds are located, as well as fifteen acres owned by the University of Georgia (UGA), home to the Center for Research and Education at Wormsloe (CREW). The entirety of this research effort, from the trees’ initial planting to present, has been made possible only with the support of CREW, the Wormsloe Foundation, and the Barrows.





*Figure 3. Orthomosaic of the longleaf pine field and its surroundings from an April 2018 drone flight.*

Researchers from the UGA College of Environment and Design, led by Dr. Jon Calabria, selected the field for the restoration effort because its observed characteristics such as elevation, soil type (moderately well-drained sandy soil), and existing vegetation (loblolly pines and grasses) indicated its suitability for recreating a maritime longleaf pine ecosystem similar to that which existed on the Isle of Hope prior to Wormsloe's founding.

Historically both the field and the lands adjacent to it have seen multiple changes in land use, mainly alternating between forest and cleared agricultural land (Campbell & Morris, 2018; Swanson, 2012). This land use history is worth mentioning for the impact it may be having on current vegetation growth patterns, as analysis of 3D vegetation structure at Wormsloe by Burda (2011) showed a relationship between the past frequency of land use transitions and present-day forest structure. At the beginning of the restoration effort, the field underwent yet another transformation as its existing vegetation was nearly entirely cleared to make way for the new pine seedlings.

In the spring of 2016, 10,000 longleaf pine seedlings were ordered, and approximately 9,800 of these were planted in the field in a curvilinear pattern – this pattern helps give the trees the visual appearance of a natural forest (when seen from the ground) rather than that of a plantation with perfectly straight rows (Figure 4). All of the trees are genetic clones which, although not ideal in an ecological sense, is useful when it comes to studying the influence of non-genetic environmental factors on their growth and survival over time. Property owner Craig Barrow also made the decision to plant the seedlings at a relatively high density; this qualified the planting effort to be partially funded by the U.S. Department of Agriculture (USDA), but it means that the field has a higher tree density than what would exist naturally in a maritime longleaf pine ecosystem. In addition to the seedlings, researchers planted a variety of local forbs and grasses – a healthy longleaf pine forest requires these species to thrive, as they increase diversity and productivity (Aschenbach et al., 2010) and provide fuel for periodic fires. Finally, for conducting long-term monitoring of the seedlings, researchers delineated six 20-m x 20-m plots spaced throughout the field and divided each plot into four sections, allowing for experimentation with a variety of clearing and planting methods in each section. Since 2016, continued management of the field has included semi-regular

prescribed burns, which serve as a viable forest management tool in the absence of natural wildfires (Brethauer et al., 2021).



**A****B**

*Figure 4. (A) aerial and (B) ground-level views of longleaf pines in the field. Images were taken in September 2022 and December 2022, respectively. Aerial UAS image courtesy of Dr. Thomas Jordan.*

## **Objectives**

This study uses state-of-the-art geospatial technologies to evaluate the current state of the longleaf pines in the restoration area by creating 3D models and accurate estimates of sapling count, height, and distribution. It also explores spatiotemporal trends in tree growth between their 2016 plant date and the most recent data collection in 2023. This research seeks to provide insight into the efficacy of these geospatial techniques for evaluating similar longleaf pine restoration or conservation efforts. Specific objectives include the following.

### ***1. Assess UAS-based geospatial methods for accurately measuring the heights of longleaf pine trees.***

To achieve Objective 1, this research compares the efficacy of two unmanned aerial system (UAS)-based data collection and analysis methods, photogrammetric Structure from Motion (SfM) and Light Detection and Ranging (LiDAR), for generating 3D point clouds of the study area and remotely measuring the heights of the longleaf pines. UAS flights of the study area to collect overlapping optical imagery (used to generate SfM results) and LiDAR data were conducted. At the same time, within a subset of the overall study area, a select number of longleaf pines were precisely geolocated and their heights were measured from the ground; these heights are compared to the heights derived from canopy height models (CHMs) produced by (1) SfM, (2) LiDAR, and (3) a combination of both types of data. Additionally, this step of the research looks at how changing UAS flight parameters for optical imagery collection affects the accuracy of the height models produced by SfM.

***2. Remotely sense, monitor, and analyze longleaf pine sapling survival using UAS imagery and GeoAI.***

Using the most recent UAS imagery dataset (February 2023) and GeoAI analysis, Objective 2 estimates the total number of surviving longleaf pines in the study area, determines their approximate spatial distribution and height distribution, and explores environmental factors that may have influenced their health and survivability. This objective utilizes a deep learning workflow to detect the locations of all surviving longleaf pines that are visible in the drone imagery. Combining these tree locations with the results of Objective 1 yields accurate heights for all longleaf pines identified in the study area. Finally, these results are compared to select environmental variables to find potential correlations between environmental conditions and longleaf pine survival and growth.

***3. Incorporate the optical remote sensing data from earlier UAS flights to create time series maps that visualize longleaf pine growth and survival between 2016 and 2023.***

To achieve Objective 3, the SfM process used in Objective 1 is repeated using optical imagery from multiple UAS data collections between 2016 and 2022 to create a time series of orthomosaics and CHMs. Since data collections have occurred regularly (on a mostly annual to biannual basis) between the seedlings' plant date and present, this time series is ideal for visualizing spatiotemporal trends occurring in the field. This effort is focused on smaller plots within the overall study area. Longleaf pines are identified in each plot for each year's orthomosaic, and each identified tree is assigned an estimated height value from the corresponding CHM.

***4. Lay the groundwork for future UAS-based longleaf pine research at Wormsloe by documenting best practices for data collection and establishing baselines that can serve as the backbone for a more comprehensive evaluation of landscape performance.***

The data collected at the study area to date constitute a robust collection of geospatial information, and there is much potential for further research that may benefit foresters, conservationists, land managers, and others with interest in monitoring longleaf pine forests. Planning for such future research in the present can help ensure its success. Objective 4 includes projects such as installing permanent ground control points around the field for drone flights, establishing a comprehensive record of all past drone flight metadata, and recording best practices for future data collections.

## CHAPTER 2

### LITERATURE REVIEW

#### **A Brief Longleaf Pine-Centered Land Use History of Wormsloe**

This section is wholly derived from the comprehensive account of Wormsloe's environmental history provided by Swanson (2012).

The longleaf pines at Wormsloe have seen many rises and falls since the arrival of Europeans to the Lowcountry. At Wormsloe's founding in 1736, a mixed pine forest of longleaf pine and loblolly pine was one of two dominant forest types on the Isle (the other being live oak hammock). These pine forests tended towards the higher, sandier areas further from the marsh and were kept clearer of undergrowth than the oak hammocks, likely from lightning-induced wildfires. Beyond use by Native Americans, it is likely that some impact by European settlers on the local pine forest ecosystem had begun even before the founding of Savannah or Wormsloe: the openness and abundance of grasses made them ideal foraging grounds for free-ranging cattle, both cattle raised by the English (including Noble Jones) but also cattle left behind by Spanish expeditions along the coast in the sixteenth and seventeenth centuries. These cattle, and likely hogs as well, would have noticeably impacted the longleaf pine ecosystem by killing seedlings, compacting soil, spreading invasive plant species, and disrupting wild animal habitats. But this was largely the limit of the impacts to Wormsloe's longleaf pine forests throughout the prerevolutionary era. While livestock roamed the woods, and some timber was harvested, overall Wormsloe remained mostly forest and marsh (Swanson, 2012).



Between the end of the American Revolution and the start of the Civil War, however, the landscape saw dramatic changes as Wormsloe evolved into a slavery-dependent plantation focused on the production of sea island cotton. This cotton grew best directly along the coast in fast-draining, flat, sandy soils – exactly the kind of soils historically dominated by pine forest (Swanson, 2012). By the eve of the Civil War, a significant section of oak and pine forest on the northern section of the property had been replaced by corn and cotton fields, and the property as a whole had become “more farm than forest, more manicured landscape than marsh” (Swanson, 2012, p. 94).

Immediately after the Civil War, agriculture continued to play an important role in the Wormsloe landscape, but eventually, the drastic economic and societal changes wrought by Reconstruction took their toll, and agriculture was slowly fading from prominence at Wormsloe as it moved into the twentieth century. Though this ran counter to the general trend in the South, it matched the trend of Chatham County and the rest of the Georgia Lowcountry, which saw notable declines in large-scale agriculture during this time period. Compounding the effects of this agricultural trend, changing sentiments about open range livestock resulted in an 1895 law in Chatham County requiring stock owners to fence their animals. By ending more than 150 years of frequent livestock presence that had kept the Wormsloe woods relatively free of undergrowth (including fragile, young longleaf pine seedlings), the new law allowed a process of natural ecological succession to take hold, and longleaf pines began to recolonize parts of their former habitat. By the 1940s, agricultural operations had completely ceased, and due to both this and the effects of the livestock law, the majority of Wormsloe’s land was undergoing slow reforestation. Its woods were soon thicker than they had been for hundreds of years (Swanson, 2012).

This natural reforestation and succession lasted until 1974, when a southern pine beetle (*Dendroctonus frontalis*) outbreak was discovered. The Georgia Department of Natural Resources (DNR), which had recently taken control of most of the site, ultimately decided to cull the infected trees to prevent further spread of infestation. Though the original plan called for the removal of only 25 acres of the forest, Union Camp, the company tasked with clearing the trees, would go on to remove virtually all of the pines at Wormsloe across 750 acres of land. This operation denuded the landscape and left behind ruts and piles of debris that significantly damaged many of the park's roads and allowed for the accumulation of stagnant water, creating a mosquito infestation. When this brief but destructive period was over, there was discussion of reforesting with longleaf pines; however, no significant reforesting occurred, and it was natural succession that eventually filled in the bare land with a mix of shrub species, pines, and hardwoods to create the landscape seen today (Swanson, 2012).

As much history and landscape change as Wormsloe has seen, in recent decades it has slowly transitioned into a site primarily for the protection and interpretation of colonial historical artifacts, as well as for recreation, tourism, and general enjoyment of nature. Much evidence of the other history wrought on its landscape has faded, making it easy for first-time Wormsloe visitors to presume that they are visiting a place where much of the land has remained relatively undisturbed since the founding of Savannah. This modern emphasis on the undisturbed natural side of Wormsloe has covered up past periods of intensive land use and frequent environmental changes, including changes that took place at the site of the longleaf pine field (Swanson, 2012). It is relevant to keep this environmental history of the local landscape in mind when thinking about the longleaf pine restoration project, since it

too has now become a part of the landscape's history. It represents a small but important modern thread in the much larger tapestry of Wormsloe's rich past.

### **Wormsloe's Significance as a Longleaf Pine Restoration Site**

Perhaps the clearest significance of the longleaf pine restoration site is that the maritime longleaf pine ecosystem that was once abundant at Wormsloe has been given the chance to make a comeback and again provide habitat for the unique and varied flora and fauna that thrive in it (Figure 5). But it is arguably noteworthy for reasons deeper than simple ecosystem restoration because of the way it fits into the long history of human-environment interactions at Wormsloe. Swanson (2012) argues that Wormsloe has been a dynamic landscape of experimentation, reinvention, and constant exchanges between people and the natural Lowcountry environment since the day it was founded. Much of the experimentation at the site has been agricultural or horticultural in nature, such as the introduction of new crops (for agricultural production and economic benefit) or new plants (for ornamental use in the gardens). It has also long been a site for experimenting with the idea of preservation, such as when the Jones family, Wormsloe's stewards, sought to preserve characteristics of the colonial and Antebellum South in the decades following the Civil War (Swanson, 2012). These long-enduring forms of experimentation continue into the present day, from the meticulous planting of hundreds of varieties of heirloom vegetables in Wormsloe's gardens by former CREW executive director Sarah Ross to the Historic Site's interpretive programs and museum displays that seek to preserve Wormsloe's past for modern-day visitors. The longleaf pine ecosystem restoration site is yet another way that the exchange between Wormsloe's people and its natural and cultural environment continues today, but it is quite different from many of the other human-landscape interactions that have taken place in the past. By attempting to grow an entire ecosystem from scratch, this project seeks to shape a

small piece of Wormsloe's woods into something more reminiscent of the landscape that existed before the arrival of Europeans.



*Figure 5. Resident gopher tortoise in its burrow near the edge of the study area, taken February 2023. Image courtesy of Charles Perrie.*

The effort is also noteworthy beyond Wormsloe for what it can contribute to longleaf pine-related land management and restoration across the southeastern U.S. While planting longleaf pines has become more popular in the South in recent years (Brethauer et al., 2021), the total acreage of longleaf pine forests is still a fraction of what it was historically. Every additional tree, even at a relatively small restoration site like Wormsloe's, plays a part in reversing that trend. Furthermore, despite the field's small size, it is a site with some valuable attributes that not all such projects are guaranteed to have: (1) myriad resources for monitoring and research due to close affiliation with a public land-grant research university, (2) the opportunity for public visibility given the field's location alongside the biggest attraction at a popular historic site (Wormsloe's famous Oak Avenue), and (3) strong landowner support. Many otherwise willing landowners may lack the resources or the

commitment to undertake an endeavor as difficult and involved as ecosystem restoration, especially when taking long-term monitoring and research goals into account. The early success of longleaf pine restoration at Wormsloe owes itself largely to the resources and commitment of the Barrow family, the UGA researchers at CREW, and the Georgia DNR.

Of course, that is not to suggest that there are not other regional initiatives and organizations protecting longleaf pines and restoring their habitat. Groups such as Tall Timbers, The Longleaf Alliance, and The Jones Center at Ichauway collectively conserve hundreds of thousands of acres of land, including many longleaf pine forests, and have planted millions of longleaf pine seedlings (The Jones Center at Ichauway, 2024; The Longleaf Alliance, 2024; Tall Timbers, 2023b). Organizations such as these also advocate for the tree's protection by building relationships with landowners, government agencies, industry leaders, researchers, and other stakeholders (The Longleaf Alliance, 2021; Tall Timbers, 2023a); working with private landowners is particularly crucial since an estimated 38% of existing longleaf pine forest currently sits on unprotected private land (Florida Natural Areas Inventory, 2023). Collectively these organizations and many others are leading the push to increase the amount of healthy longleaf pine habitat in the South, and their efforts have often proven successful – in their most recent annual report, America's Longleaf Restoration Initiative (2023) documented 168,000 acres of newly established and newly protected longleaf pine forest across the tree's native range. So while the longleaf pine field at Wormsloe is unique in several ways, it is just one small piece in a network of numerous such revitalization efforts throughout the South that all share many of the same overarching goals.

A final argument for the significance of restoration lies in the idea that longleaf pines, as the centerpiece of an ecosystem that has been shown to be resilient in the face of climate change, can play a major role in carbon sequestration and other climate-smart forestry

efforts across their native range (Lord, 2022). In addition to being highly fire resistant, longleaf pines are more resistant to insects, disease, wind, and drought when compared to other native pine species in the Southeast (Franklin, 2009; Lord, 2022). These valuable traits are expected to become even more valuable in the future, as extreme weather events including heat waves, droughts, and hurricanes are predicted to continue increasing in frequency and intensity throughout the Southeast in coming decades due to climate change (Binita et al., 2015; Camelo et al., 2020). Because of these trends, the presence of longleaf pines in Southeastern forests will become increasingly valuable as the twenty-first century progresses, especially in areas of their habitat such as Wormsloe that are directly adjacent to the coast and have some of the highest vulnerability to climate change impacts (Binita et al., 2015). By providing methods that can help manage climate-smart longleaf pine restorations, research conducted at Wormsloe has the potential to help the Southeast as a whole adapt to twenty-first century climate trends.

### **Brief History of UAS, Structure from Motion, and LiDAR for Forestry and Ecological Monitoring**

#### ***Evolution of Unmanned Aerial Systems for Environmental Monitoring***

The term *unmanned aerial system* (UAS) describes the devices that are also frequently called *unmanned aerial vehicles* (UAVs) or simply *drones*. The terms are often used interchangeably, but there is a slight difference: while *UAV* or *drone* refers specifically to the aircraft, *UAS* describes the entire system, which typically includes a ground control station (GCS), the aircraft itself, and the communications system linking the aircraft to the GCS (Colomina & Molina, 2014).

While remote sensing of forests via manned aircraft for aerial surveys and forest mapping was pioneered in the early twentieth century (Leckie, 1990; Lund et al., 1997; Spurr, 1948; Thelen, 1919), and satellite remote sensing of forests began with the Landsat program in 1972 (Iverson et al., 1989; Thorley, 1975), it took longer for UAS to begin seeing regular use for such research. It can trace its roots to military technology, with the earliest instances of military use of UAS going all the way back to the 1910s and further military-led UAS developments taking place over the following six decades (Colomina & Molina, 2014). It was around this time, during the 1970s, that the use of the technology for non-military purposes began to receive some consideration, partly due to advances in integrated circuitry and radio-controlled systems technology. However, at this early stage, it was primarily developed by forward-thinking private sector companies and civil aviation authorities and was not yet seeing regular use in academic research (Colomina & Molina, 2014). The 1990s saw the development and miniaturization of new technologies that made the production of more advanced UAS systems feasible (Deliry & Avdan, 2021), but it took until the twenty-first century for UAS to really explode in mainstream popularity – towards the end of the first decade of the 2000s, Google searches with the word “drone” began to surge, and around the same time, there was a notable increase in the volume of UAS-related environmental studies being published as well as a stronger focus on UAS topics at photogrammetry and remote sensing conferences (Colomina & Molina, 2014; Manfreda et al., 2018).

More recent trends from the 2010s have shown that UAS continue to be used ever more frequently, including for the purpose of monitoring forested lands via remote sensing (Anderson & Gaston, 2013; Jaakkola et al., 2010; Singh & Frazier, 2018; Tang & Shao, 2015). They offer powerful data collection capabilities while remaining relatively cheap and also

highly customizable with regards to parameters such as flight time, sensor type, and spatial and temporal resolution (Sharma, 2019).

### ***Evolution of Structure from Motion for Environmental Monitoring***

The use of conventional photogrammetry predates the development of LiDAR – in fact it was used to assess the accuracy of early efforts to study forests with LiDAR (Nelson et al., 1984) – but modern SfM photogrammetry is a more recent invention. According to Granshaw (2018), the phrase *structure from motion* was first used in the doctoral research of computer scientist Shimon Ullman in the late 1970s (i.e., Ullman, 1979), when the computer vision techniques behind SfM – many of which were developed earlier during the 1950s – were being incorporated into computer software (Förstner & Gülch, 1987; Gruen & Baltsavias, 1988; Gruen et al., 2004). Over the next few decades, researchers made significant progress in the field of photogrammetry-related computer vision, including the development and refinement of techniques such as feature correspondence and bundle adjustment that became vital components of the SfM workflows commonly used today (James et al., 2019; Snavely et al., 2008; Westoby et al., 2012). These techniques were highly robust and flexible and addressed some of the limitations of traditional photogrammetric methods, allowing for high-quality 3D shape recovery with less stringent input data requirements, including no need for detailed camera position and orientation data (Dellaert et al., 2000; Snavely et al., 2008).

As a result of these developments, by the mid-2010s (notably, at around the same time that the use of UAS was becoming commonplace), SfM had undergone a steady growth in popularity in a variety of fields, and it quickly became the preferred photogrammetric technique used in the geosciences (Granshaw, 2018). This included an increase in the use of SfM for forest structure characterization and other forest-related inventory and monitoring projects (e.g., Bohlin et al., 2012; Ni et al., 2018; Ullah et al., 2017; Zarco-Tejada et al., 2014).



Such popularity is not surprising, as collecting data with a modern UAS-based SfM workflow has several advantages over the traditional aerial photogrammetry process. In addition to the aforementioned flexibility that comes with using a UAS, SfM uses cheaper equipment and requires less precision, expertise, and time (Deliry & Avdan, 2021). And yet another reason for the newfound popularity of SfM during this time period, besides simply being a cheaper and more user-friendly alternative to traditional photogrammetry and LiDAR (Granshaw, 2018), was a surge in the availability of tools for implementing it. The early 2000s, which saw the drone industry fully take off, also saw consumer-grade digital cameras come into widespread use alongside various easy-to-use software products; this allowed even amateur users to begin applying digital photos to SfM applications (Fraser & Cronk, 2009).

### ***Evolution of LiDAR for Environmental Monitoring***

Though the idea of using light to measure distance had been experimented with as early as the 1930s, the development of modern LiDAR really began in the 1960s after the invention of the laser, and it was developed largely for military and aerospace endeavors, including several of NASA's Apollo missions (McManamon, 2019). Over the following decades, the technology evolved and slowly became more mainstream, and it began seeing use in other fields. This expansion, coupled with improvements in aerial navigation and positioning systems, opened the door for geospatial applications of airborne LiDAR technology (Lim et al., 2003; Renslow, 2012). Early uses of LiDAR for modelling trees focused more on forestry, such as remotely measuring tree height, basal area, and other forest stand characteristics (e.g., Means et al., 1999; Nelson et al., 1984; Nilsson, 1996). More recently, however, LiDAR applications have expanded to include ecological research such as canopy gap detection, fuel assessment and fire prevention, and vertical forest structure characterization (Maltamo et al., 2014; Miura & Jones, 2010). Such tasks were conventionally quite challenging due to

the complex 3D structure of trees and undergrowth, but LiDAR excels at providing insights into complex vegetation structures (Miura & Jones, 2010).

Early instances of LiDAR landscape analysis were usually done from manned aircraft, and manned aircraft continue to be used, but recent years have seen rapid expansion of the market for ground-based LiDAR, often called terrestrial laser scanning (TLS), as well as UAS-based LiDAR, also referred to as UAV laser scanning (ULS). This type of LiDAR, which uses a UAS platform for a LiDAR sensor, lessens the expense and logistical challenge of aerial LiDAR data collection (Hartley et al., 2020), and it is expected to continue growing in popularity. Recent predictions have estimated a nearly 30% annual growth rate and a more than \$350 million overall increase in the value of the global LiDAR drone market between 2022 and 2027 (Markets and Markets, 2022). This includes forestry and landscape ecology applications in addition to many other applications such as precision agriculture and utility corridor mapping.

### **Technical Overview of UAS-Related Data Acquisition and Processing Methods**

Canopy height measurements provide basic but critical data that is needed to evaluate and manage forests around the world (Tang & Shao, 2015). Manual data collection, such as collecting individual tree coordinates and heights for forest studies, is painstaking and expensive, but UAS-based sensors offer an accurate and cost-effective alternative to traditional data collection methods (Gyawali et al., 2022; Rodríguez-Puerta et al., 2022).

### ***Structure from Motion***

Structure from Motion (SfM) is a photogrammetric technique with origins in the field of computer vision (Dellaert et al., 2000; Fonstad et al., 2013; Westoby et al., 2012). The concept behind SfM lies in its name: the 3D structure of an object or landscape can be

modelled by moving a camera around the object of interest and taking multiple overlapping photos (Figure 6). In order to reconstruct the scene successfully, there must be enough overlap for any given feature to appear in multiple images (Fonstad et al., 2013; Westoby et al., 2012). This allows the photos to be processed into 3D models using photogrammetry software. The software employs image matching algorithms to recognize the matching points in the images and align them, creating a model of individual photo locations, or *cameras*, that represent where each image was taken in 3D space (Snavely et al., 2008; Westoby et al., 2012). From there, the images can be further processed into products such as dense point clouds, 3D models, and orthomosaics. This process can be done relatively simply by using a handheld camera or smartphone to photograph a single item, but it can be applied to very broad scales as well, such as by using a drone-mounted camera to photograph and model vast swaths of land. It should be noted that this process does not have the ability to penetrate vegetation, so the details captured in an SfM-derived point cloud of a forest, for instance, will disproportionately be from the tree canopy and not from ground level. Sometimes this makes tree height measurements difficult as there is usually a negative correlation between tree height accuracy and canopy density (Sankey et al., 2017), but in many situations SfM can still be used for the creation of an accurate canopy height model (Rodríguez-Puerta et al., 2022).

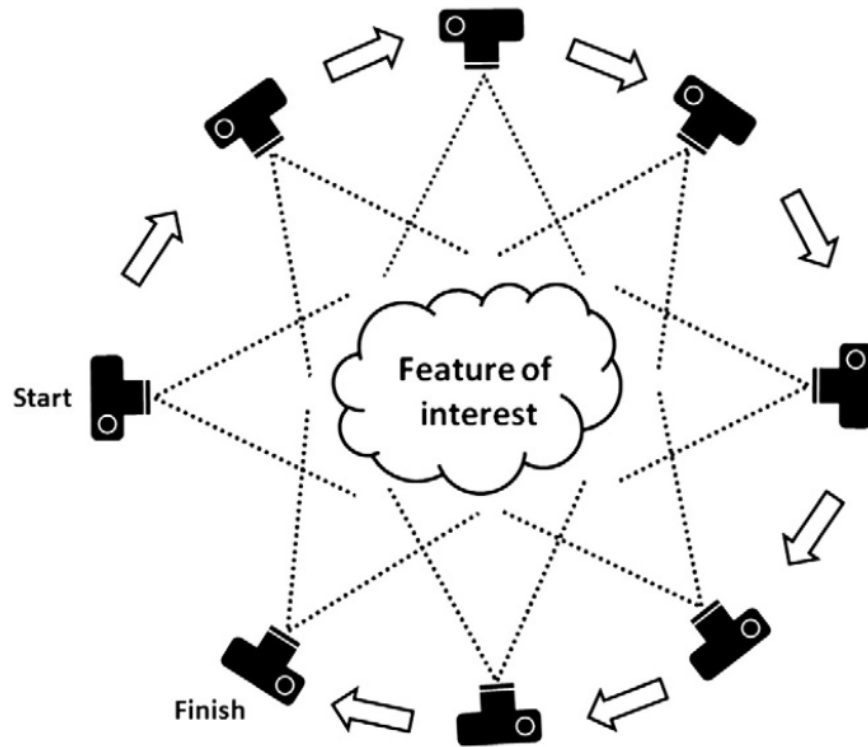


*Figure 6. Visualizing Structure from Motion. Multiple overlapping photographs are required to model the feature of interest. Taking many photographs from multiple angles with a high degree of overlap will typically yield higher quality results. Image credited to Westoby et al. (2012).*

### **Ground Control Points and GNSS Data Collection**

SfM generates point clouds and derived data products in a relative coordinate system, meaning that features of interest will not have real-world coordinates unless a true coordinate system is assigned (Westoby et al., 2012). While the digital images used for SfM do typically contain the geolocation data necessary for assigning a coordinate system, this data can be rather inaccurate since images are usually collected with mid-grade drones that lack high accuracy positioning systems (Dinkov & Kitev, 2020). Therefore, it is advantageous to collect accurate coordinates for ground control points (GCPs) on the ground before a UAV flight to ensure that SfM results will be accurately georeferenced (Madden et al., 2019). The use of an appropriate number of evenly distributed GCPs has been shown to be one of the

most crucial factors for obtaining accurate geospatial data with UAS-based SfM (Deliry & Avdan, 2021; Sanz-Ablanedo et al., 2018). Though there are alternatives to using GCPs such as direct georeferencing of individual UAS camera locations, and such approaches may be necessary when a study area will not accommodate the use of GCPs, a traditional GCP-based approach tends to yield the best accuracy (Dinkov & Kitev, 2020; Turner et al., 2012).

GCP locations (as well as the locations of other objects such as trees) can be determined with centimeter-level accuracy through the use of GNSS (Global Navigation Satellite System) receivers. One technique for resolving highly accurate coordinates via GNSS is known as the post-processed kinematic (PPK) method. Unlike the real-time kinematic (RTK) method, in which a GNSS receiver applies corrections to positional data in real time by communicating with a base station, PPK involves fixing positional inaccuracies by applying base station corrections in the office after data collection is finished (Dinkov & Kitev, 2020; Pirtti, 2021). As long as receivers are sufficiently visible to the overhead satellite network, both methods are effective for obtaining centimeter-level accurate coordinates; however, one may be preferred over the other depending on data collection goals and study area characteristics. RTK is advantageous for producing corrected results in the field and reducing office processing time, but PPK arguably offers more overall flexibility in the field – it does not require a real-time connection to a base station, and there is no need to resolve base station coordinates prior to data collection (Pirtti, 2021).

### ***LiDAR***

LiDAR (Light Detection and Ranging) is an active form of remote sensing that sends pulses of electromagnetic energy, typically in optical or infrared wavelengths of the electromagnetic spectrum, from a sensor and then receives a reflected signal back (Renslow, 2012). By measuring the time needed for a pulse of energy to bounce off an object and return to the

sensor, the distance between the sensor and object can be calculated (McManamon, 2019). In this manner, a rapid stream of pulses sent from an airborne LiDAR sensor over a landscape can precisely determine the distance to many different points on the ground and visualize an entire landscape's surface in three dimensions. Perhaps LiDAR's greatest attribute is that each pulse can also penetrate layers of vegetation, often sending multiple returns back to the sensor at different intensities that correspond to various layers in the forest canopy as well as the ground underneath (Figure 7). This allows for detailed mapping of both 3D vegetation structure and the structure of underlying terrain (Wulder et al., 2012). In order to ensure that this data is both highly detailed and geospatially accurate, airborne LiDAR relies on three technologies: the laser scanner itself; an inertial navigation system (INS) that records pitch, roll, and yaw; and a Global Navigation Satellite System (GNSS) that records position (Lefsky et al., 2002). The two primary types of systems are *full waveform* LiDAR, which records the entirety of each pulse's reflection as a waveform, and *discrete return* LiDAR, which interprets the energy peaks of each pulse's reflection as discrete objects and assigns each peak a point, building a cloud of points (Wulder et al., 2012).

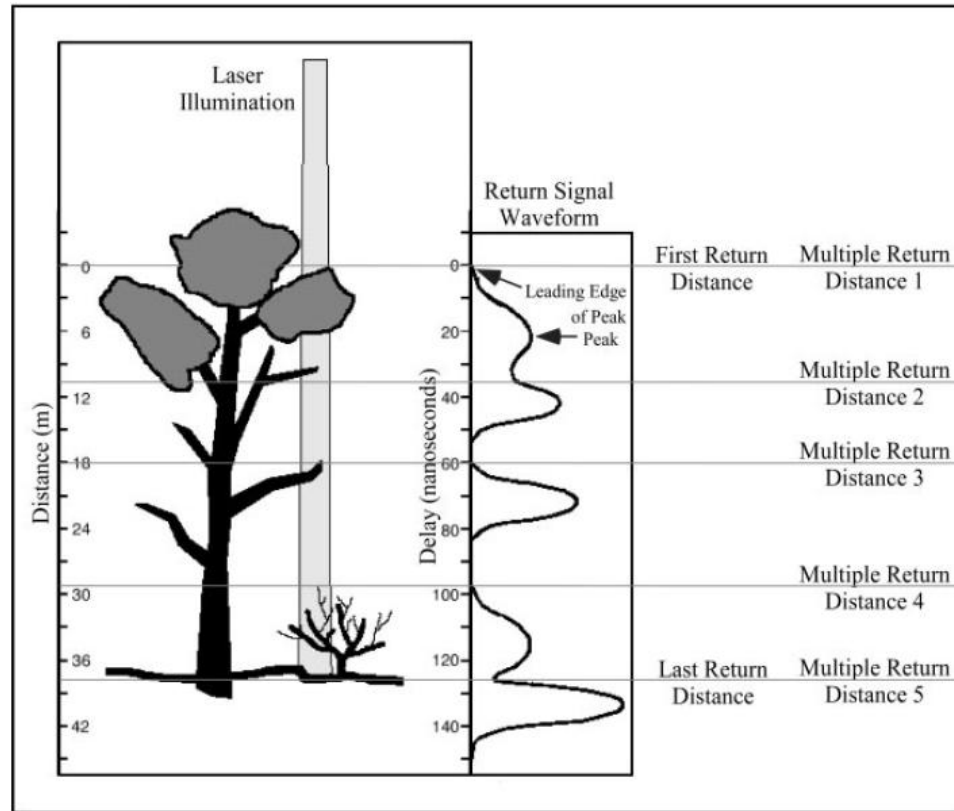


Figure 7. An example of a pulse from an airborne LiDAR sensor. As it hits vegetation, some energy passes through multiple layers, reaches the ground, and returns to the sensor (left side of figure). The return signal might resemble a wave (full waveform LiDAR, center), or it might be processed into a number of discrete returns, or points (discrete return LiDAR, right). Image credited to Lefsky et al. (2002).

### **SfM and LiDAR Accuracy**

Though these two methods are generally very accurate, point clouds may still lack points equating to the exact ground level or the uppermost bits of forest canopy. If either or both occur, canopy height values will be underestimated (Hyypä et al., 2008). As a result, SfM tends to underestimate tree height (e.g., Hao et al., 2021; Zarco-Tejada et al., 2014), as does LiDAR (e.g., Nilsson, 1996; Persson et al., 2002; Picos et al., 2020; Rodríguez-Puerta et al., 2022); this is especially the case for shorter trees. Though many studies have found some variation of this trend, they used a variety of data collection and processing methods and

were applied to stands with a variety of heights, tree species, canopy structures, and terrain characteristics, all factors that can affect the magnitude of height underestimation (Abdullah & Munjy, 2019). Examples of how differing methodologies and study area characteristics affect SfM accuracy specifically can be seen in Goodbody et al. (2021), which studied the effects of image overlap, forest structure, and terrain characteristics; Kameyama & Sugiura (2021), which compared the accuracy of multiple SfM software options; and Deliry & Avdan (2021), whose review of relevant literature found that higher UAV flight heights consistently diminish accuracy and that choice of SfM software consistently affects accuracy.

Previous studies have directly compared the two methods as well, though research comparing SfM to LiDAR is less common in the literature than research utilizing one method or the other. Furthermore, comparison studies looking at young, plantation-style forests with relatively open canopies and regular spacing between trees (i.e., forests similar to the longleaf pine field at Wormsloe) are even rarer (Gyawali et al., 2022). Many of these comparison studies, including those focused on younger forest stands, have found similar trends; namely, that SfM and LiDAR both produce acceptable tree height estimates, LiDAR's results are usually slightly more accurate, and again, both methods underestimate height and do so to a greater extent for shorter trees (e.g., Gyawali et al., 2022; Hartley et al., 2020; Mielcarek et al., 2020). However, some studies' results contrast with the general trends, such as Wu et al. (2020), which studied horticultural tree crops and reported that SfM produced more accurate tree heights. Again, though, it should be noted that different data collection parameters, study area characteristics, and post-processing software settings can yield different results. Thus, the trends in tree height error seen in these studies may not equate to the trends seen when measuring Wormsloe's longleaf pines, and it is important to



make SfM-LiDAR comparisons and quantify tree height error for the specific set of factors present in this study.

### ***The Significance of Making SfM-LiDAR Comparisons***

Although both methods can create useful 3D point clouds and derived products, each comes with its own set of advantages and disadvantages. For instance, SfM usually creates a relatively dense point cloud and includes extra spectral data such as RGB values for points – this is good for creating detailed 3D models, but the extra data can cause processing difficulties when working with large study areas. Conversely, LiDAR often produces a sparser point cloud and no additional spectral data for points, but it is much better at extracting the ground surface from beneath vegetation (Hartley et al., 2020; Rodríguez-Puerta et al., 2022). Also, both the technologies used to capture data and the software needed to process it can have notable differences in price and accessibility. SfM data, for instance, can be collected with a relatively inexpensive mid-level drone and camera; however, the post-processing needed to create high-quality, accurately georeferenced outputs may be disproportionately time-consuming and computationally demanding (Westoby et al., 2012), and depending on project goals, it may be impossible to complete at all without sufficient expertise and access to expensive photogrammetry software. Yet in spite of these potential pitfalls, SfM is generally still the cheaper and easier option (Granshaw, 2018; Mlambo et al., 2017). LiDAR collection, besides necessitating a much more expensive sensor than the consumer-grade cameras frequently used for SfM, typically requires a professional-grade drone capable of carrying a heavier payload and a highly experienced remote pilot who can minimize the risk of damaging such valuable equipment while in the field – a full UAS-based LiDAR setup will likely come to more than \$50,000. Post-processing software for LiDAR data can cost tens of thousands of

dollars as well, though there are also cheaper and even free, open-source options available (Van Tassel, 2021).

In short, anyone interested in the data that can be acquired with these technologies, whether it be for academic research or commercial purposes, has many logistical and financial factors to consider. The results of tree height accuracy comparisons can provide additional valuable information when deciding between methods, particularly for a forestry or ecological monitoring project.

### **Overview of Instance Segmentation with Deep Learning**

In order to obtain tree heights from a point cloud, it is crucial to know where the trees are and where they are not. While traditional individual tree detection (ITD) and crown delineation from point clouds or canopy height models (CHMs) of a pine plantation is typically feasible (e.g., Rodríguez-Puerta et al., 2022), those methods worked poorly for this study due to the short heights of some trees, occasional overlapping crowns, the prevalence of surrounding vegetation, and the need to isolate longleaf pines from shrubs and other pines that have taken root in the field. Previous studies also found that factors such as these lowered the accuracy of ITD algorithms (e.g., Hao et al., 2021; Véga & Durrieu, 2011).

Fortunately, alternative techniques now exist thanks to the field of GeoAI (geospatial artificial intelligence), which has seen multiple breakthroughs in recent years on its way to becoming the face of novel, innovative data analysis in the geosciences. More specifically, geospatial deep learning, a component of the GeoAI toolset, is now being used for rapid, advanced analysis of subtle and complex patterns in geospatial data (Li & Hsu, 2022). Convolutional neural networks (CNNs), a type of deep learning algorithm, offer an alternative approach to detecting trees based on analysis of patterns in raster data (Goodfellow et al., 2016). As GeoAI has grown, the ability to analyze photographs and other raster data with

CNNs has seen rapid advancements in speed, efficiency, and scalability, including for the task of *instance segmentation* (He et al., 2017). Unlike *object detection*, which classifies objects and assigns each a bounding box, or *semantic segmentation*, which classifies all input pixels into categories, instance segmentation is able to identify objects and simultaneously delineate their exact extents in pixels, essentially blending the capabilities of object detection and semantic segmentation. This makes it an ideal solution for tasks such as building footprint extraction and tree crown delineation (Dersch et al., 2023; Esri Academy, 2020; He et al., 2017).

The exact performance level of CNNs trained to detect trees in aerial imagery can vary significantly for a variety of reasons. For example, a model trained to detect multiple tree species in a forest may perform better than a model trained to detect a single species in the same study area (Beloïu et al., 2023). Alternatively, the nature of the study area itself may cause inconsistencies: models applied to heterogeneous forests with dense, complex canopies will likely have reduced accuracy compared to those applied to more homogenous, plantation-style forests (Beloïu et al., 2023; Zhang et al., 2022); it has also been observed that that morphology of a particular species may render it more or less suitable for detection via CNN (Beloïu et al., 2023). However, in spite of these potential limitations, neural network-based approaches to tree crown detection and segmentation have proven quite capable of outperforming most conventional approaches (Dersch et al., 2023).

Mask Region-Based Convolutional Neural Network (Mask R-CNN) is an example of a CNN that was developed specifically for instance segmentation. It was originally proposed by He et al. (2017) as an extension of the pre-existing Faster R-CNN (Ren et al., 2016) used for object detection. Both CNNs use a two-stage architecture for object detection, making them more computationally demanding but better performing than one-stage algorithms

(Katal et al., 2022). However, unlike Faster R-CNN, Mask R-CNN delineates masks for detected objects in addition to bounding boxes (Figure 8), allowing for precise segmentation while still remaining flexible, high-performing, and easy to train (He et al., 2017).

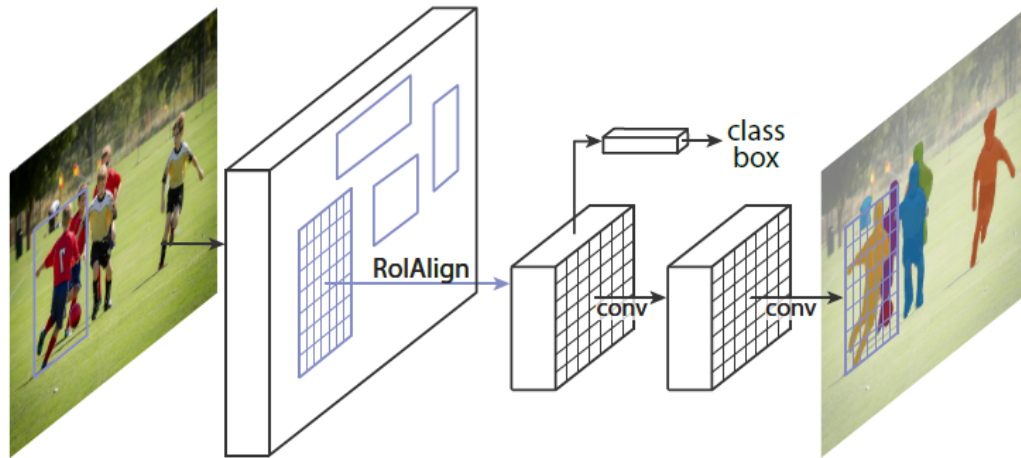


*Figure 8. A simple visualization of the Mask R-CNN framework. Mask R-CNN adds functionality for delineating object masks in addition to creating bounding boxes. Image credited to He et al. (2017).*

Mask R-CNN and related deep learning algorithms have proven to be powerful, customizable, and highly accurate tools capable of quickly accomplishing geospatial analyses of forested lands in a manner that previously would have been impossible. With these capabilities now pairable with readily available, high-resolution remote sensing data such as that from UAS flights, it is no surprise that geospatial deep learning is rapidly becoming a familiar component of many forestry and ecology studies (BeloIU et al., 2023).

## **CHAPTER 3**

### **METHODOLOGY**

#### **UAS Flights**

UAS collection of RGB imagery of the field at Wormsloe began in 2016 when the longleaf pines were planted and has been repeated on a mostly annual to semiannual basis ever since (there are a few data gaps, as data was not collected in 2020 or 2024 and has yet to be collected in 2025). The flights from the early years were conducted primarily for general site monitoring and did not necessarily have the more detailed analysis objectives of this research in mind; however, they still provide useful time series data. The more recent flights within the timeline of this research effort occurred during two field missions in September 2022 and February 2023. A detailed map of the field and the research plots within it is presented in Figure 9.

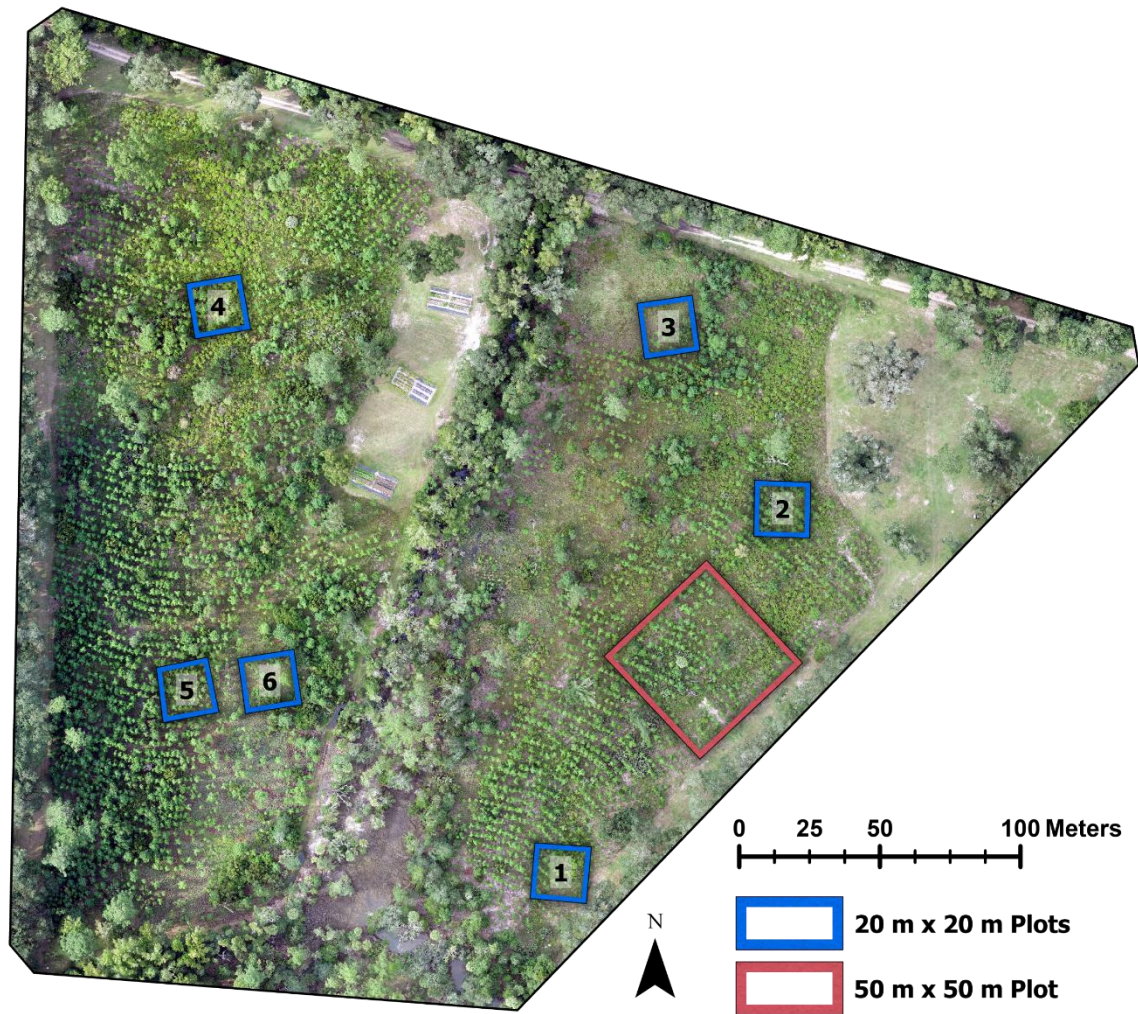


*Figure 9. Detail map of the longleaf pine field shown using an orthomosaic from September 2022.*

The purpose of the September 2022 UAS flights was twofold. First, five separate flights to collect RGB imagery were conducted over a 50 x 50-m sample plot in the field (Figure 9) at flight heights ranging from 40 to 120 m at 20-m intervals, obtaining spatial resolutions ranging from 1.1 to 3.3 cm. The purpose of these flights was to assess the effect of drone flight height on SfM-derived tree height accuracy. These flights also used five GCPs, which were placed in the sample plot to allow for accurate georeferencing. The GCPs were



2-ft. x 2-ft. plywood squares with a black 'X' painted on a white background. After collecting data at the sample plot (Figure 10), RGB imagery was collected for the whole field at a height of 120 m to continue the ongoing time series of data going back to 2016. All flights were done using a DJI Phantom 4 Pro and built-in 20 MP camera, and they were flown in a back-and-forth single grid flight pattern with the camera angled at nadir. Flight planning was done on a tablet with the Map Pilot app for iOS.



*Figure 10. Dr. Thomas Jordan changes UAV batteries for the DJI Phantom 4 Pro in between flights during the September 2022 data collection.*

The February 2023 flights were the first data collection to obtain both UAS imagery for SfM and UAS LiDAR data, allowing for direct comparison of the two methods. As before, RGB imagery collection was conducted for the whole field with a DJI Phantom 4 Pro using a single grid flight pattern with the camera angled at nadir; however, this time the flight height

was set to 60 m for the purpose of obtaining imagery with a higher spatial resolution (1.6 cm) and allowing for more accurate tree height estimates. This flight was also able to take advantage of eight permanent rebars that had recently been installed to mark GCP locations. The LiDAR collection was flown on the same day with a Freefly Alta X UAV and a LiDAR USA Revolution 120 sensor capable of up to three discrete returns (Figure 11). The flight collected data at a pulse rate of 300 kHz, and like the RGB imagery collection, it was conducted over the whole field using a single grid flight pattern. Full parameters for all UAS flights from 2016-2023 are displayed in Tables 7-9 in Chapter 4.



*Figure 11. Dr. Sergio Bernardes gets the Freefly Alta X ready for flight during the February 2023 data collection.*



### **Ground-Based Data Collection**

Multiple data collection and field work-related tasks were carried out on the ground in addition to the UAS flights.

#### ***GNSS with Emlid Reach Receivers***

Ground-based GNSS receivers were employed during both recent data collections. Both the field and the post-processing aspects of the GNSS workflow are largely based on Pratt-Sitaula et al. (2022). During the September 2022 mission, an Emlid Reach M2 receiver was set up as a base station at the north end of the study area and initially collected data for over four hours – four or more hours of base station occupation ensures accurate trilateration of the station’s location with Precise Point Positioning (PPP) during post-processing. With the base station running, the Emlid Reach RS2 receiver was set up as a GNSS rover. It collected the coordinates of GCPs for the drone flights and the coordinates of 36 trees in the 50 x 50-m sample plot (Figure 12). Both GNSS receivers were configured and managed via the Emlid Flow app (formerly called ReachView 3), which was operated on a smartphone that accompanied the receivers in the field. During the second round of data collection in February 2023, the base station-rover GNSS setup was used again in a similar manner to collect GCP coordinates. However, two changes were made to improve the quality of data and hopefully resolve more accurate coordinates. First, a new base station location, the center of the large field west of the study area, was used so that the receiver would be more visible to the satellite network. Additionally, the GNSS rover collected data for 2 minutes at each point instead of the recommended 30-second interval that was used initially.



*Figure 12. The GNSS base station (left) and rover (right) being used to record individual tree coordinates in September 2022. Right image courtesy of Dr. Thomas Jordan.*

### ***Tree Height Measurements***

During the GNSS data collection in September 2022, each of the 36 trees whose coordinates were collected was marked and numbered with pink flagging tape. These trees' heights were then manually measured with a telescopic measuring pole. This was a two-person job, where one person held the telescopic pole and the second person used field binoculars to observe and record height values. The measuring of tree heights was repeated in the same manner during the February 2023 field mission in order to have up-to-date ground truth data to compare to the heights derived from UAS data (Figure 13). It should be noted that these measurements, despite being considered “true” tree heights, may have a few centimeters of error, as determining the measurement on the telescopic pole that was most level with the uppermost pine needles proved challenging at times. Appendix D contains a record of the measured heights and positional data for all 36 trees.



*Figure 13. Charles Perrie assists with measuring tree heights with the telescopic pole in February 2023.*

### ***Permanent Ground Control Points***

In February 2023, 8 steel rebars were installed around the field to serve as permanent locations for GCPs. Each rebar extended one foot out of the ground and was spray-painted pink and capped with an orange safety cap to be as visible as possible (Figure 14). They were strategically placed throughout the study area so as to be easily accessible to humans, highly visible to UAS sensors from above, and useful for accurate georeferencing of drone imagery. The goal of installing these rebars was to eliminate the need for collecting GCP coordinates during future drone flights, thus increasing data collection efficiency.





*Figure 14. Capped rebar in the southwest corner of the study area.*

### **Structure from Motion and LiDAR Data Processing**

#### ***GNSS Post-Processing***

Before processing the RGB imagery into SfM products, it is important to process the GNSS raw data into accurate GCP coordinates. To do this, base station logging data was first sent to the Canadian Spatial Reference System Precise Point Positioning (CSRS-PPP) service offered by Natural Resources Canada (NRCan). NRCan used the data logs to determine the base station coordinates with centimeter-level accuracy. The next step was to correct the coordinates collected by the GNSS rover via a post-processed kinematic (PPK) workflow in the post-processing software Emlid Studio, Version 1.5 (Emlid, 2023). After entering the base station logging data, the rover logging data, the base station coordinates reported by the PPP

service, and the uncorrected coordinates into Emlid Studio's "Stop & Go with Emlid Flow" tool (Figure 15), the software output corrected x, y, and z-coordinates for each point.

Most points had high enough quality data to achieve a *fix* solution, meaning that the corrections provided by the base station resolved all positional ambiguities. However, some points only achieved a *float* solution. Coordinates with float solutions are less accurate because not all of their positional ambiguities have been resolved, though their accuracy may still be sufficient depending on the nature of the task at hand (Emlid, n.d.; Madikyzy, 2024). To help quantify accuracy, each adjusted coordinate also includes root mean square (RMS) error values for latitude, longitude, and elevation, as well as a position dilution of precision (PDOP) value indicating the quality of the overhead satellite geometry (Madikyzy, 2024). After studying the accuracy metrics, some slight adjustments were applied to the Emlid Studio processing settings, and the software yielded fix solutions for nearly all points with accuracy metrics showing good PDOP values ( $< 2$ ) and low RMS values (generally no greater than 2 cm).

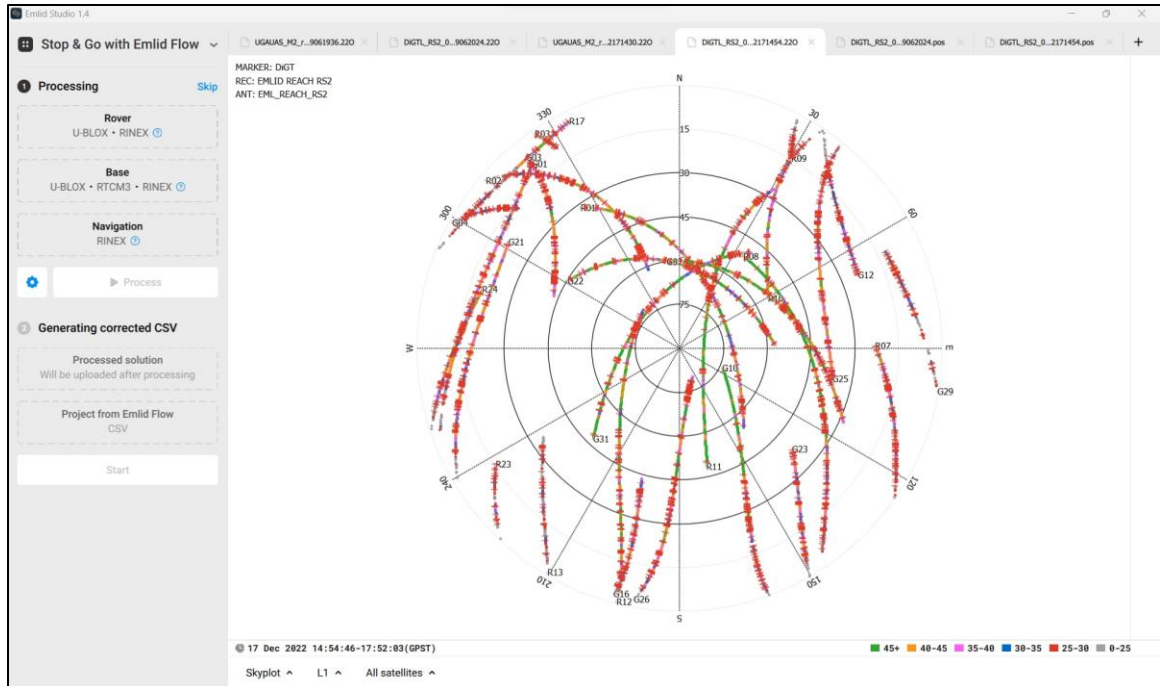


Figure 15. Visualization of the Emlid Studio interface. Data files for post-processing can be added to the left panel. In this screenshot, the main window shows a sky plot of satellite positions and movements during a data logging event.

### SfM Workflow

The SfM processing was completed in the photogrammetry software Agisoft Metashape Professional, Version 1.8.1 using guidelines presented in the user manual (Agisoft LLC, 2022) in conjunction with workflows provided by Bernardes & Madden (2021) and Over et al. (2021). After the initial steps of loading the images into Metashape and aligning them to create a sparse point cloud, the software allows for the addition of GCPs for more accurate georeferencing (Figure 16). This is where the GCP coordinates, corrected for accuracy during the PPK workflow described above, were added to the SfM workflow. It should be noted that not all the RGB imagery collected used traditional GCPs; for flights that did not use GCPs, the coordinates of landmarks in the field (i.e., tree trunks, fence posts, etc.) were derived and used in place of traditional GCPs.

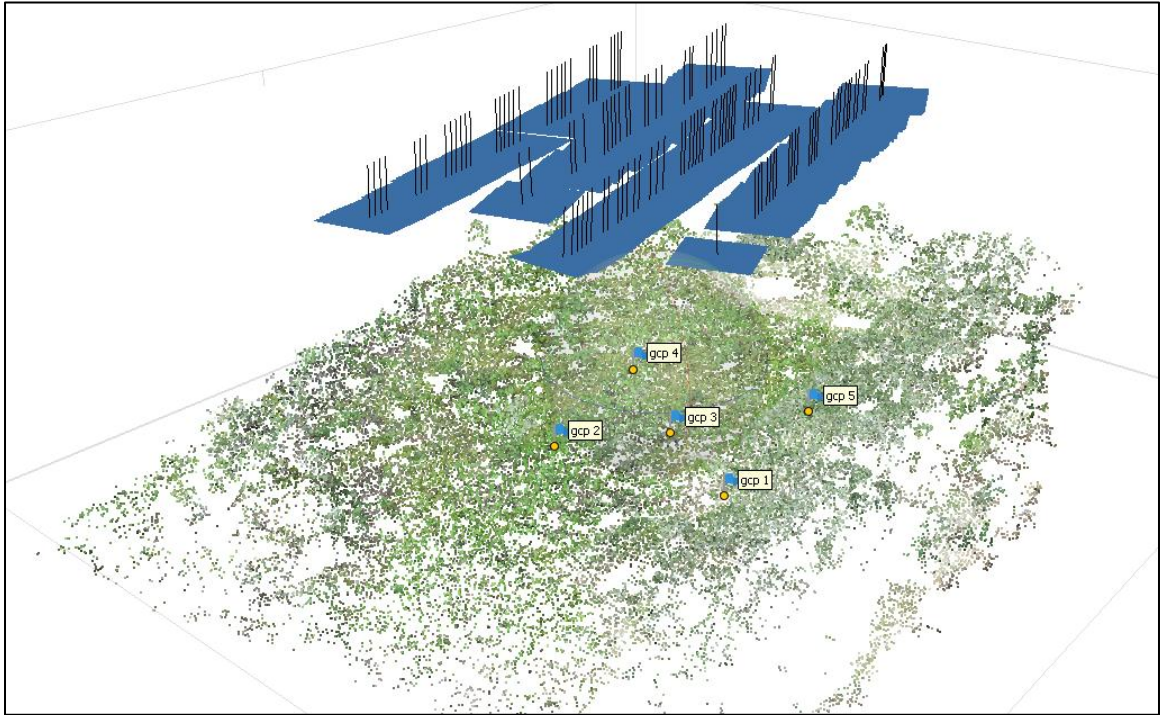
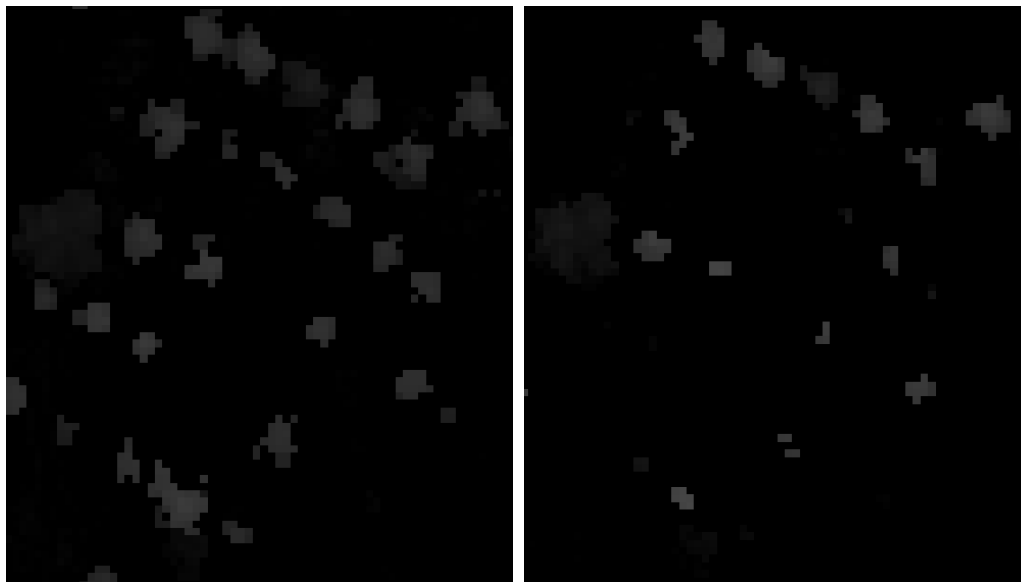


Figure 16. The aligned photos (blue rectangles), GCPs (labelled blue flags), and sparse point cloud visualized in Agisoft Metashape for one of the five flights of the sample plot in September 2022.

For each UAS flight, after adding and positioning the GCP markers, the aligned images were used to create a high-quality dense point cloud, which was then exported as a LAS point cloud file for further processing. Finally, a digital elevation model (DEM) was built from the point cloud, and an orthomosaic was built from the DEM. As with the dense point cloud, each orthomosaic was exported as an image file to be used in later steps of the analysis.

A series of additional processing steps collectively referred to as *gradual selection* is often added to the Agisoft Metashape workflow as well. The gradual selection process refines the sparse point cloud, gradually removing points with lower accuracy and higher

uncertainty until error metrics reach suitable thresholds. However, when this process was applied to the February 2023 data, it shrank the tree crown size of many longleaf pines and even seemed to completely remove some trees from the dense point cloud and derived CHM (Figure 17). Applying gradual selection less aggressively might have improved data quality without causing large decreases in tree crown size, but this was not tested. Gradual selection was not included in the workflow to generate final SfM results for any of the datasets.



*Figure 17. Two versions of the 2023 CHM for part of the field, without gradual selection (left), and with gradual selection (right). Brighter pixels represent larger canopy height values where trees are located.*

### ***LiDAR Processing***

Cleaning of the LiDAR dataset was completed in the open source point cloud processing software CloudCompare, Version 2.13.2. First, noise points were removed from the entire point cloud with the Statistical Outlier Filter (SOR) tool. Additionally, since the dataset



consisted of four separate swaths, a translation tool was applied to better align the individual point cloud swaths with each other (Figure 18). Swaths were only translated in the x and y-directions; all point cloud z-values remained unchanged since there was no visible misalignment in the z-direction.

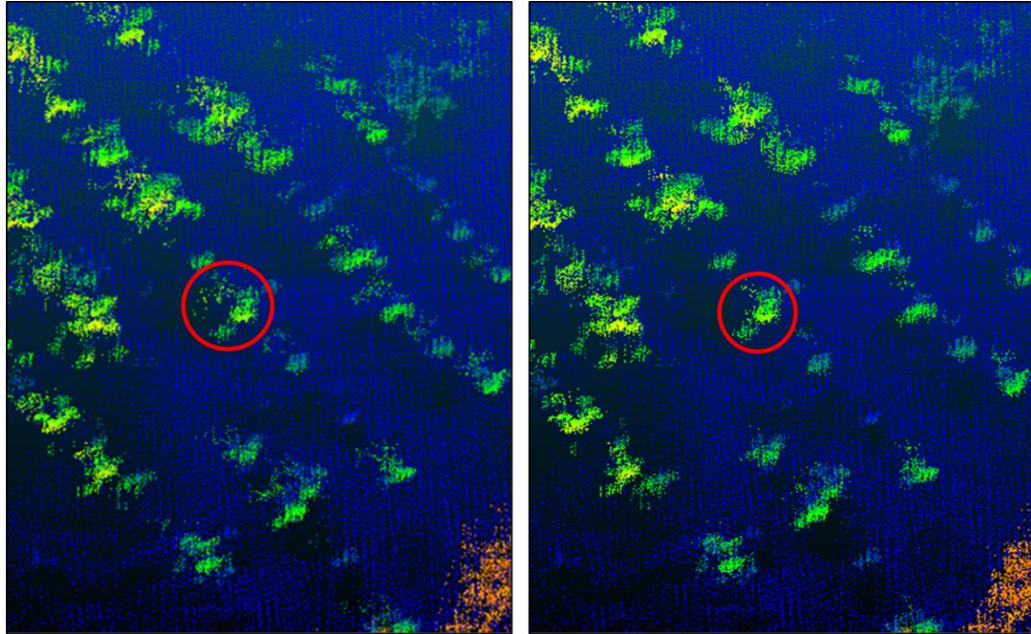


*Figure 18. Nadir view of the point cloud before (left) and after (right) improving the alignment of two overlapping swaths. Longleaf pine saplings (such as the one circled in red) show up as green and yellow points.*

CloudCompare was also used to create a joint LiDAR-SfM point cloud that combined the 2023 data from both methods into a single 3D dataset (Figure 19). To correct slight positional discrepancies between the two point clouds, they were registered to each other automatically using the Fine Registration-Iterative Closest Point (ICP) tool before being exported as a single LAS file.

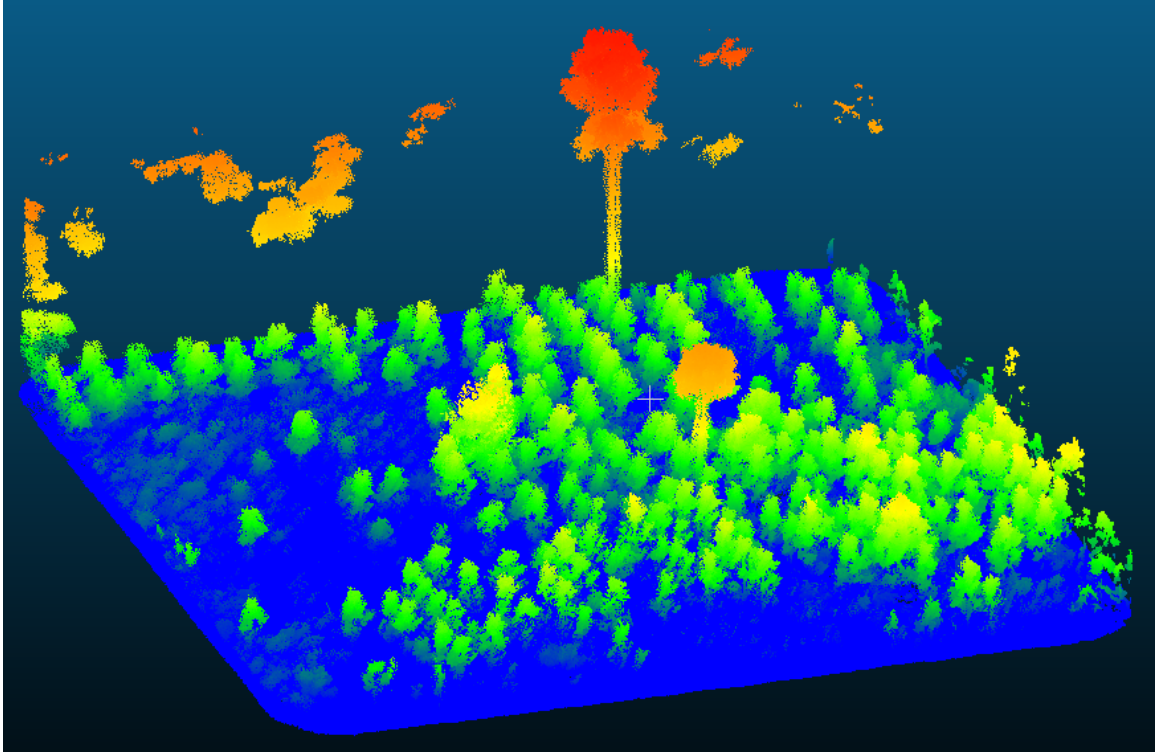


*Figure 19. The SfM and LiDAR point clouds merged into one in CloudCompare. The area shown is the 50 x 50-m plot on the east side of the field.*

### ***Creation of Canopy Height Models***

All point clouds exported from Agisoft Metashape and CloudCompare were processed into CHMs in R 4.2.0, primarily using the R package *lidR*, Version 4.0.0 (Roussel & Auty, 2022; Roussel et al., 2020). The functions offered by *lidR* can perform a wide variety of data cleaning and processing tasks for point clouds. To create a CHM, it first classifies ground points to create a digital terrain model (DTM). Then, the point cloud is normalized based on the elevation values of the DTM (Figure 20). Finally, the normalized point cloud is used to create a CHM raster that can be exported for further analysis in traditional desktop GIS software.

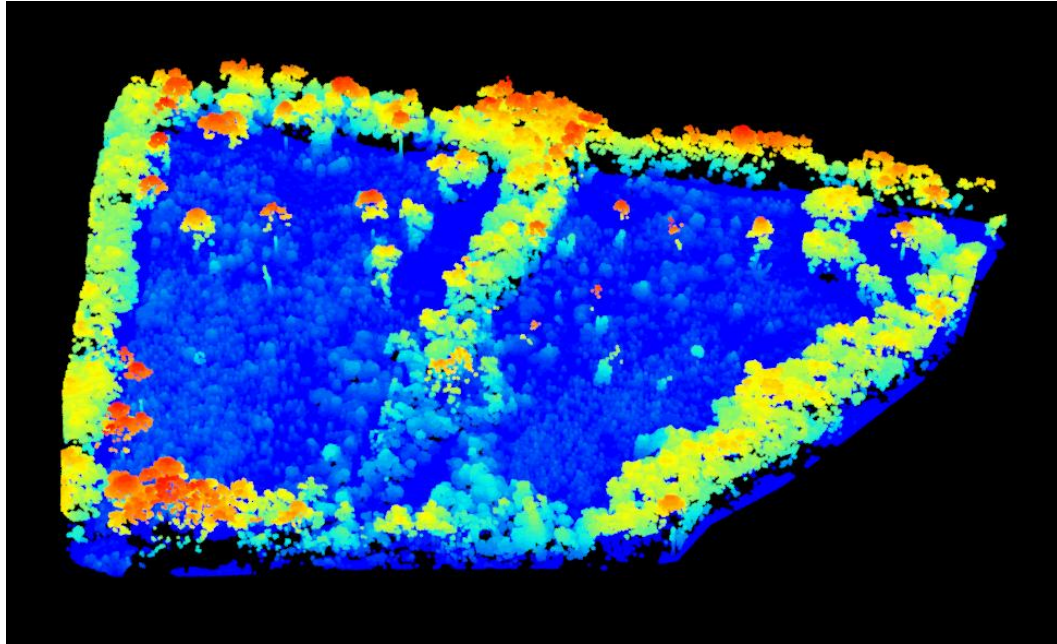


*Figure 20. A normalized point cloud of the study area created using the R package lidR. The point cloud is from the September 2021 data collection and was used to create a CHM for that year.*

All CHMs were created at a spatial resolution of 0.25 m. While finer resolution CHMs tend to result in more accurate tree heights (Picos et al., 2020), DTM (and thus CHM) resolution is limited by the number of ground points in the point cloud. As ground points are sometimes sparse in point clouds created via SfM, 0.25 m was the highest resolution that could be interpolated relatively accurately for all point clouds of the field.

### **Deep Learning for Individual Tree Segmentation**

A deep learning workflow utilizing instance segmentation via a CNN was implemented to detect the locations of longleaf pines in the 2023 data. This method was chosen with the goal of reducing erroneous detections of non-longleaf pine vegetation that is common in the study area and would skew estimates of tree count and average height.

Performing deep learning tasks can be very computer resource-intensive, usually requiring either cloud computing or access to a powerful local machine that can handle heavy workloads; this particular workflow relied on ArcGIS Pro geoprocessing tools running on a local machine. Using these deep learning geoprocessing tools required an Image Analyst license as well as a separate installation of the ArcGIS Pro Deep Learning Libraries. Additionally, the specific neural network implemented, Mask R-CNN, required a CUDA-compatible NVIDIA GPU. The final model training and implementation, which is explained in more detail below, was done in ArcGIS Pro 3.0.0 on a computer with an 8.0 GB Nvidia GeForce RTX 3070 GPU and running a Windows 11 operating system.

#### ***Creation of a Multiband Composite Raster***

Object detection for identifying tree crowns in RGB imagery is a commonly performed task, but in this study area, it mistakenly identified too many bushes and pieces of nearby mature forest canopy as longleaf pines. Fortunately, such deep learning tasks can often be aided by the inclusion of additional spectral bands such as near-infrared (Gani et al., 2021). The UAS flights at Wormsloe have not collected data for any bands beyond the visible spectrum, but there are other alternatives to spectral data that may also be used to improve deep learning results when RGB data by itself proves insufficient. In this case, using CHM height data to complement the RGB orthomosaic improved model results. Tree detection using the CHM only would also be insufficient – such methods are more error-prone when identifying younger, smaller trees (Rodríguez-Puerta et al., 2022) and would not be able to isolate longleaf pines from other species. However, combining the two types of data gave the deep learning model more training data and avoided the limitations of using only one dataset or the other.

Several more datasets were also appended to the RGB data as additional raster bands. To help the model identify pines with intersecting crowns as separate trees, canopy height and pixel greenness datasets from earlier years (when the tree crowns were smaller) were added. The pixel greenness datasets were calculated from the bands of the RGB orthomosaics using the formula  $Greenness = Green / (Red + Green + Blue)$ , and the output rasters were smoothed slightly via focal statistics tools to estimate local vegetation greenness. Finally, a Euclidean distance raster indicating distance from the nearest row of longleaf pines was included; this essentially defined an area of interest, telling the model where objects (trees) were most likely to exist. The final product was a 10-band composite raster (Figure 21) that provided high-quality training data for instance segmentation.



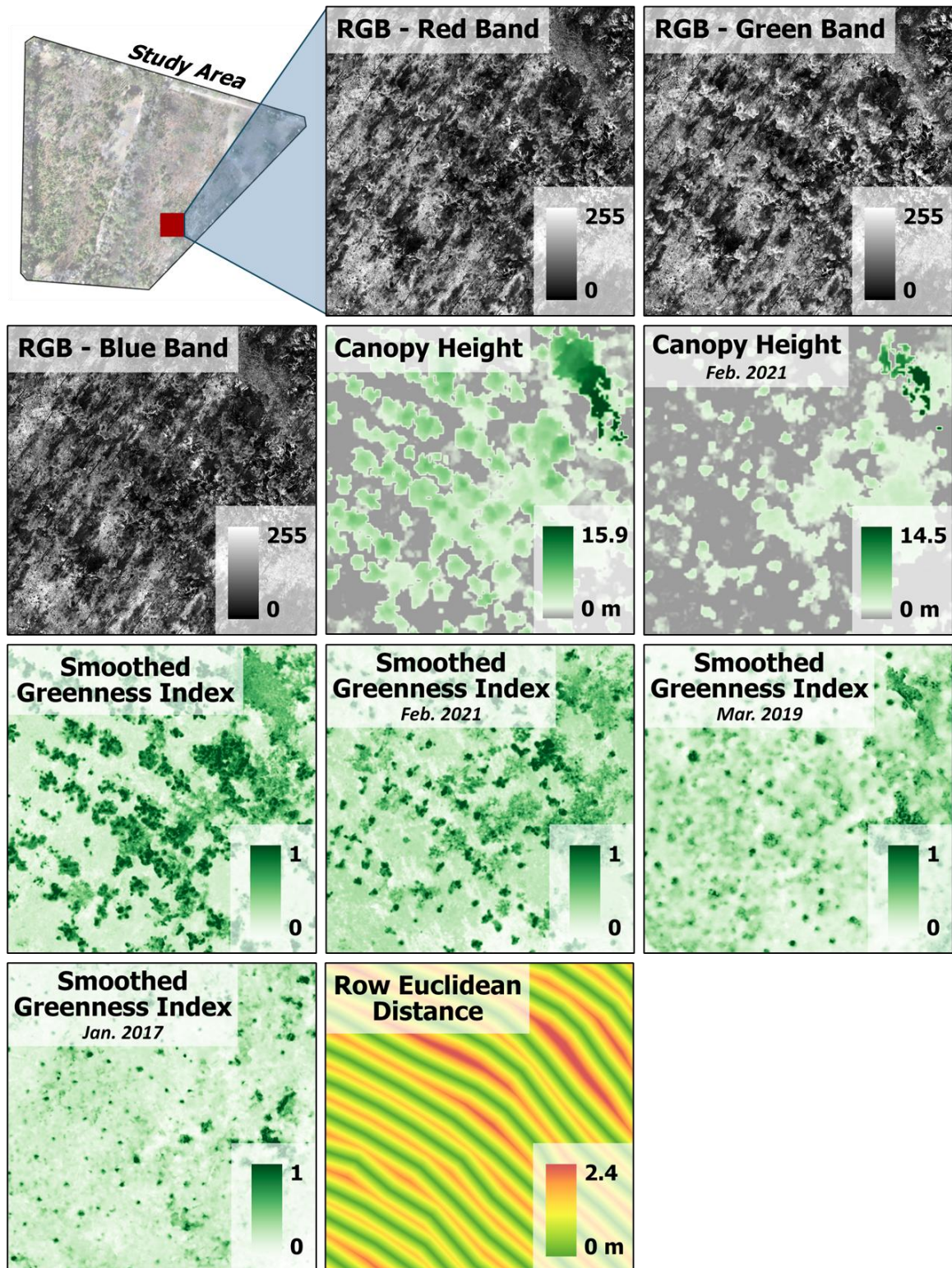


Figure 21. A close-up visualization of all ten bands in the raster dataset used for deep learning model training.

***Deep Learning Model Workflow***

This process detected trees using the Mask R-CNN neural network implemented with ArcGIS Pro Deep Learning Libraries, Version 3.0. Many of the steps explained here, as well as many of the hyperparameter values used in model training, are based on similar deep learning workflows described by Lenhardt (2022) and Mathew & Yadav (2021).

Creating training, validation, and testing data for the model first required the digitization of longleaf pine tree crowns. For this task, portions of the field were established as “training/validation zones” and “testing zones,” and each longleaf pine within these zones was carefully annotated (Figure 22). In total, 716 trees were annotated, 533 (74%) of which comprised the training/validation dataset. The zones were chosen to reflect the variety of tree crown sizes and tree surroundings present in the study area in order to give the model a healthy variety of data to learn from. Once this data was annotated, it was exported to image chips to ensure a usable format for model training.





*Figure 22. Training/validation and testing zones with completed data annotations in the northwest corner of the field. Trees annotated in yellow were used for model training and validation, and trees annotated in purple were saved for testing model accuracy.*

The model was trained using the Train Deep Learning Model tool in ArcGIS Pro. The model's hyperparameters were set to Batch Size = 16, Training-Validation Ratio = 90/10, and Max Epochs = 200. Early stopping was enabled to prevent model overfitting, and the backbone model, a preconfigured CNN that forms the foundation of the newly trained model, was ResNet-50. The backbone model was unfrozen before it began training with the 10-band raster; this is because backbone models such as ResNet-50 are usually pre-trained on 3-band RGB images. Unfreezing the model allows its weights and biases to be adjusted to fit the training samples, which lengthens the training process but usually produces better results when working with multispectral data (Esri Developer, n.d.).



After the model was trained, it conducted instance segmentation of the 10-band raster for the whole study area. The initial output was set to include objects that were detected with at least 20% confidence; however, this 20% confidence threshold would be adjusted later during the accuracy assessment. Finally, since CNNs used for instance segmentation tend to detect objects multiple times, non-maximum suppression was applied to remove duplicate features with greater than 15% overlap.

### ***Accuracy Assessment***

A portion of the annotated data (183 trees or 26% of the annotations) were part of testing zones, meaning that they were left out of the deep learning model training process and used exclusively for testing. The accuracy assessment compared this testing data to the model's results within the zones; it used an Intersection over Union (IoU) ratio of 50%, meaning that if an annotated tree and a tree detected by the model did not overlap by at least 50%, it was not considered a match.

There are multiple metrics that can provide insight into a model's results. The *average precision* (AP) metric is commonly used to quantify model performance, but in this instance it was necessary to look at additional metrics in order to adjust the confidence threshold (originally set at 20%) to a more suitable value. The confidence threshold was raised until reaching a point where *precision* (describing the frequency of false positives) and *recall* (describing the frequency of false negatives) values were similar, and the *F1 score* (a weighted average of precision and recall) was high. Once this ideal threshold was chosen, it was used to filter out lower confidence results and create the final output.

### **Tree Height Calculation and Comparison to Environmental Variables**

The final results of the deep learning model, a polygon feature class indicating all 2023 longleaf pine locations, were overlaid with the 2023 SfM-derived CHM to obtain height values for all identified trees. Since it was known that this CHM dataset tended to underestimate true tree height, the height values were adjusted using the formula from a simple linear regression model that compared SfM height estimates to ground truth heights measured in the 50 x 50-m sample plot.

After the height calculation was complete, it became the dependent variable in a multiple regression model that assessed how six environmental variables correlated with longleaf pine height. The six independent variables used in the model were (1) elevation, (2) slope, (3) Topographic Wetness Index (TWI), (4) site preparation method (i.e., whether or not residual debris was cleared before planting seedlings), (5) distance from the edge of the planting area, and (6) mean solar radiation.

Topographic wetness for a given point can be expressed as  $TWI = \ln(a / (\tan(\beta)))$ , where  $a$  represents the local upslope catchment area and  $\beta$  represents slope measured in radians (Beven & Kirkby, 1979), though the exact method to calculate this formula varies as there are multiple algorithms available. The TWI calculation for this study area used a DEM created in lidR from the 2023 LiDAR point cloud (Appendix A). Small topographic sinks (< 0.75 m deep) were filled to smooth the DEM prior to calculating TWI, and upslope catchment area  $a$  was calculated using the D-INF (D-Infinity) algorithm in ArcGIS Pro.

The solar radiation values used were an estimate of average solar radiation measured in kWh/m<sup>2</sup>/yr. These values were calculated by applying the digital surface models (DSMs) from the 2016 through 2019 UAS flights to the Area Solar Radiation tool in ArcGIS Pro; this

attempts to estimate the relative amount of sunlight individual longleaf pines received during the first few years of their lives.

Finally, in addition to the longleaf pine height regression model, a second regression model was employed to compare the six environmental variables to tree survival. Local longleaf pine survival was determined at 3,369 random points throughout the field (a sample size of 3,369 was chosen to match the sample size of the longleaf pine height data set). Local survival percentages were calculated by comparing 2023 tree totals to 2016 tree totals within a 10-meter radius surrounding each point; the locations of longleaf pines in 2016 are estimates based on a total of 9,800 seedlings being originally planted in rows and spaced equidistant throughout the field. This longleaf pine survival data was compared to the six environmental variables via multiple regression in the same manner as the longleaf pine height data.

## CHAPTER 4

### RESULTS & DISCUSSION

#### **Effects of UAS Flight Parameters on SfM Accuracy**

For each of the five UAS flights of the 50 x 50-m plot, tree heights calculated by the SfM process were compared to 36 tree heights measured on the ground with a telescopic measuring pole. All five flights yielded tree height estimates with a high degree of correlation with the ground truth data ( $R^2$  values between 0.92 and 0.94). However, the differences in drone flight parameters caused differing magnitudes of error for each of the five datasets; the flight conducted at 120 m was the least accurate (RMSE = 0.881 m), and the flight conducted at 60 m was the most accurate (RMSE = 0.589 m). Full accuracy metrics are shown in Table 1; the differences in accuracy for different flights are also displayed graphically in Figures 23 and 24.

*Table 1. SfM tree height errors for the five UAS flights of the 50 x 50-m sample plot. RMSE values are in meters.*

Flight Height (m)	Overlap	Sidelap	$R^2$	RMSE	MAPE
40	80%	80%	0.928	0.753	14.94%
60	95%	80%	0.935	0.589	11.42%
80	95%	80%	0.944	0.719	14.51%
100	95%	80%	0.921	0.782	15.58%
120	95%	80%	0.937	0.881	18.08%

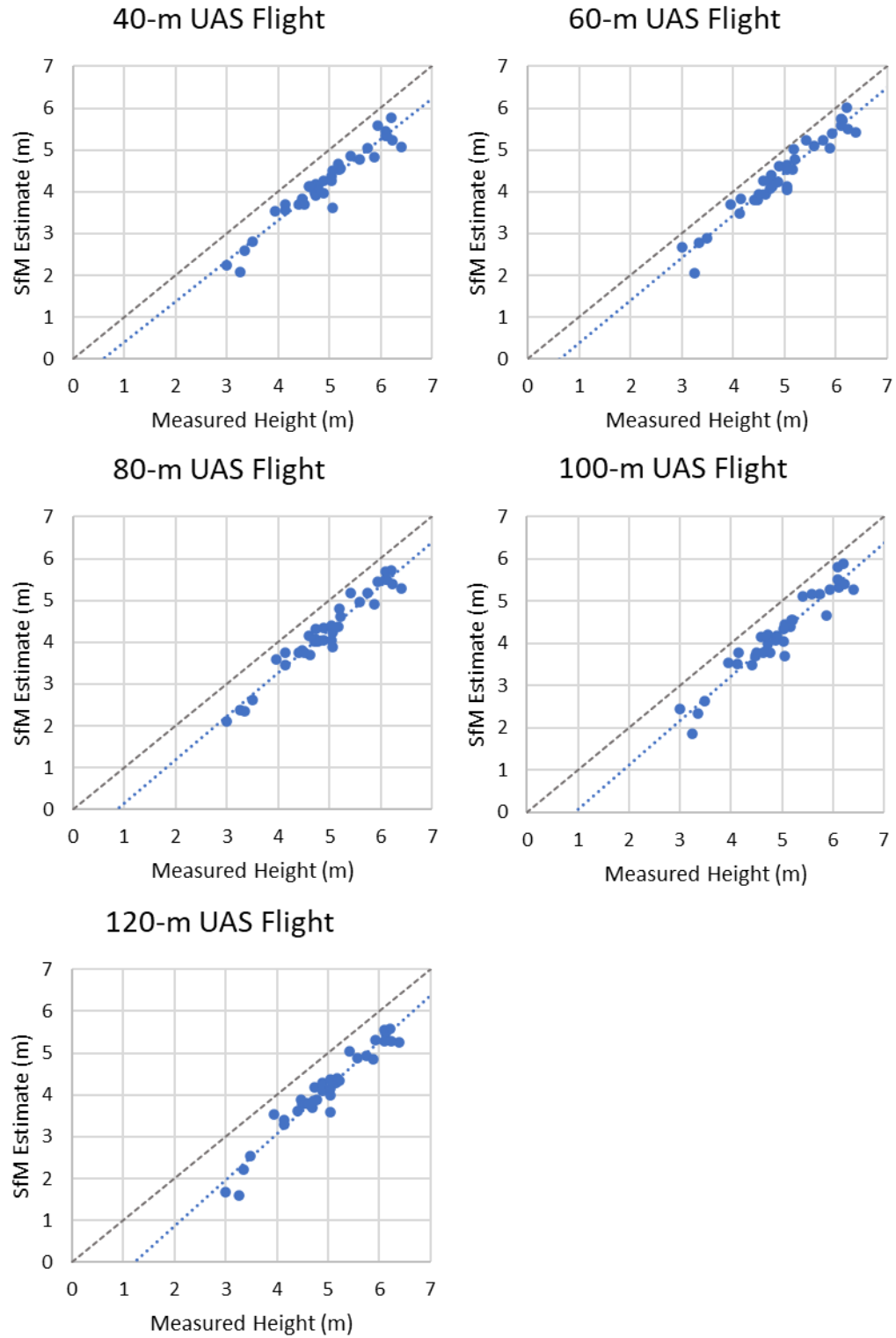


Figure 23. Field-measured tree heights plotted against SfM-measured tree heights for the five UAS flights of the sample plot.

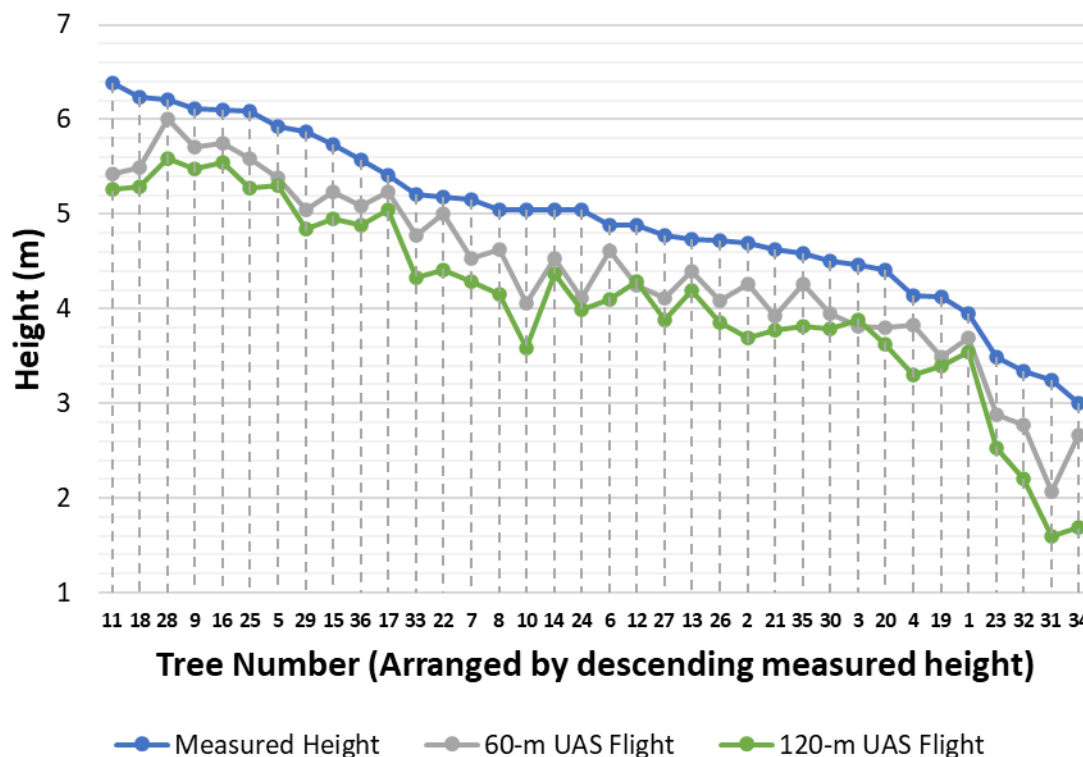


Figure 24. Comparing SfM tree height accuracy for the 60-m UAS flight and the 120-m flight.

These five flights were intended to help determine the best flight parameters for a subsequent data collection when SfM would be compared to LiDAR. While they were intended to primarily quantify the effect of flight height on SfM accuracy, along-track photo overlap ended up being tested as well due to an unusual UAS malfunction: four of the five flights had 95% overlap despite the overlap parameter being set to 80% in the Map Pilot flight planning app.

The inadvertent use of a different photo overlap parameter for the 40-m flight (which correctly used 80% instead of 95%), seemed to create a noticeable increase in tree height error. In fact, the RMSE data in Table 1 suggests that the effect of the 15% overlap decrease was similar to if the flight's height had been changed from 40 m to approximately 90 m. It is impossible to say from this single data point that the increase in error from a 15% overlap

decrease truly equates to that from a 50-m height increase, but it is nevertheless surprising that the change in overlap had such a large effect on RMSE. Of course, other unidentified factors may have influenced this result as well – after all, the 40-m flight was the only one of the five that was flown on a different day, at a different time of day, and with a UAV that operated as expected. Making more definitive conclusions about the flight overlap parameter's effect on height estimates for young longleaf pines would probably require additional data, such as collecting photos at three or more unique overlap settings while all other parameters are held constant.

### ***Comparisons to Similar Studies***

These results (namely, that RMSE increases when flight height increases and decreases when overlap increases) may seem straightforward, but they do not necessarily agree with the findings of other studies. With regards to overlap, a study by Goodbody et al. (2021) at a mixed forest site in southeastern Quebec, Canada, found that above 60%, further overlap and sidelap increases did not consistently improve canopy height accuracy. While they collected their data with manned aircraft rather than UAS, UAS-SfM studies have seen similar results. For instance, Ni et al. (2018), who tested UAS-SfM parameters at a boreal (coniferous) forest in northern China, found that overlaps from 90% down to 70% all yielded similar results; it was not until 60% that  $R^2$  decreased significantly (from 0.9 to 0.8) and RMSE increased significantly (from 1.2 m to 1.8 m).

With regards to flight height, it has been noted that the overall vertical accuracy of UAS-SfM models consistently decreases as height above ground level increases (Deliry & Avdan, 2021). Yet when it comes to looking specifically at tree height accuracy, this has often not been the case. Swayze et al. (2021) conducted UAS flights at an experimental forest in Colorado dominated by ponderosa pine (*Pinus ponderosa*) to examine how multiple forest

structure metrics, including tree height accuracy, changed across three flight heights (65, 90, and 115 m). Their linear regression analysis assessing the relationship between flight height and tree height RMSE was not statistically significant.

The results of studies like Swayze et al. (2021) and Ni et al. (2018) seem somewhat contradictory to the results shown in Table 1 and Figures 23-24, but one possible explanation for the discrepancy could be tree size. The trees in these studies were much taller on average than those in the Wormsloe study area, and Goodbody et al. (2021) reported that lower canopy height values were more strongly impacted by changes to photo overlap and spatial resolution. In other words, height estimates of taller objects (i.e., mature trees in the aforementioned studies) may be less responsive to changes in flight parameters than shorter objects like young longleaf pines.

### **Comparison of SfM and LiDAR-Derived Tree Heights**

For the LiDAR dataset and the most recent SfM dataset (both collected on the same day in February 2023), the tree heights in their respective CHMs were compared to ground-measured heights of the same 36 trees that previously provided ground truth data in 2022. Heights from a third CHM created by combining the SfM and LiDAR data were also compared to the ground truth data. Each of the three techniques yielded very high correlations with the ground-measured tree heights ( $R^2 > 0.97$ ). However, LiDAR (RMSE = 0.148 m) outperformed SfM (RMSE = 0.274 m) in terms of accuracy, while the results of the combined dataset were nearly identical to that of the LiDAR dataset. All three methods tended to underestimate height, though they did so to differing extents. The full accuracy metrics are shown in Table 2; differences in accuracy between the techniques are also displayed graphically in Figures 25 and 26.



Table 2. 2023 tree height errors for SfM, LiDAR, and the combined SfM-LiDAR dataset. RMSE values are in meters.

Technique	R <sup>2</sup>	RMSE	MAPE
SfM	0.983	0.274	5.04%
LiDAR	0.973	0.148	2.18%
Combined	0.975	0.141	1.97%

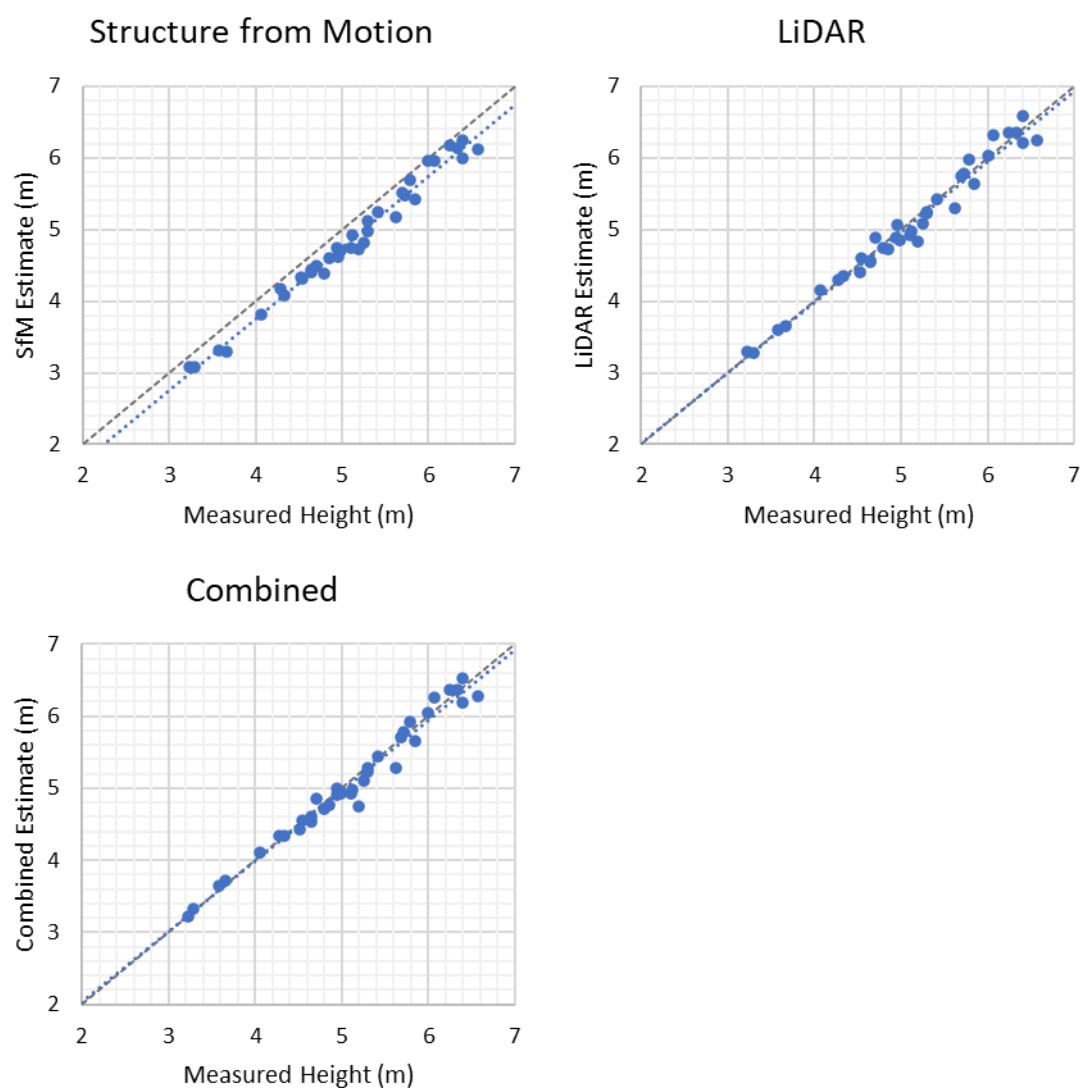


Figure 25. Field-measured tree heights plotted against tree height estimates for each UAS-based technique.

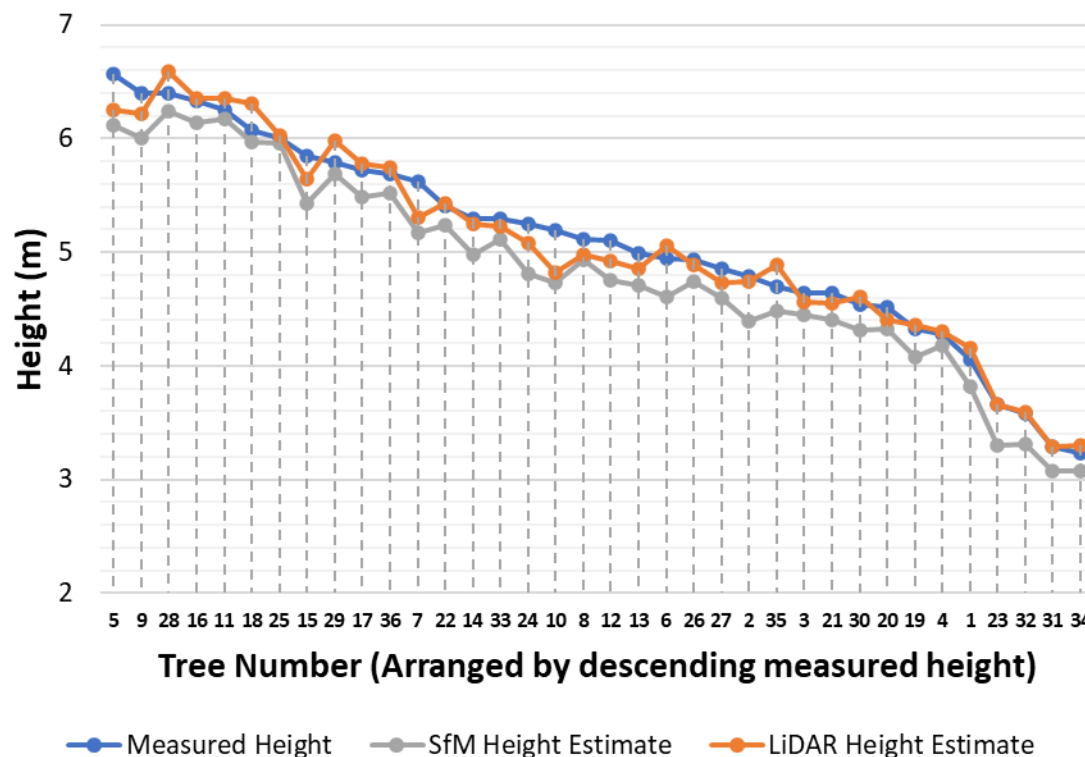


Figure 26. Comparing the accuracy of tree height measurements using SfM versus LiDAR.

Interestingly, there was a notable increase in tree height accuracy for SfM when compared to all five of the flights that were conducted in September 2022. The flight with the best results from the earlier data collection, the 60-m flight, had an  $R^2$  of 0.94 and an RMSE of 0.589 m, compared to an  $R^2$  of 0.98 and an RMSE of 0.274 m for this latest flight. There were no significant changes in the methods for data collection or processing between the two field missions, so it is likely that the improvement in accuracy is simply a result of site conditions. The earlier flights occurred in September, when vegetation in the field is at its thickest, covering up the ground and reducing the accuracy of SfM-based DTMs that are needed to measure canopy height. Conversely, the 2023 flight occurred in February and shortly after a prescribed burn (Figure 27). Both the winter conditions and the recent burn thinned much of the ground-level vegetation in the study area, improving SfM results.



*Figure 27. Aerial views of vegetation density in the 50 x 50-m plot in September 2022 (left) versus February 2023 (right).*

Though the SfM results improved as a result of the leaf-off field conditions and recent prescribed burn, LiDAR still outperformed SfM on average. In many instances, LiDAR underestimated tree height but to a smaller degree than SfM. However, some of the LiDAR results were actually overestimates compared to the ground truth data (see Figure 26). One possible reason for this could be that the noise reduction process in CloudCompare that cleaned the LiDAR point cloud was not aggressive enough to remove all noise points from above the trees, thus artificially inflating their heights. Other factors such as errors in ground truth measurement or point cloud registration could have contributed as well.

As for the third technique, the combined SfM-LiDAR method, height accuracy for most trees was very similar to the accuracy of the LiDAR data by itself. Creating a CHM from the combined dataset also necessitated more data wrangling, since the two point clouds were not well-aligned with each other in the z-direction. In short, it was a more time-consuming and challenging workflow than dealing with either method by itself, and since it

did not yield substantially different results, there seems to be little reason to continue exploring it, at least as it relates to the goals of this research.

### ***Comparisons to Similar Studies***

These SfM-LiDAR comparison results are generally comparable to other studies. For example, Gyawali et al. (2022) assessed both methods at a young mixed forest site in southeast Finland with average heights of 10-15 m; though the study area contained mixed forest, results were provided separately for different species. For Scots pine (*Pinus sylvestris*), the site species most similar morphologically to longleaf pine, LiDAR ( $R^2 = 0.86$ , RMSE = 1.44 m) yielded more accurate heights than SfM ( $R^2 = 0.71$ , RMSE = 2.13 m). This study saw a weaker correlation with field measurements and higher RMSE compared to the results from the Wormsloe study area, but this was probably at least partially due to the field measurements at the Finland site not being obtained until well after the UAS data were collected. Hartley et al. (2020) compared UAS-based SfM and LiDAR at a young plantation forest of Monterey pine (*Pinus radiata*) on the North Island of New Zealand; these trees had a smaller average height of just 2.6 m. The  $R^2$  and RMSE values of this study (LiDAR:  $R^2 = 0.99$ , RMSE = 0.15 m; SfM:  $R^2 = 0.94$ , RMSE = 0.48 m) were fairly similar to the results seen in Table 2. However, a comparison of the differences in RMSE between the two techniques shows that LiDAR's accuracy advantage over SfM was markedly greater for the New Zealand study than for the Wormsloe data.

Though there are certainly differences between the results of these two studies and the results from the longleaf pine field, they all share a couple of trends: LiDAR outperformed SfM for tree height measurements, and both methods tended to underestimate when compared to ground truth data. Still, it is worth reiterating that even though a majority of studies may have found similar results, there is a minority of studies whose results differ

(e.g., Wu et al., 2020); furthermore, among the studies that have seen LiDAR outperform SfM, the difference in accuracy is often slight and may not be enough to justify the additional logistical and financial challenges that tend to accompany LiDAR data collection. So, while the SfM-LiDAR comparison presented here is highly relevant for the specific study area and workflow used to conduct it, its results should not be interpreted as a broadly applicable consensus on the better method.

### **Assessment of Deep Learning Results**

With the early stopping parameter enabled, model training finished after 35 epochs. After training completion, ArcGIS Pro output a model metrics summary for assessing how well the model had learned from the training data; this included the generation of a learning curve graph (Figure 28). A learning curve that demonstrates a well-fitted model typically has loss values that gradually decrease to a point of stability and similar final values for training and validation loss, though it is normal for training dataset loss to be slightly lower than validation dataset loss. The graph output by ArcGIS Pro contained these characteristics.

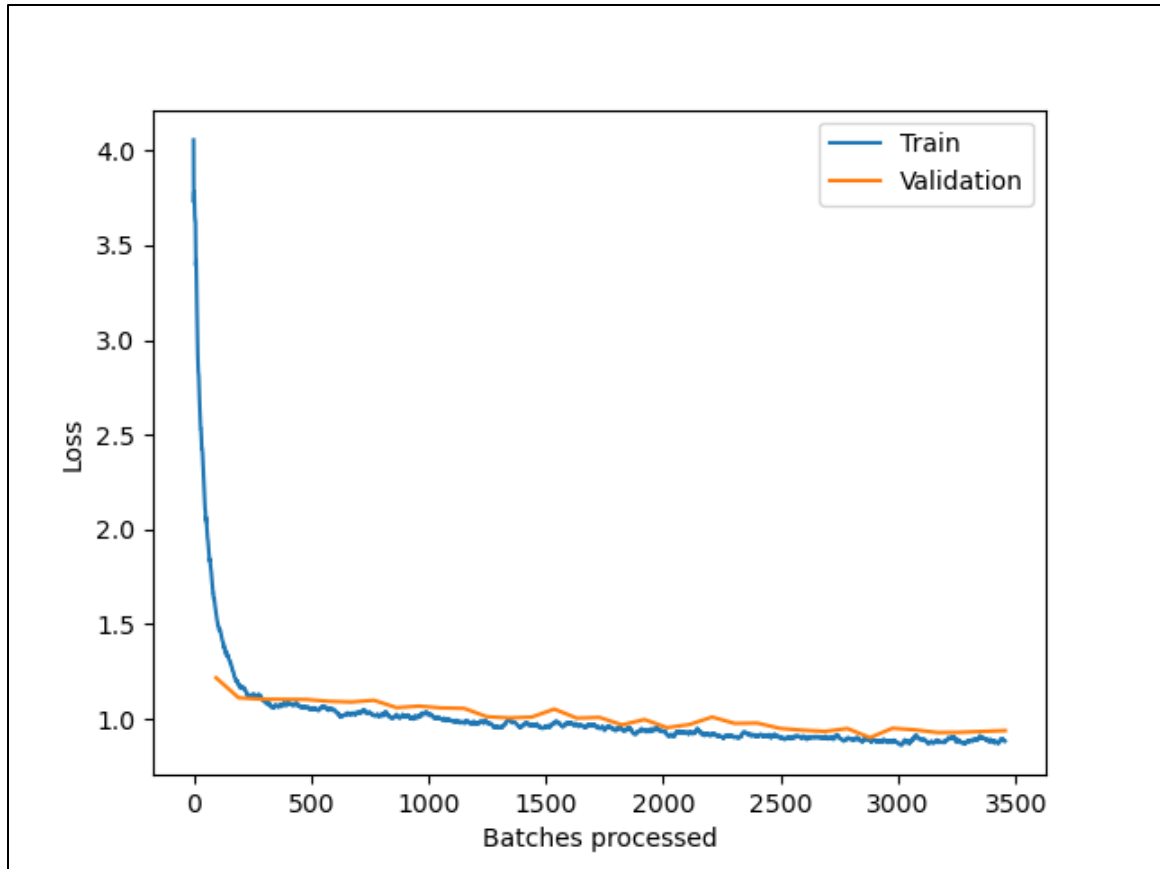


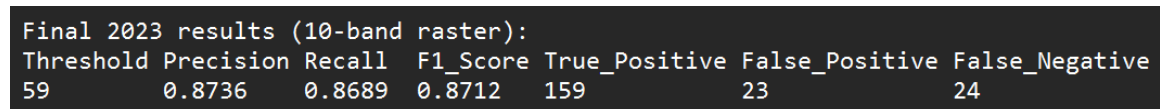
Figure 28. Final learning curve results for the deep learning model.

The trained model identified longleaf pines in the 10-band raster dataset. After running the model, but prior to calculating any accuracy metrics from its results, the following post-processing steps were carried out:

- 1) The initial confidence threshold was set to 20%. Objects detected with less than 20% confidence were therefore excluded.
- 2) Non-Maximum Suppression (NMS): For detected objects that overlapped significantly with each other (i.e., having an IoU threshold of 15% or greater), NMS removed the object(s) with lower confidence values to eliminate duplicate detections.
- 3) Artefacts (i.e., polygons with a zero or near-zero area) were deleted.

- 4) A small number of objects whose corresponding canopy height values classified them as statistical outliers were removed.

After refining the model's raw output over these four steps, a comparison of model results to the testing dataset (using an IoU threshold of 50%) yielded an average precision (AP) of 0.8547. The final step was to raise the 20% confidence threshold; a threshold of 59% achieved a balance between the rates of occurrence for false positives and false negatives and resulted in accuracy metrics with values around 0.87 (Figure 29).

A screenshot of a terminal window showing model accuracy metrics. The text is as follows:

```
Final 2023 results (10-band raster):
Threshold Precision Recall F1_Score True_Positive False_Positive False_Negative
59          0.8736    0.8689  0.8712    159             23             24
```

Threshold	Precision	Recall	F1_Score	True_Positive	False_Positive	False_Negative
59	0.8736	0.8689	0.8712	159	23	24

*Figure 29. Screenshot showing model accuracy metrics using the chosen confidence threshold of 59% and an IoU threshold of 50%.*



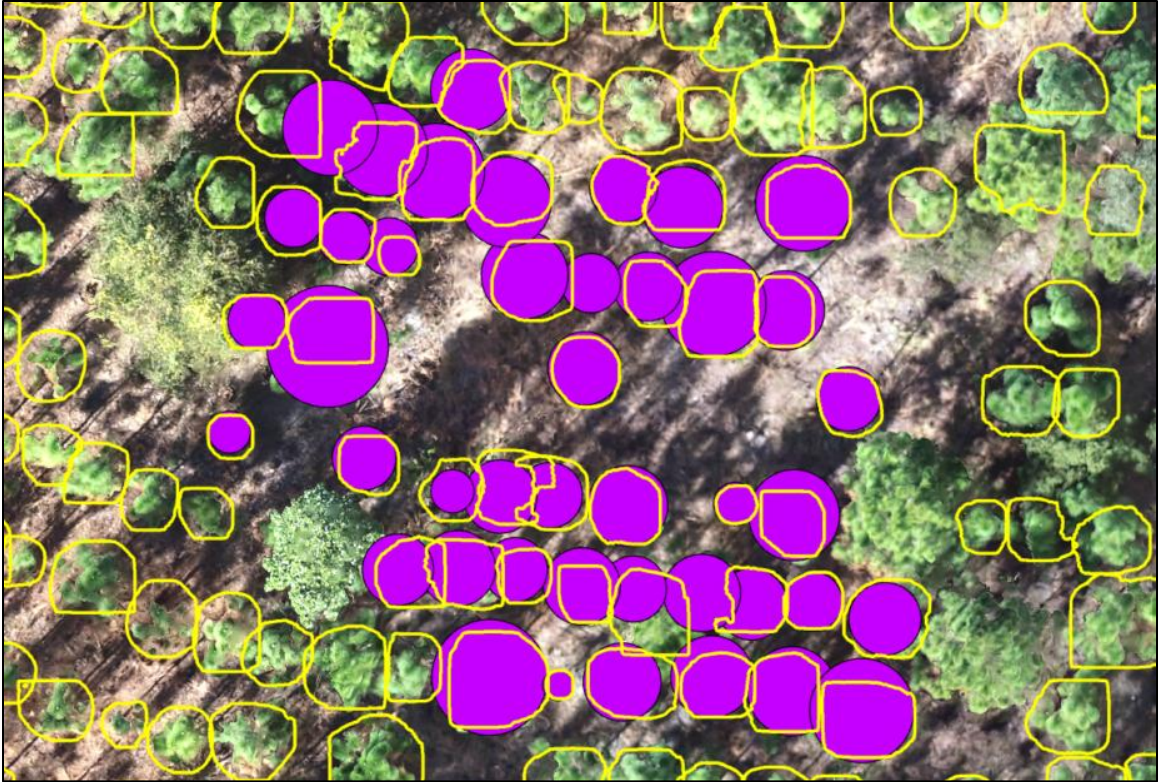


*Figure 30. Visualizing accuracy by comparing model results (yellow polygons) to annotated data from a testing zone (purple circles).*

Visual inspection of model results seems to validate the reported metrics and indicates that the trained model did a rather good, if not perfect, job at identifying longleaf pines and distinguishing them from other trees. In Figure 30, all but a couple of the data annotations (purple circles) are paired with yellow polygons, indicating a true positive match. Likewise, much of the non-longleaf pine vegetation in the image (e.g., the two trees with large canopies in the bottom-right) was correctly passed over by the model.

The inclusion of four additional raster bands representing data from earlier years absolutely had a positive effect on model accuracy. The first iteration of deep learning for the 2023 imagery only used six bands of raster data as opposed to ten, and its accuracy was lower than expected, likely due to the overlapping of tree canopies as well as slight blurring



in parts of the orthomosaic. There was no easy workaround for the blurring, but the four extra raster bands (the 2021 CHM plus the 2021, 2019, and 2017 smoothed greenness index layers) improved the model's ability to correctly segment trees with overlapping canopies. As a result, the F1 score increased from 0.78 to 0.87 (though it should also be noted that a few of the testing zone locations in the field were shifted between model iterations, which could have had a slight impact on the change in F1 score as well).

The accuracy metrics are generally comparable to other recent studies that have used Mask R-CNN and Faster R-CNN to detect trees in forest imagery (e.g., Beloiu et al., 2023: average F1 score = 0.76; Dersch et al., 2023: F1 scores = 0.83-0.92; Zhang et al., 2022: F1 scores = 0.77-0.92). However, since the raster dataset used to train this model was rather unusual, and the number of data points used for model training was much smaller than typical ( $n = 533$ ), making direct comparisons to other studies may be of limited usefulness.

For many study areas, the inclusion of additional high-resolution UAS data from earlier years to improve model performance would probably be impossible because that data would not exist in the first place. However, other more attainable types of data might be used in their place to similar effect. For instance, creating a point density raster(s) from a LAS point cloud would probably be helpful in highlighting tree trunk locations and could be an alternative way to aid the segmentation process in denser forest canopies.

Even though it would probably be impractical to replicate the deep learning portion of this study elsewhere given the unique combination of raster data and other unusual techniques that were used to implement it, the results are useful for demonstrating the potential value of incorporating unorthodox data sources into deep learning model training processes. As was the case here, taking such steps may in fact be the only way to achieve

higher accuracy if the standard data (i.e., RGB imagery or other spectral data) available for annotation is limited in quality or quantity.

### **2023 Tree Distribution and Height Estimates for the Full Study Area**

The deep learning model produced a polygon feature class of 3,369 longleaf pine tree crowns whose spatial distribution across the study area is shown in Figure 31. Within each tree crown polygon, the maximum canopy height value was extracted (the model used for this was a 2023 SfM-based CHM that had been corrected based on ground truth data). The resulting distribution of heights is presented in Figure 32.

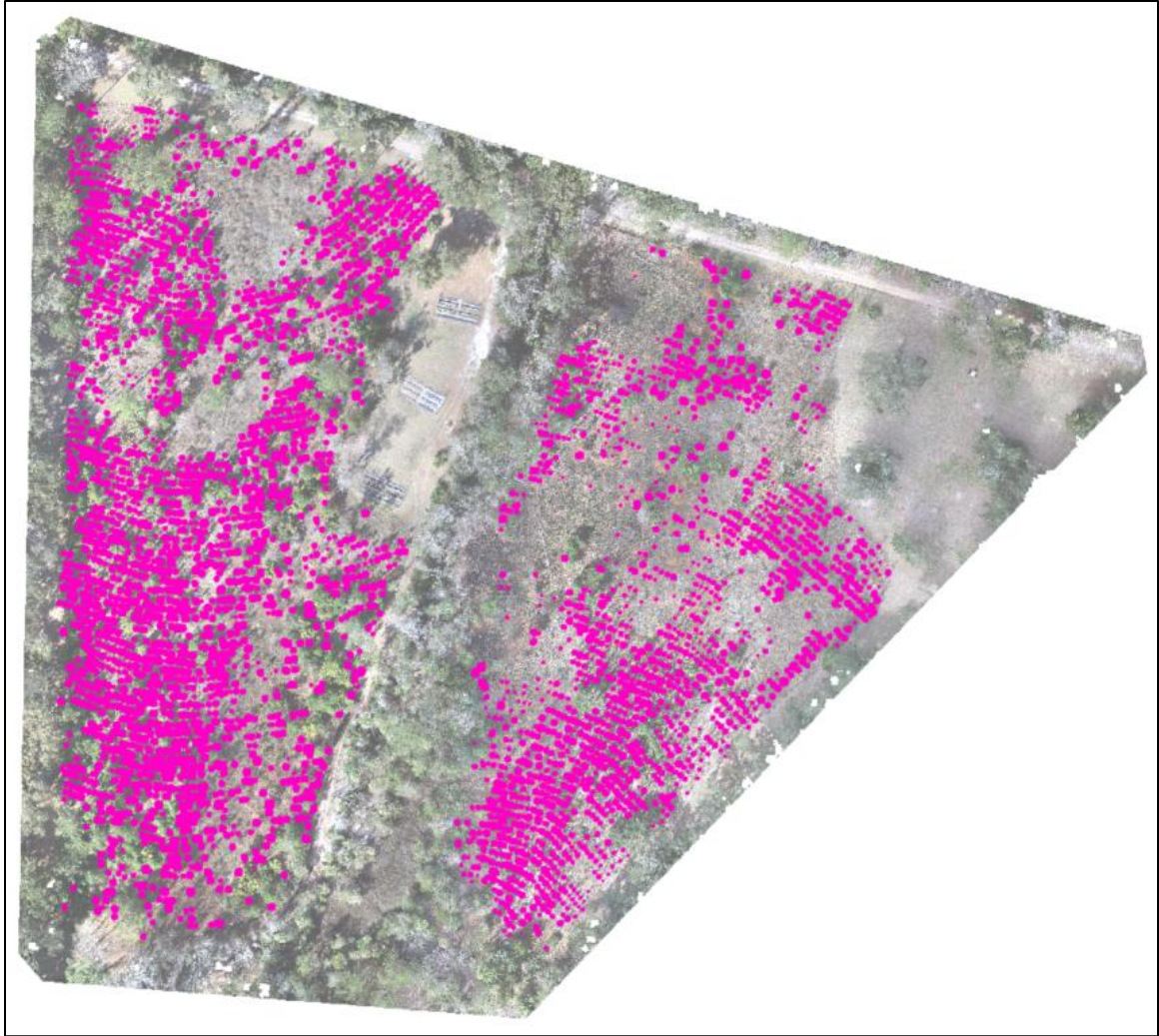


*Figure 31. Final results showing the spatial distribution of 3,369 objects (pink dots) that the deep learning model identified as longleaf pines as of February 2023.*

As previously discussed, there are certainly a number of false positives and false negatives within this dataset, as would be the case for the output of any model whose precision and recall metrics are less than 100%. Yet on the whole it provides an accurate and useful summary of longleaf pine distribution in the study area. There are a few obvious spatial patterns: areas with higher and lower densities of longleaf pine as well as a few empty patches where no surviving pines remain (the initial density in 2016 was virtually uniform throughout the field). In some instances the reasons for these patterns are easily identifiable.

For example, the general lower density through the middle of the study area (alongside the old irrigation ditch and strip of mature forest that splits the field into two halves) appears to largely be the result of the lower elevations in that area. In other locations, however, the reasons for the variation in density are not readily obvious, though variables including elevation, soil saturation, and solar radiation levels all likely play a role. A non-comprehensive set of six variables that are potentially affecting the distribution of longleaf pines is explored in more detail during the discussion of linear regression results in the subsequent section.

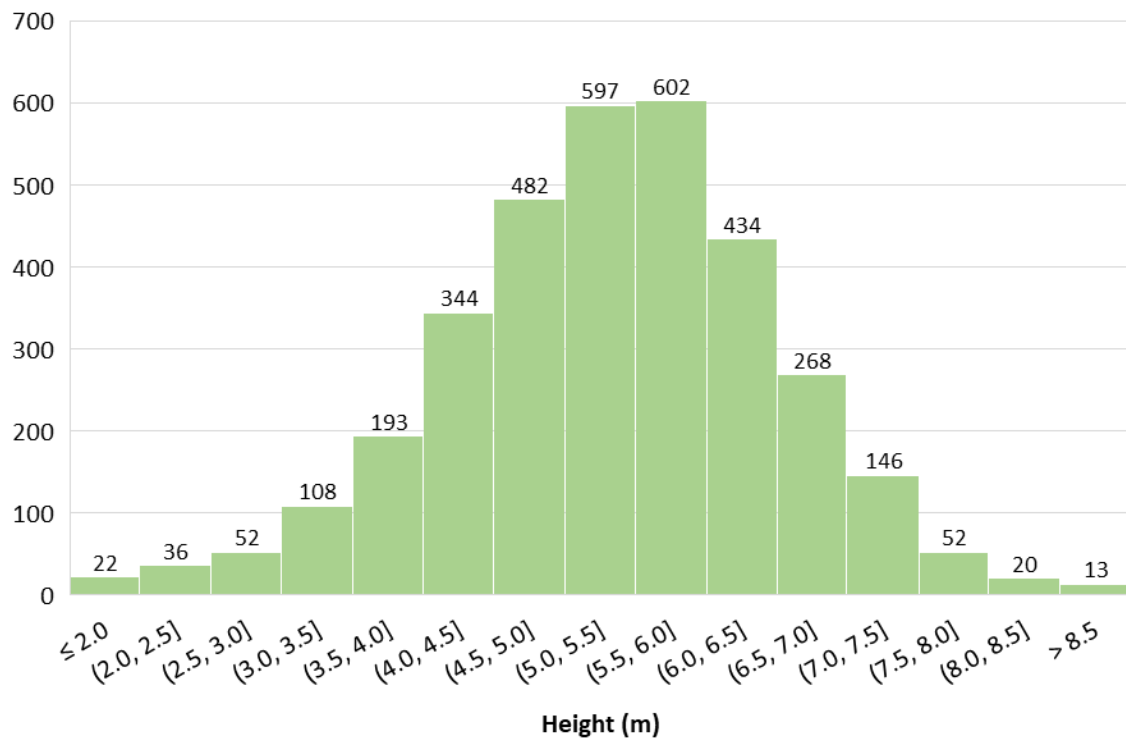


*Figure 32. Approximate distribution of longleaf pine heights in the study area in February 2023. The median height is 5.37 m.*

The distribution of tree heights for the entire field generally matches the distribution of heights from the ground truth data collected in the 50 x 50-m sample plot, though some

extreme values are present. Some of these extreme values are false positives detected by the deep learning model; in other words, they are not actually longleaf pines. However, many of the highest and lowest observed heights do correspond with longleaf pines. The lowest values ( $< 1$  m in some instances) may indicate pines that have spent a longer time in the initial grass stage of their lives before beginning to grow upwards due to less favorable growing conditions. Conversely, some of the highest values presumably correspond to pines that have had the best growing conditions – a few of the tallest trees in the southwest portion of the study area are over 8 m tall.

A few of the highest values can also be attributed to errors caused by the adjacency of other trees to longleaf pines. This was a limitation of the data collection and processing methodology: it was difficult to get accurate data for longleaf pines growing close to taller, more mature trees. Many of these trees, both hardwoods and pines, have been growing in and around the field since well before 2016 and are tens of meters tall. Their canopies overhang nearby longleaf pines, often resulting in inaccurate height values from the CHM, or in some cases completely obscuring longleaf pines from aerial view.

### **Relationships Between Environmental Conditions and Observed Heights and Survival**

Multiple linear regression was used to test for correlations between six environmental variables and 2023 longleaf pine height. The overall regression model was statistically significant ( $R^2 = 0.10$ ,  $F(6, 3362) = 62.3$ ,  $p < 0.01$ ). Of the six variables included in the model, four significantly predicted tree height: elevation ( $p = 0.04$ ), slope ( $p < 0.01$ ), presence of residual debris during planting ( $p < 0.01$ ), and mean solar radiation ( $p < 0.01$ ). Two variables did not significantly predict tree height: topographic wetness ( $p = 0.24$ ) and distance from the edge of the planting area ( $p = 0.59$ ). Of the four significant variables, higher elevations and

solar radiation levels correlated with an increase in tree height, while higher slopes and the clearance of residual debris correlated with a decrease in tree height.

Multiple linear regression was also used to test for correlations between these six environmental variables and longleaf pine local survival as of 2023. This model was also statistically significant ( $R^2 = 0.35$ ,  $F(6, 3362) = 300.9$ ,  $p < 0.01$ ). All six of the variables in the model were significant predictors of local survival: elevation ( $p < 0.01$ ), slope ( $p < 0.01$ ), topographic wetness ( $p < 0.01$ ), presence of residual debris during planting ( $p < 0.01$ ), distance from the edge of the planting area ( $p < 0.01$ ), and mean solar radiation ( $p < 0.01$ ). Increases for three of the variables (elevation, clearance of residual debris, and mean solar radiation) correlated with an increase in local survival, while for the other three variables (slope, topographic wetness, and distance from the edge of the planting area), increases in their magnitude were correlated with a decrease in local survival.

The full results for both models are presented in Table 3 and Table 4; additional details, including a more intuitive interpretation of variable slope estimates and estimated  $R^2$  contributions for individual variables, are shown in Tables 5 and 6. Finally, scatterplots showing each variable's individual relationship with longleaf pine height and survival can be found in Appendix B.

Table 3. Longleaf pine height regression model results (Model 1).

**MODEL INFO:**

Observations = 3369

Dependent Variable = Longleaf Pine Height

Type = OLS Linear Regression

**MODEL FIT:**

F(6, 3362) = 62.303, p = 0.000

 $R^2 = 0.100$ Adjusted  $R^2 = 0.099$ 

Residual Std. Error = 1.125

**Residuals:**

Min	1Q	Median	3Q	Max
-5.035	-0.718	0.017	0.730	4.466

	Estimate	Standard Error (OLS)	Lower 95% CI	Upper 95% CI	t-statistic	p-value	VIF
(Intercept)	0.981	0.319	0.357	1.606	3.081	0.002 **	
Elevation	0.104	0.049	0.007	0.201	2.108	0.035 *	1.028
Slope	-0.042	0.010	-0.061	-0.023	-4.353	0.000 ***	1.077
Topographic Wetness Index	0.009	0.008	-0.006	0.024	1.179	0.239	1.065
Site Preparation	-0.499	0.097	-0.689	-0.309	-5.149	0.000 ***	1.004
Distance from Edge of Field	-0.001	0.002	-0.004	0.002	-0.542	0.588	1.425
Mean Solar Radiation	0.003	0.000	0.003	0.004	15.125	0.000 ***	1.413

*Table 4. Longleaf pine survival regression model results (Model 2).*

**MODEL INFO:**

Observations = 3369

Dependent Variable = Local Longleaf Pine Survival

Type = OLS Linear Regression

**MODEL FIT:**

$F(6, 3362) = 300.854, p = 0.000$

$R^2 = 0.349$

Adjusted  $R^2 = 0.348$

Residual Std. Error = 0.154

**Residuals:**

Min	1Q	Median	3Q	Max
-0.476	-0.103	0.005	0.112	0.448

	Estimate	Standard Error (OLS)	Lower 95% CI	Upper 95% CI	t-statistic	p-value	VIF
(Intercept)	-0.274	0.036	-0.344	-0.205	-7.702	0.000 ***	
Elevation	0.128	0.006	0.115	0.140	20.229	0.000 ***	1.136
Slope	-0.016	0.003	-0.021	-0.010	-5.839	0.000 ***	1.112
Topographic Wetness Index	-0.023	0.001	-0.025	-0.020	-19.623	0.000 ***	1.095
Site Preparation	0.360	0.027	0.308	0.412	13.594	0.000 ***	1.015
Distance from Edge of Field	-0.002	0.000	-0.003	-0.002	-9.583	0.000 ***	1.531
Mean Solar Radiation	0.000	0.000	0.000	0.000	19.615	0.000 ***	1.474



Table 5. For both regression models, the predicted change in the value of the dependent variable based on changes in the value of each independent variable.

Model	Dependent Variable (y)	Independent Variable (x)	$\Delta x$	$\Delta y$ Estimate	Lower 95% CI	Upper 95% CI	t-statistic	p-value
1	Longleaf Pine Height	Elevation	+1 m	+0.10 m	+0.01 m	+0.20 m	2.108	0.035 *
		Slope	+10°	-0.42 m	-0.61 m	-0.23 m	-4.353	0.000 ***
		Topographic Wetness Index	+10	+0.09 m	-0.06 m	+0.24 m	1.179	0.239
		Site Preparation	Debris Cleared = Yes	-0.50 m	-0.69 m	-0.31 m	-5.149	0.000 ***
		Distance from Edge of Field	+10 m	-0.01 m	-0.04 m	+0.02 m	-0.542	0.588
		Mean Solar Radiation	+100 kWh/m <sup>2</sup> /yr	+0.31 m	+0.27 m	+0.35 m	15.125	0.000 ***
2	Local Longleaf Pine Survival	Elevation	+1 m	+12.8 %	+11.5 %	+14.0 %	20.229	0.000 ***
		Slope	+10°	-15.6 %	-20.8 %	-10.3 %	-5.839	0.000 ***
		Topographic Wetness Index	+10	-22.7 %	-24.9 %	-20.4 %	-19.623	0.000 ***
		Site Preparation	Debris Cleared = Yes	+36.0 %	+30.8 %	+41.2 %	13.594	0.000 ***
		Distance from Edge of Field	+10 m	-2.2 %	-2.6 %	-1.7 %	-9.583	0.000 ***
		Mean Solar Radiation	+100 kWh/m <sup>2</sup> /yr	+3.8 %	+3.4 %	+4.2 %	19.615	0.000 ***

*Table 6. The estimated relative weight of each independent variable used in multiple regression. Calculations were done via the Lindemann-Merenda-Gold (LMG) method using the R package relaimpo, Version 2.2-7 (Groemping, 2006).*

Model	Dependent Variable	R <sup>2</sup>	Adjusted R <sup>2</sup>	Independent Variable	Partial R <sup>2</sup> Approximation
1	Longleaf Pine Height	0.100	0.098	Elevation	0.001
		0.100	0.098	Slope	0.008
		0.100	0.098	Topographic Wetness Index	0.001
		0.100	0.098	Site Preparation	0.006
		0.100	0.098	Distance from Edge of Field	0.010
		0.100	0.098	Mean Solar Radiation	0.073
2	Local Longleaf Pine Survival	0.349	0.348	Elevation	0.117
		0.349	0.348	Slope	0.017
		0.349	0.348	Topographic Wetness Index	0.091
		0.349	0.348	Site Preparation	0.047
		0.349	0.348	Distance from Edge of Field	0.009
		0.349	0.348	Mean Solar Radiation	0.068

Both models are statistically significant, which demonstrates that there is a relationship between the six environmental conditions that were assessed and the two dependent variables, longleaf pine height and longleaf pine survival; however, the six variables are a notably better predictor of survival than height as indicated by the difference in R<sup>2</sup> values between the models.

There were also notable differences in how effectively individual variables predicted height and survival. Across the two models, ten of the twelve variables tested had a statistically significant correlation with their model's dependent variable. However, only five of those ten make what might be considered a large contribution to the overall predictive power of their respective models based on how much they contribute to overall R<sup>2</sup> (Table 6). For Model 1, the longleaf pine height model, mean solar radiation is the only variable that fits these criteria. As such, it accounts for the bulk of that model's predictive ability, estimating

a 0.31-m increase in tree height for every 100-kWh/m<sup>2</sup>/yr increase in 2016-2019 mean solar radiation. The other four variables that are statistically significant and contribute substantially to R<sup>2</sup> are all associated with Model 2, the local longleaf pine survival model. This model estimates a 12.8% increase in survival for every 1-m elevation gain, a 22.7% decrease in survival for every 10-point TWI increase, a 36.0% increase in survival when residual debris is cleared prior to seedling planting, and a 3.8% increase in survival for every 100-kWh/m<sup>2</sup>/yr increase in 2016-2019 mean solar radiation. These coefficient estimates generally align with what would be expected in accordance with basic longleaf pine ecology: longleaf pines prefer soils that are well-drained and low in organic matter, and they thrive when there is less competition with surrounding vegetation for light and nutrients (Georgia Forestry Commission, 2020). It is also worth noting that the +36% figure associated with the site preparation variable reaffirms the findings from earlier research conducted by the UGA College of Environment and Design that found in 2018 that in the six research plots, cleared areas had more pines surviving than areas left with residual debris.

In summary, the models show that mean yearly solar radiation (specifically, radiation based on site conditions during the first four years after planting) is a useful predictor of longleaf pine height; that elevation, topographic wetness (TWI), site preparation method, and mean yearly solar radiation are useful predictors of longleaf pine survival; and that the remaining variables are not very strongly correlated with height or survival. Based on these results, it seems clear that additional environmental factors not included in either model have significant effects on longleaf pine health, which is not surprising. There are a few variables that ideally would have been included in this analysis, as it is very likely that they correlate with pine health, but they were excluded due to insufficient data. These include prescribed burn frequency as well as soil characteristics (lime buffering capacity, a

fundamental property of soil, was previously found to correlate with percent survival in the six research plots).

In addition to being limited by the inability to include environmental variables for which there was no data, it is likely that both models were slightly limited by the quality of data that was put into them. The longleaf pine height data, for instance, was derived from deep learning model results with an F1 score of 0.87, meaning that some longleaf pines were erroneously left out and some non-longleaf pine trees were erroneously included; by default, these same inaccuracies would have also affected the longleaf pine survival data. Some of the independent variable datasets were undoubtedly imperfect as well. TWI, for instance, is an estimate of relative soil moisture based on the flow of water across topography, but it does not account for variability in soil characteristics or the presence of buildings, vegetation, impervious surfaces, or other landscape features that affect the way water accumulates on the landscape. The site preparation variable is limited for a very different reason: despite it being a simple binary variable not prone to calculation errors, the clearance of residual debris only took place across a very small percentage of the study area (in three of the six 20 x 20-m plots), meaning a very large quantity of “uncleared” data points were compared to a much smaller quantity of “cleared” data points. Finally, the mean solar radiation values are rather rough estimates as they were calculated using DSMs that ignore the complexity of 3D forest structure, such as the ways sunlight passes between gaps in vegetation or the way solar radiation at a point changes during leaf-on versus leaf-off conditions.

In spite of these models’ limitations, both might still be considered useful as long as certain amounts of error are acceptable. The height regression model predicted nearly two-thirds (65%) of tree heights to within 1 m of their actual height (Figure 33). Similarly, the

survival regression model predicted two-thirds (67%) of local survival rates to within 15 percentage points of the true rate, and more than four-fifths (81%) were predicted to within 20 percentage points of the true rate (Figure 34). This indicates that even though both models lack multiple variables that might have made them more robust, they do still have some predictive power in their current form.

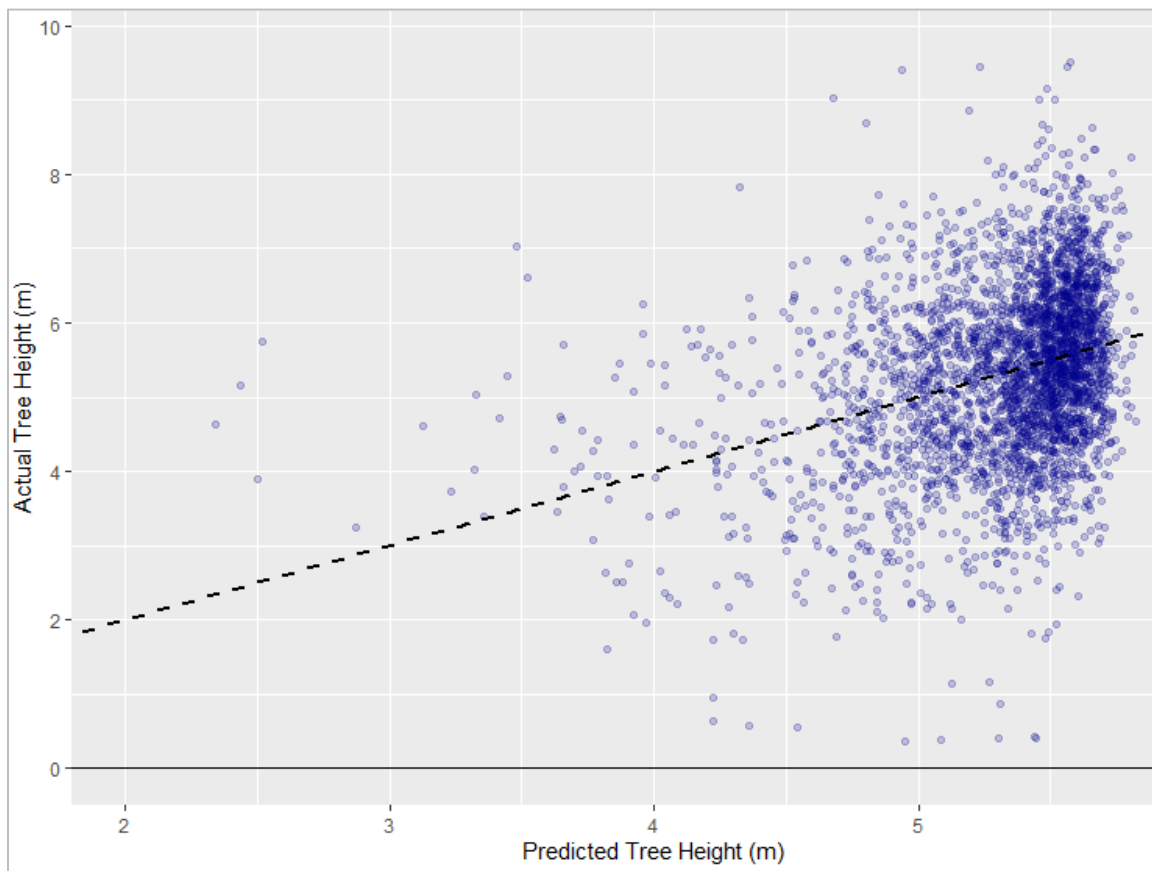


*Figure 33. Longleaf pine heights compared to heights predicted by multiple regression model 1.*

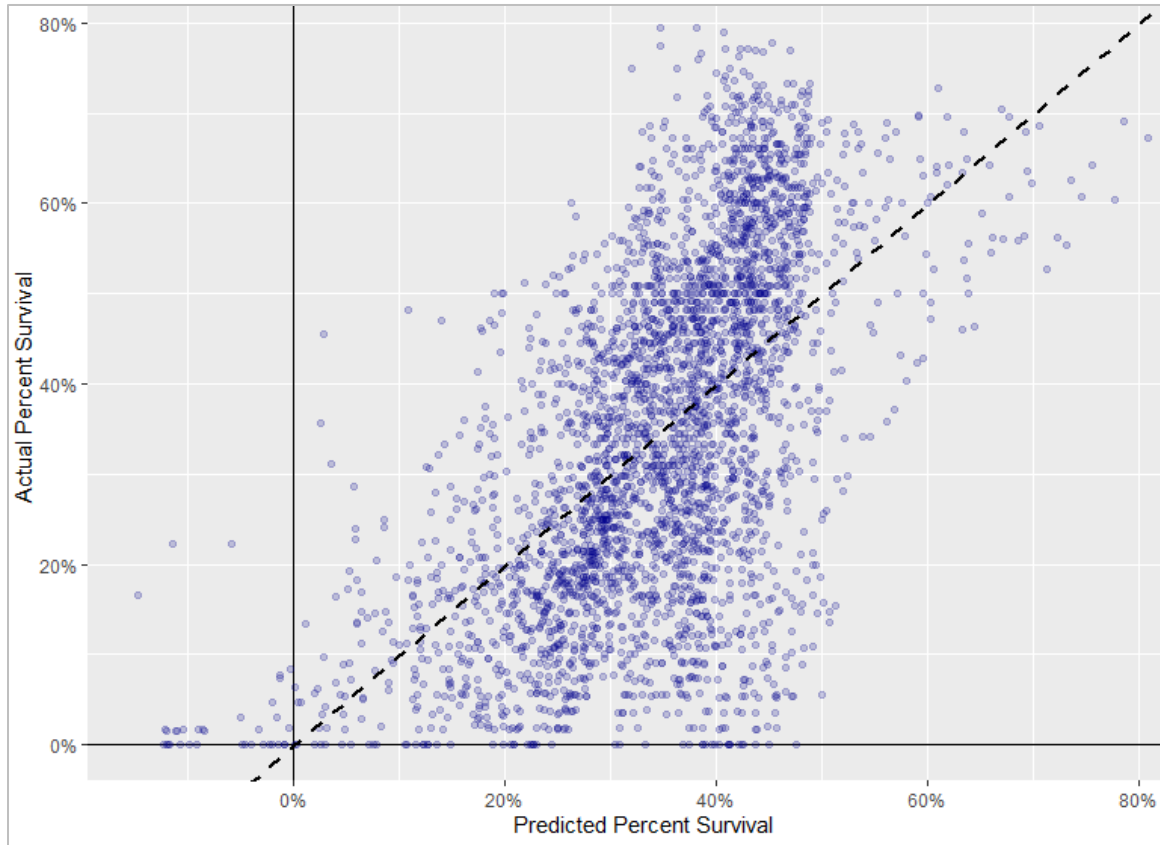


*Figure 34. Longleaf pine local survival (defined as percent survival within a 10-meter radius of each point) compared to survival values predicted by multiple regression model 2.*

### **Time Series Analysis of Tree Heights**

A total of nine sets of UAS RGB imagery of the full study area, collected between 2016 and 2023, were processed in photogrammetry software; LAS point clouds, orthomosaic images, and CHMs were created for each (Figure 35 shows an example of these outputs; orthomosaics and CHMs for all years are displayed in Appendix C). Eight of the nine datasets (the 2016 data was excluded as it was acquired just prior to the longleaf pines' planting) became part of a time series analysis that examined longleaf pine growth and spatial distribution patterns over time. The analysis focused on the six 20 x 20-m plots that were established by UGA researchers in 2016. During the period of over six years covered by the

time series, the number of surviving longleaf pines in the plots decreased from 279 to 206, while the median height increased from 0.10 m to 4.88 m (Figures 36 and 37).

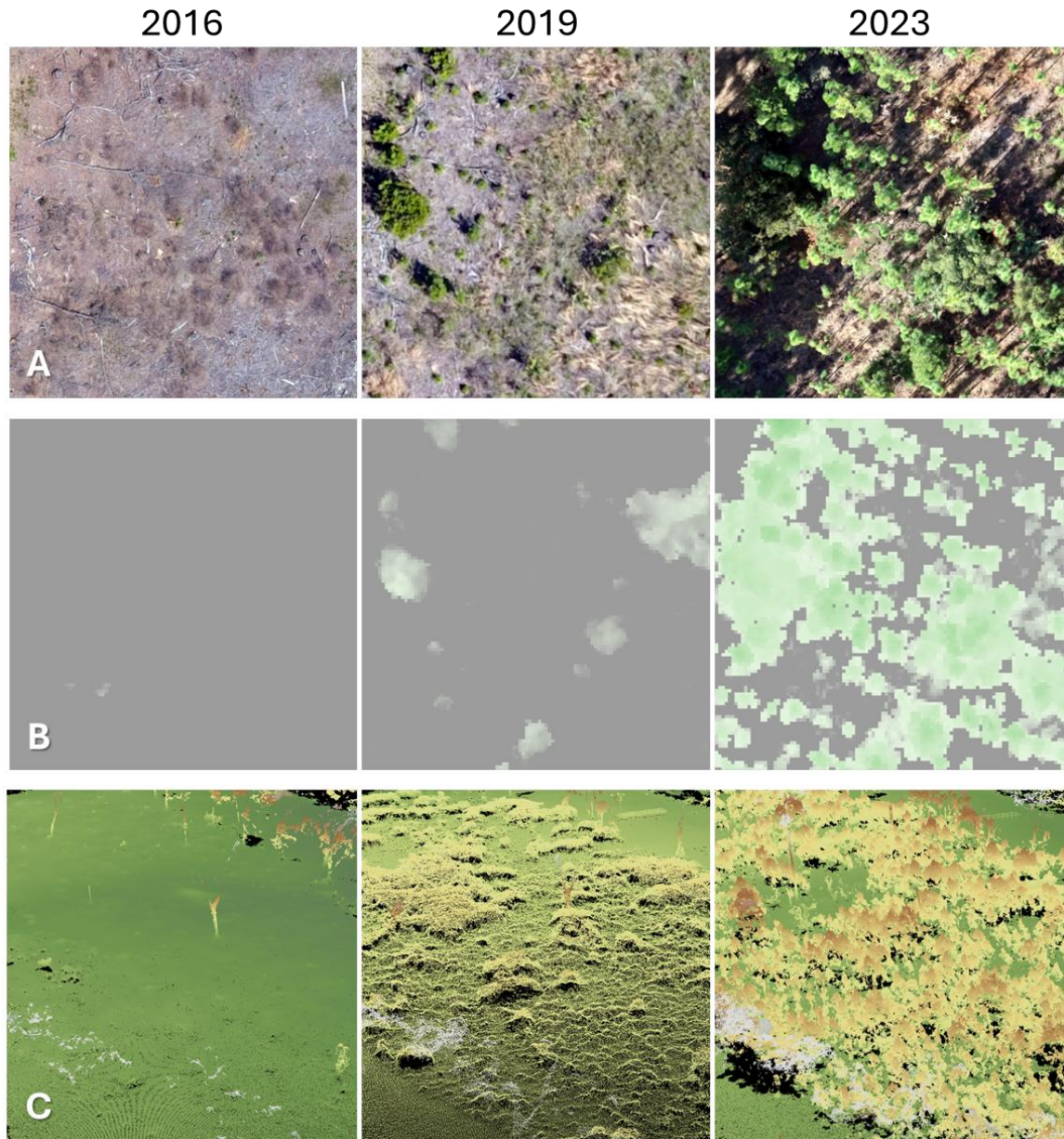


Figure 35. (A) orthomosaics, (B) CHMs, and (C) oblique LAS point cloud views showing part of the west side of the field during three different years.



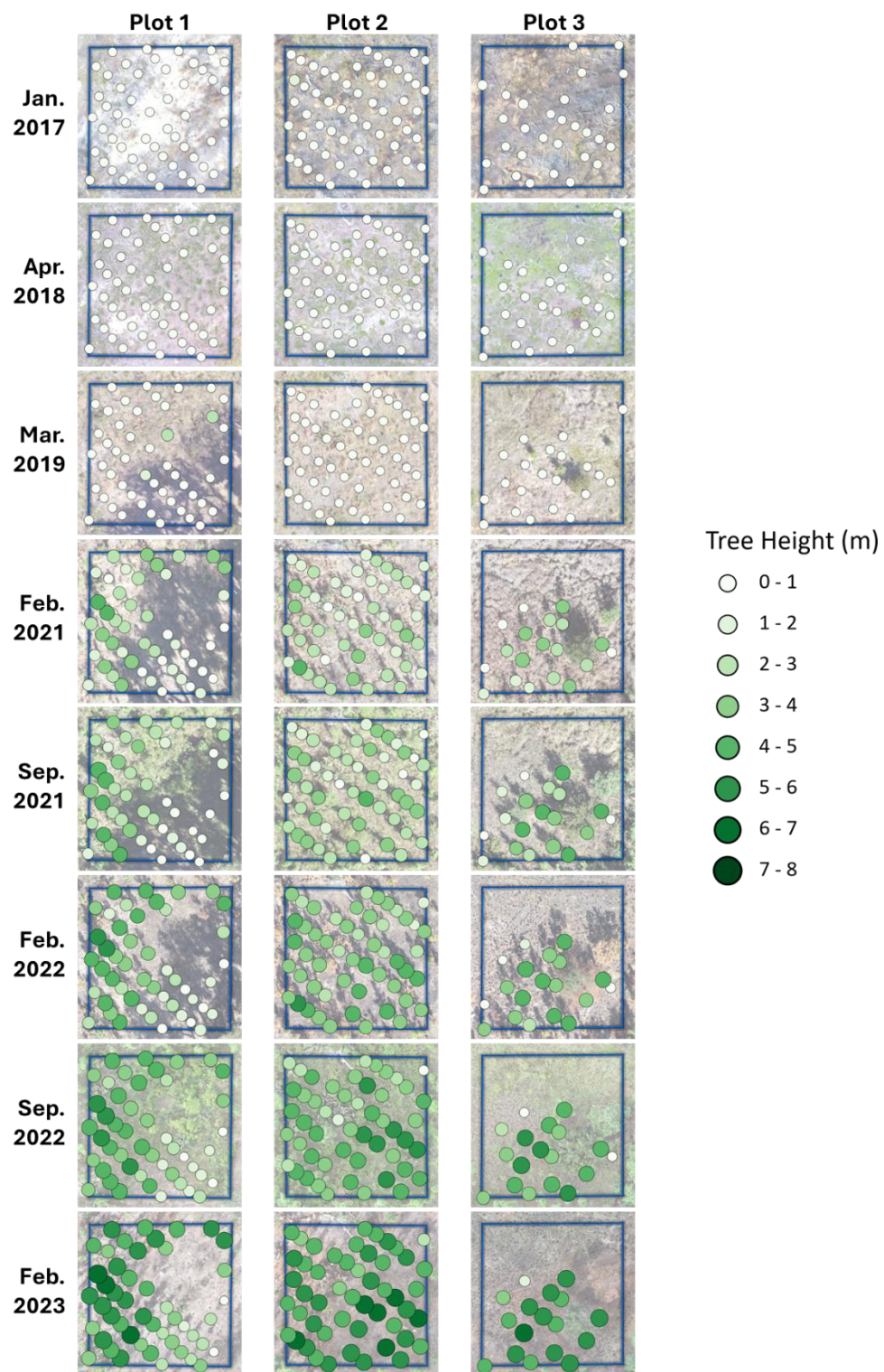


Figure 36. Longleaf pine changes over time, Plots 1-3.



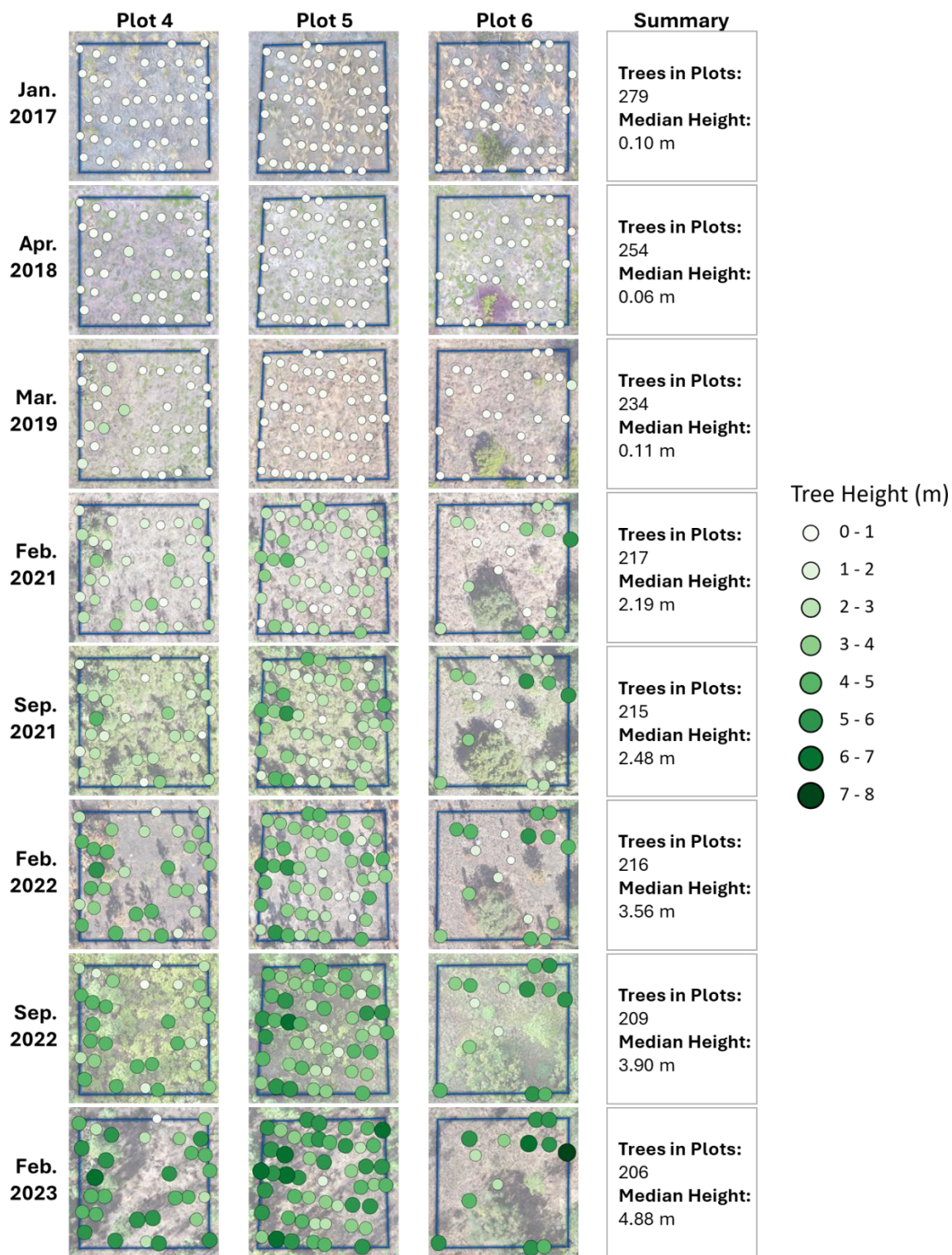


Figure 37. Longleaf pine changes over time, Plots 4-6.

It is important to note that unlike the heights used for other analyses in this report, none of the time series tree heights have been corrected or adjusted. This is because the data was collected by multiple pilots using different UAS models and a wide variety of flight parameters, and for the majority of them there is no ground truth data available, making the calculation of true height values difficult or impossible. Since the amount of error in these height estimates is so uncertain, especially for the earlier years, the results are more useful for providing an overarching view of change over time rather than an exact measure of longleaf pine heights at specific points in their lifecycle.

There are a couple of overall trends in height and survival across all six plots. 22% of the seedlings in the plots died between 2017 and 2021, but after 2021, the remaining pines had become fairly well-established, and very few have died since. As for median height, seedling heights remained virtually unchanged between 2017 and 2019. However, sometime between the March 2019 and February 2021 data collections, the majority of the pines completed the grass stage of the longleaf pine life cycle and began to quickly grow upward on their way to becoming saplings and eventually mature trees. Through the most recent data collection, steady growth has continued.

By looking at some of the plots individually, the time series can also serve as a visual companion to the results of the regression analyses. For example, the low number of remaining trees in Plot 3 is likely the result of high TWI values, as the top half of the plot lies in one of the wettest areas where longleaf pines were planted. A similar occurrence took place in Plot 6: this plot did not have TWI values as high as those found in Plot 3, but it still had some areas of high TWI and a relatively low average elevation. Conversely, Plot 2 provides an example of part of the field where all growing conditions were apparently quite good, as longleaf pine survival is close to 100% and many of the trees have grown to 5 m or

more in height; Plot 2 was also one of the plots (along with Plots 1 and 5) where residual debris clearance was tested. Finally, Plot 1 contains an example of a pattern that is not well-explained by any of the six variables used for regression analysis. The hole in the middle of this plot where no trees survived may be the result of local variations in soil composition or some other unknown factor.

### **Recommended Best Practices for Future Data Collections**

After carrying out field missions in 2022 and 2023 and conducting many analyses of the resulting data, some recommendations can be made regarding optimal conditions and parameters for future UAS flights at the study area. The metadata that were collected and aggregated for these flights as well as all of the older flights are displayed in Tables 7-9 and can serve as a resource for future data collections.

### ***Ideal Site Conditions for UAS Flights for SfM***

The best time of year for flights that intend to collect RGB imagery for SfM is generally late winter or early spring, especially if prescribed burning has recently taken place. The minimal ground cover caused by these conditions results in more accurate DTMs, which are crucial for determining tree heights, and the presence of less green vegetation makes it easier to identify longleaf pines in the images and orthomosaics. With regards to weather conditions, cloudy (not rainy) weather – with flights conducted around midday for minimum shadows and maximum brightness levels – generated the best orthomosaics. Sunny weather is acceptable, but dark shadows can make it harder to observe parts of the field; partly cloudy weather causes fluctuating brightness levels that can affect imagery quality and create variations in the appearance of otherwise similar parts of the study area, potentially making tree identification more difficult for both humans and machine learning models. Of course,

while these are ideal conditions, waiting for them may not always be realistic, as it can be difficult enough just to plan around rain and thunderstorms in the humid subtropical Savannah climate.

### ***Ideal Flight Parameters for UAS Flights for SfM***

The UAS-based RGB imagery that has been collected at the study area over the years has seen a wide variety of flight parameters used. A good standard for such UAS missions in the future is to use flight parameters from the February 2023 data collection (Table 7): a flight height of 60 m, 85% endlap, 75% sidelap, and the camera angled at nadir and flown in a standard single grid flight pattern. Assuming that the UAV being used has similar capabilities and image resolution to the Phantom 4 Pro, these parameters should produce high quality results without putting too much strain on data processing and storage capabilities. The resulting orthomosaic should be detailed enough to make identifying longleaf pines and distinguishing them from other species a straightforward process, and the point cloud should be detailed enough to create an accurate CHM (though as the trees continue to age and grow, these recommended parameters may need to be revisited).

*Table 7. UAS flight metadata for all optical imagery collected at the study area. Cells highlighted in yellow show flight parameters that had to be approximated due to the absence of the original metadata.*

Date	Used for Analysis?	UAV Make & Model	Mega-pixels	Pilot	Flight Pattern	Flight Height (m)	% Endlap	% Sidelap	Camera Angle (degrees, 90 = nadir)	Ground Sampling Distance (cm/px)	Ground Control Points Used?
4/22/2016	Yes	DJI Phantom 4	12	Tommy Jordan	Single grid (2)	60	80	80	90	2.56	No
1/15/2017	Yes	DJI Phantom 4	12	Tommy Jordan	Single grid (2)	60	80	80	90	2.56	No
4/4/2018	Yes	DJI Phantom 4	12	Tommy Jordan	Single grid (2)	110	80	80	90	4.70	No
3/24/2019	Yes	DJI Phantom 4	12	Tommy Jordan	Single grid	110	80	80	90	4.70	No
1/10/2021	No	DJI Mavic Air	12.3	Marguerite Madden	Single grid	110	70	60	90	3.72	No
2/3/2021	Yes	DJI Phantom 4 Pro	20	Claudia Venherm	Double grid	50	85	75	90	1.36	Yes
9/26/2021	Yes	DJI Phantom 4 Pro	20	Tommy Jordan	Single grid	120	75	80	90	3.27	No
2/23/2022	Yes	DJI Phantom 4 Pro	20	Claudia Venherm	Single grid	120	90	85	90	3.27	No
9/7/2022	Yes	DJI Phantom 4 Pro	20	Tommy Jordan	Single grid	120	95	80	85	3.3	No
2/19/2023	Yes	DJI Phantom 4 Pro	20	Sergio Bernardes	Single grid	60	85	75	90	1.63	Yes

Table 8. UAS flight metadata for all optical imagery collected for the 50 x 50-m plot.

Date	Used for Analysis?	UAV Make & Model	Mega-pixels	Pilot	Flight Pattern	Flight Height (m)	% Endlap	% Sidelap	Camera Angle (degrees, 90 = nadir)	Ground Sampling Distance (cm/px)	Ground Control Points Used?
9/8/2022	Yes	DJI Phantom 4 Pro	20	Tommy Jordan	Single grid	40	80	80	85	1.1	Yes
9/7/2022	Yes	DJI Phantom 4 Pro	20	Tommy Jordan	Single grid	60	95	80	85	1.6	Yes
9/7/2022	Yes	DJI Phantom 4 Pro	20	Tommy Jordan	Single grid	80	95	80	85	2.2	Yes
9/7/2022	Yes	DJI Phantom 4 Pro	20	Tommy Jordan	Single grid	100	95	80	85	2.7	Yes
9/7/2022	Yes	DJI Phantom 4 Pro	20	Tommy Jordan	Single grid	120	95	80	85	3.3	Yes
2/19/2023	No	DJI Phantom 4 Pro	20	Sergio Bernardes	Double grid	60	85	75	70	1.63	No

Table 9. UAS flight metadata for the LiDAR data collected at the study area.

Date	Used for Analysis?	UAV Make & Model	Sensor	Pulse Rate (kHz)	Pilot	Total Points	Flight Height (m)	Flight Speed (m/s)	Flight Line Spacing (m)	Estimated Point Density (points/m <sup>2</sup> )
2/19/2023	Yes	Freefly AltaX	LiDAR USA Revolution 120	300	Sergio Bernardes	97,841,589	40	5.0	70	555.7

### ***The Merits of SfM Versus LiDAR at the Study Area***

The LiDAR data unquestionably yielded more accurate tree height estimates, and even under the best site conditions, SfM did not produce a bare-earth DEM approaching the quality of the bare-earth DEM produced by the LiDAR data. However, SfM still performed well overall,

and the logistics of data collection for it were less challenging than for LiDAR. So while LiDAR appears to be the better option if solely focusing on data accuracy for tree studies, SfM is and should continue to be an acceptable technique for estimating longleaf pine heights, especially if flights are conducted in leaf-off conditions and periodic prescribed burning continues. If prescribed burning were to cease, it is possible that any CHMs produced by SfM would become increasingly inaccurate as time passes due to thick undergrowth vegetation, and it would no longer be an acceptable option. However, even if the field were to enter a state where SfM could not yield accurate tree height estimates, it would still be prudent to collect optical UAS imagery because it provides a visual record of the field's appearance at the time of data collection.

#### ***Additional Thoughts and Recommendations***

The steel rebar permanent GCPs that were installed in February 2023 (Table 10) worked well initially, as they were used to help georeference the UAS images that were collected at that time. However, the rebars have since proved to be insufficiently permanent for long-term repeated use. In December 2023, ten months after their installation, multiple rebars were missing their orange caps – making them less visible and a safety hazard (Figure 38) – or in some cases missing entirely. The use of permanent GCPs to facilitate drone data collection is still a feasible idea for the study area, but better materials and installation procedures should be used in the future.

Table 10. Corrected positional data for the permanent GCP markers.

GCP	Latitude	Longitude	Orthometric Height (m)
1	31.96846813	-81.06898036	2.588
2	31.96781340	-81.06842448	2.172
3	31.96850599	-81.06659675	2.569
4	31.96924434	-81.06567826	2.620
5	31.97058349	-81.06585674	3.691
6	31.97013574	-81.06772927	2.346
7	31.97128314	-81.06878799	2.961
8	31.97030841	-81.06896712	3.258



Figure 38. Rebar marking a GCP location that has been damaged and is missing its safety cap.

A few miscellaneous recommendations regarding future data collections may be made as well. If field measurements of tree heights are taken again, an alternate measuring method such as a laser rangefinder will likely be required, as the telescopic measuring pole used previously was already almost too short to measure some of the trees in 2023. Additionally, if ground truth trees need to be labelled for a long period of time, it may be



prudent to invest in semi-permanent labels such as engraved metal tags affixed to each tree. This is because temporary markers like flagging tape are likely to melt when prescribed burning takes place, which renders them useless and is environmentally harmful.

## **CHAPTER 5**

### **CONCLUSIONS**

Several advanced geospatial techniques were collectively utilized to monitor a small (23-acre) longleaf pine ecosystem restoration site at Wormsloe State Historic Site on the Isle of Hope near Savannah, Georgia. A maritime longleaf pine ecosystem was historically one of the dominant ecosystem types found on the Isle of Hope, but it has been unable to thrive there for centuries in the face of agriculture, development, and a myriad of other human-caused landscape alterations; this makes the restoration effort an important new chapter in the history of Wormsloe, already one of the oldest and most historically and ecologically significant sites in the state of Georgia. Through the evaluation of the site with novel geospatial technologies, this study sought to test and refine techniques that have the potential to streamline the management of longleaf pine forests not just at the study area, but throughout the southeastern U.S.

The first objective was to remotely measure canopy height, specifically longleaf pine tree heights, across the restoration area through the use of two UAS-based geospatial techniques, Structure from Motion (SfM) and LiDAR, and compare both methods. Initial testing of different flight parameters for SfM showed that SfM tree height estimates were generally more accurate when flight height was low (approximately 60 m) and along-track overlap was very high (95%). Direct comparison of LiDAR and SfM showed that both methods correlated very strongly with ground truth data but that height estimates for LiDAR had lower RMSE, on the order of 0.15 m; a third method of height measurement that combined LiDAR and SfM data was also tested, and it yielded results very similar to the LiDAR dataset.

Additionally, comparison of SfM accuracy between the September 2022 data and February 2023 data collections indicated that thinner ground vegetation during winter and after prescribed burns notably improved tree height estimates.

The goal of the second objective was to use geospatial deep learning to count the number of longleaf pines in the study area, thus enabling further analysis of their spatial distribution, height distribution, and statistical relationships with local environmental conditions. A deep learning model, Mask R-CNN, was trained on a custom-made 10-band raster dataset to identify longleaf pine locations in the most recent imagery from 2023. It achieved an F1 score of 0.87 and identified 3,369 longleaf pines in the study area. Having seven additional bands of raster data appended to a simple 3-band RGB orthomosaic made for an unusual input dataset, but the extra data proved crucial for boosting model performance and demonstrated the value of using alternative, non-spectral data in CNN model training. When the deep learning results were combined with canopy height data and assessed via multiple regression, analysis of the regression models identified one variable (2016-2019 mean yearly solar radiation) that was valuable as a predictor of longleaf pine height, and four variables (elevation, topographic wetness, the presence or absence of residual debris during planting, and 2016-2019 mean yearly solar radiation) that were valuable as predictors of longleaf pine survival.

The third objective sought to use SfM to generate time series maps for visualizing the growth and survival patterns of longleaf pines over the course of their lives. To achieve this, photogrammetry and point cloud processing software packages were used to create LAS point clouds, orthomosaics, and canopy height models (CHMs) for nine separate data collections occurring between 2016 and 2023. Analysis of the time series at six small plots in the study area showed two major phases of longleaf pine growth: during the first, virtually

no vertical growth occurred, and a number of seedlings died due to intolerable growing conditions; during the second phase, which for most trees appears to have begun four to five years after planting, rapid vertical growth began to occur, and that steady growth has continued occurring all the way through the most recent dataset. The observed growth trends correspond well with the typical grass stage, bottlebrush stage, and sapling stage of the longleaf pine life cycle.

Finally, the fourth objective was to create, organize, and aggregate information that could facilitate the continued use of UAS-based remote sensing for studying the restoration site. One aspect of this, the installation of permanent ground control points (GCPs) with known high-precision coordinates, was ultimately unsuccessful as the rebar posts that were installed proved unfit for long-term repeated use. Still, this objective was met in other ways, including through the creation of a new comprehensive UAS flight metadata database, and through evaluating past results to make recommendations for future research, such as identifying specific flight parameters, weather and site conditions, and data collection methodologies that should be used or avoided.

Overall, the methods used during this research certainly allowed for a broader-scale and more thorough analysis of the longleaf pines than would have been possible without advanced GIS and remote sensing techniques. More specifically, both of the UAS-based techniques employed, SfM and LiDAR, seem to offer a more efficient and easily scalable approach to the monitoring of longleaf pine forests than ground-based methods, assuming a base level of technical knowledge on the part of the user and the ability to invest in the requisite technology. In addition, geospatial deep learning tools such as the CNN that was tested seem well-equipped to be valuable companions to UAS data collection with their ability to analyze remotely sensed data quickly and accurately. For this study, the amount of

time and effort saved by using a deep learning workflow was ultimately not very great due to the fact that multiple iterations of data annotation and model training were conducted and due to the relatively small number of objects being detected. Yet even with these limitations, the total amount of data annotated was less than what would have been required if tree detection was done manually. For a much larger area of interest, such as forest sites with tens or hundreds of thousands of trees, the benefits of eliminating tedious manual digitization in favor of deep learning would be immeasurably greater.

While some financial and technical barriers to the use of these technologies do still exist, it is likely that they will become more easily surmountable with time as more tools and educational resources become available and as use of the technology itself becomes more widespread. This means that UAS-mounted remote sensors and geospatial deep learning techniques should absolutely have an important part to play in the work that foresters, private landowners, and conservation organizations do to conserve, monitor, and restore longleaf pine habitat. If fully embraced, these technologies can be instrumental in helping a remarkable and resilient tree continue making a comeback across its historic range.

### **Future Work**

Probably the single most important task that should be at the center of all future work is to continue collecting data to add to the existing time series. Even if there is no in-depth research using it at the time, simply obtaining UAS imagery annually or biannually adds to an already robust data record that can be used in the future, just as some of the imagery collected between 2016 and 2022 went largely unused for a while before it was incorporated into this research.

One of the most enticing options for future study would be further analysis of the 3D forest models, either those created by SfM, LiDAR, or both. This research primarily used the

models to extract tree heights, but canopy height is just one of many ways to study forest structure. Point clouds can be used to calculate a variety of metrics, from common forestry measurements like basal area and diameter at breast height (DBH) to more complex forest characterizations such as tree crown morphology, tree volume, woody debris volume, and biomass and carbon sequestration estimates.

There are also a seemingly infinite number of experiments that could be done to study and improve deep learning model performance. For instance, it would be very interesting to compare the performance of different neural networks. Mask R-CNN is known as a high-performing neural network, but it was introduced in 2017, and in an age of booming GeoAI, newer models are introduced every year, some of which may outperform Mask R-CNN. There are multiple ways to change and potentially improve the nature of the model's input data as well, such as testing the efficacy of a model trained on multiple tree species as opposed to a single species, experimenting with raster bands by quantifying which bands affect accuracy the most, or introducing multispectral imagery in addition to RGB imagery. It would also be possible to forgo Mask R-CNN entirely in favor of deep learning tools that are designed to learn from 3D data. This would allow for working with point cloud data directly instead of using rasters (CHMs) derived from point cloud data.

To allow for better comparison of longleaf pine characteristics like height and survivability to environmental conditions, it would be useful to conduct more detailed soil surveys of the field, though admittedly it may be quite labor-intensive to gather this data for the whole restoration site; previous soil data was only collected in small plots within the larger study area. It would also be prudent to start accumulating data regarding the frequency and spatial extent of prescribed burns, as these burns undoubtedly impact the longleaf pines. A rough idea of the timing and extent of previous burns can be gathered by

examining the orthomosaics from older UAS flights, but since the flights were not necessarily conducted with this goal in mind, it is difficult to know how accurate or complete the burn-related data from them really is.

With continued support from the Barrow family, the Wormsloe Foundation, CREW, and UGA, there is no limit to the possibilities for further research that can add to our knowledge of the restoration site and how it changes over time as the longleaf pines continue to mature.

## REFERENCES

- Abdullah, Q., & Munjy, R. (2019). sUAS data accuracy in photogrammetric workflows. In J.B. Sharma (Ed.), *Applications of small unmanned aircraft systems: Best practices and case studies* (pp. 1-15). CRC Press. <https://doi.org/10.1201/9780429244117-1>
- Agisoft LLC. (2022). *Agisoft Metashape user manual: Professional edition, version 1.8*. [https://www.agisoft.com/pdf/metashape-pro\\_1\\_8\\_en.pdf](https://www.agisoft.com/pdf/metashape-pro_1_8_en.pdf)
- America's Longleaf Restoration Initiative. (2023). *2023 range-wide accomplishments*. <https://americaslongleaf.org/media/wfmbhh0k/2023-alri-accomplishment-report.pdf>
- Anderson, K., & Gaston, K. J. (2013). Lightweight unmanned aerial vehicles will revolutionize spatial ecology. *Frontiers in Ecology and the Environment*, 11(3), 138-146. <https://doi.org/10.1890/120150>
- Aschenbach, T. A., Foster, B. L., & Imm, D. W. (2010). The initial phase of a longleaf pine-wiregrass savanna restoration: Species establishment and community responses. *Restoration Ecology*, 18(5), 762-771. <https://doi.org/10.1111/j.1526-100X.2009.00541.x>
- Beloiu, M., Heinzmann, L., Rehush, N., Gessler, A., & Griess, V. C. (2023). Individual tree-crown detection and species identification in heterogeneous forests using aerial RGB imagery and deep learning. *Remote Sensing*, 15(5), Article 1463. <https://doi.org/10.3390/rs15051463>
- Bernardes, S., & Madden, M. (2021). Digital preservation of historical heritage using 3D models and augmented reality. In A. E. Frazier & K. K. Singh (Eds.), *Fundamentals of capturing and processing drone imagery and data* (pp. 283-304). CRC Press.
- Beven, K. J., & Kirkby, M. J. (1979). A physically based, variable contributing area model of basin hydrology. *Hydrological Sciences Bulletin*, 24(1), 43-69. <https://doi.org/10.1080/02626667909491834>
- Binita, K. C., Shepherd, J. M., & Gaither, C. J. (2015). Climate change vulnerability assessment in Georgia. *Applied Geography*, 62, 62-74. <https://doi.org/10.1016/j.apgeog.2015.04.007>



- Bohlin, J., Wallerman, J., & Fransson, J. E. (2012). Forest variable estimation using photogrammetric matching of digital aerial images in combination with a high-resolution DEM. *Scandinavian Journal of Forest Research*, 27(7), 692-699. <https://doi.org/10.1080/02827581.2012.686625>
- Brethauer, D. K., Sharma, A., Vogel, J. G., Miller, D. L., & van Santen, E. (2021). Longleaf pine seedling growth and survival: Effects of season and intensity of simulated prescribed burning. *Forest Ecology and Management*, 502, Article 119719. <https://doi.org/10.1016/j.foreco.2021.119719>
- Burda, C. (2011). *Placing a historical plantation in an ecological context: Evaluating effects of land use legacies on vegetation patterns using discrete return LiDAR* [Master's thesis, University of Georgia]. UGA GIL-Find Catalog. [https://getd.libs.uga.edu/pdfs/burda\\_carey\\_201108\\_ms](https://getd.libs.uga.edu/pdfs/burda_carey_201108_ms)
- Camelo, J., Mayo, T. L., & Gutmann, E. D. (2020). Projected climate change impacts on hurricane storm surge inundation in the coastal United States. *Frontiers in Built Environment*, 6, Article 588049. <https://doi.org/10.3389/fbuil.2020.588049>
- Campbell, J. H., & Morris, L. A. (2018). Land use and soil legacy in the Lower Coastal Plain: A case study of Wormsloe State Historic Site, Georgia. *Journal of Soil and Water Conservation*, 73(4), 386-399. <https://www.tandfonline.com/doi/pdf/10.2489/jswc.73.4.386>
- Colomina, I., & Molina, P. (2014). Unmanned aerial systems for photogrammetry and remote sensing: A review. *ISPRS Journal of Photogrammetry and Remote Sensing*, 92, 79-97. <https://doi.org/10.1016/j.isprsjprs.2014.02.013>
- Deliry, S. I., & Avdan, U. (2021). Accuracy of unmanned aerial systems photogrammetry and structure from motion in surveying and mapping: A review. *Journal of the Indian Society of Remote Sensing*, 49(8), 1997-2017. <https://doi.org/10.1007/s12524-021-01366-x>
- Dellaert, F., Seitz, S. M., Thorpe, C. E., & Thrun, S. (2000). Structure from motion without correspondence. *Proceedings IEEE Conference on Computer Vision and Pattern Recognition. CVPR 2000 (Cat. No.PR00662)*, 2, 557-564. <https://doi.org/10.1109/CVPR.2000.854916>

- Dersch, S., Schöttl, A., Krzystek, P., & Heurich, M. (2023). Towards complete tree crown delineation by instance segmentation with Mask R-CNN and DETR using UAV-based multispectral imagery and lidar data. *ISPRS Open Journal of Photogrammetry and Remote Sensing*, 8, Article 100037.  
<https://doi.org/10.1016/j.ophoto.2023.100037>
- Dinkov, D., & Kitev, A. (2020). Advantages, disadvantages and applicability of GNSS post-processing kinematic (PPK) method for direct georeferencing of UAV images. In T. Bandrova, M. Konečný, & S. Marinova (Eds.), *Proceedings of the 8th International Conference on Cartography and GIS: Vol. 1* (pp. 747-759). Bulgarian Cartographic Association. [https://iccgis2020.cartography-gis.com/8ICCGIS-Vol1/8ICCGIS\\_Proceedings\\_Vol1\\_\(81\).pdf](https://iccgis2020.cartography-gis.com/8ICCGIS-Vol1/8ICCGIS_Proceedings_Vol1_(81).pdf)
- Emlid. (n.d.). *Reach RS/RS+ glossary*.  
<https://docs.emlid.com/reachrs/reference/glossary/#solution-status-fix-float-single>
- Emlid. (2023). *Emlid studio land survey data collection software* (Version 1.5) [Computer software]. <https://emlid.com/emlid-studio/>
- Esri. (2024, December 18). *Terrain* [ArcGIS Living Atlas of the World image service]. Esri.  
<https://www.arcgis.com/home/item.html?id=58a541efc59545e6b7137f961d7de883>
- Esri. (2025, January 29). *World imagery* [ArcGIS map service]. Esri.  
[https://services.arcgisonline.com/ArcGIS/rest/services/World\\_Imagery/MapServer](https://services.arcgisonline.com/ArcGIS/rest/services/World_Imagery/MapServer)
- Esri Academy. (2020). *Deep learning using ArcGIS Pro* [Online course]. Esri.  
<https://www.esri.com/training/catalog/62e98b093ef3766d5391016f/deep-learning-using-arcgis-pro/>
- Esri Developer. (n.d.). *Detecting settlements using supervised classification and deep learning*. <https://developers.arcgis.com/python/latest/samples/detecting-settlements-using-supervised-classification-and-deep-learning/>
- Farjon, A. (2013). *Longleaf pine (Pinus palustris)*. The IUCN Red List of Threatened Species.  
<https://dx.doi.org/10.2305/IUCN.UK.2013-1.RLTS.T39068A2886222.en>
- Florida Natural Areas Inventory. (2023). *Southeast Longleaf Ecosystem Occurrences Geodatabase (LEO GDB) Apr. 2018 – Sep. 2023*.  
[https://www.fnai.org/PDFs/LEO\\_GDB\\_v2\\_Results\\_Quick\\_Sum\\_Sep2023.pdf](https://www.fnai.org/PDFs/LEO_GDB_v2_Results_Quick_Sum_Sep2023.pdf)

- Fonstad, M. A., Dietrich, J. T., Courville, B. C., Jensen, J. L., & Carbonneau, P. E. (2013). Topographic structure from motion: A new development in photogrammetric measurement. *Earth Surface Processes and Landforms*, 38(4), 421-430. <https://doi.org/10.1002/esp.3366>
- Förstner, W., & Gülch, E. (1987). A fast operator for detection and precise location of distinct points, corners and centres of circular features. *Proceedings of ISPRS Intercommission Conference on Fast Processing of Photogrammetric Data*, 6, 281-305. <https://cseweb.ucsd.edu/classes/sp02/cse252/foerstner/foerstner.pdf>
- Franklin, R. (2009). *Converting planted loblolly pine (or slash pine) to longleaf pine: An opportunity* (Report No. 31). Clemson University Cooperative Extension Service. [https://americaslongleaf.org/media/qcbfus0q/converting\\_loblolly\\_to\\_longleaf.pdf](https://americaslongleaf.org/media/qcbfus0q/converting_loblolly_to_longleaf.pdf)
- Fraser, C. S., & Cronk, S. (2009). A hybrid measurement approach for close-range photogrammetry. *ISPRS Journal of Photogrammetry and Remote Sensing*, 64(3), 328-333. <https://doi.org/10.1016/j.isprsjprs.2008.09.009>
- Frost, C. C. (1993). Four centuries of changing landscape patterns in the longleaf pine ecosystem. *Proceedings of the Tall Timbers fire ecology conference*, 18, 17-43.
- Gani, M. O., Kuiry, S., Das, A., Nasipuri, M., & Das, N. (2021). Multispectral object detection with deep learning. In P. Dutta, J. K. Mandal, & S. Mukhopadhyay (Eds.), *Computational intelligence in communications and business analytics: Vol. 1406. Communications in computer and information science* (pp. 105-117). Springer, Cham. [https://doi.org/10.1007/978-3-030-75529-4\\_9](https://doi.org/10.1007/978-3-030-75529-4_9)
- Georgia Forestry Commission. (2020). *Seedling care and planting guidelines* [Brochure]. <https://gatrees.org/wp-content/uploads/2020/02/Seedling-Care-And-Planting-Guidelines.pdf>
- Goodbody, T. R., White, J. C., Coops, N. C., & LeBoeuf, A. (2021). Benchmarking acquisition parameters for digital aerial photogrammetric data for forest inventory applications: Impacts of image overlap and resolution. *Remote Sensing of Environment*, 265, Article 112677. <https://doi.org/10.1016/j.rse.2021.112677>
- Goodfellow, I., Bengio, Y., & Courville, A. (2016). *Deep learning*. Massachusetts Institute of Technology Press. <https://www.deeplearningbook.org/>
- Granshaw, S. I. (2018). Structure from motion: Origins and originality. *The Photogrammetric Record*, 33(161), 6-10. <https://doi.org/10.1111/phor.12237>

- Groemping, U. (2006). Relative importance for linear regression in R: The package relaimpo. *Journal of Statistical Software*, 17(1), 1-27. <https://doi.org/10.18637/jss.v017.i01>
- Gruen, A., & Baltsavias, E. P. (1988). Geometrically constrained multiphoto matching. *Photogrammetric Engineering and Remote Sensing*, 54(5), 633-641. [https://www.researchgate.net/profile/Armin-Gruen/publication/260187986\\_Geometrically\\_constrained\\_multiphoto\\_matching/links/5706232108ae44d70ee34eeb/Geometrically-constrained-multiphoto-matching.pdf](https://www.researchgate.net/profile/Armin-Gruen/publication/260187986_Geometrically_constrained_multiphoto_matching/links/5706232108ae44d70ee34eeb/Geometrically-constrained-multiphoto-matching.pdf)
- Gruen, A., Remondino, F., & Zhang, L. (2004). Photogrammetric reconstruction of the great Buddha of Bamiyan, Afghanistan. *The Photogrammetric Record*, 19(107), 177-199. <https://doi.org/10.1111/j.0031-868X.2004.00278.x>
- Gyawali, A., Aalto, M., Peuhkurinen, J., Villikka, M., & Ranta, T. (2022). Comparison of individual tree height estimated from LiDAR and digital aerial photogrammetry in young forests. *Sustainability*, 14(7), Article 3720. <https://doi.org/10.3390/su14073720>
- Hall, L. (2024, April 29). *Parcel digest 2023* [Data set]. Savannah Area Geographic Information System. <https://data-sagis.opendata.arcgis.com/datasets/SAGIS::parcel-digest-2023-2/about>
- Hao, Z., Lin, L., Post, C. J., Jiang, Y., Li, M., Wei, N., Yu, K., & Liu, J. (2021). Assessing tree height and density of a young forest using a consumer unmanned aerial vehicle (UAV). *New Forests*, 52, 843-862. <https://doi.org/10.1007/s11056-020-09827-w>
- Hartley, R. J., Leonardo, E. M., Massam, P., Watt, M. S., Estarija, H. J., Wright, L., Melia, N., & Pearse, G. D. (2020). An assessment of high-density UAV point clouds for the measurement of young forestry trials. *Remote Sensing*, 12(24), Article 4039. <https://doi.org/10.3390/rs12244039>
- He, K., Gkioxari, G., Dollár, P., & Girshick, R. (2017). Mask R-CNN. *Proceedings of the IEEE International Conference on Computer Vision*, 2961-2969. [https://openaccess.thecvf.com/content\\_ICCV\\_2017/papers/He\\_Mask\\_R-CNN\\_ICCV\\_2017\\_paper.pdf](https://openaccess.thecvf.com/content_ICCV_2017/papers/He_Mask_R-CNN_ICCV_2017_paper.pdf)
- Hyypä, J., Hyypä, H., Leckie, D., Gougeon, F., Yu, X., & Maltamo, M. (2008). Review of methods of small-footprint airborne laser scanning for extracting forest inventory data in boreal forests. *International Journal of Remote Sensing*, 29(5), 1339-1366. <https://doi.org/10.1080/01431160701736489>

- Iverson, L. R., Graham, R. L., & Cook, E. A. (1989). Applications of satellite remote sensing to forested ecosystems. *Landscape Ecology*, 3, 131-143. <https://doi.org/10.1007/BF00131175>
- Jaakkola, A., Hyypä, J., Kukko, A., Yu, X., Kaartinen, H., Lehtomäki, M., & Lin, Y. (2010). A low-cost multi-sensoral mobile mapping system and its feasibility for tree measurements. *ISPRS Journal of Photogrammetry and Remote Sensing*, 65(6), 514-522. <https://doi.org/10.1016/j.isprsjprs.2010.08.002>
- James, M. R., Chandler, J. H., Eltner, A., Fraser, C., Miller, P. E., Mills, J. P., Noble, T., Robson, S., and Lane, S. N. (2019). Guidelines on the use of structure-from-motion photogrammetry in geomorphic research. *Earth Surface Processes and Landforms*, 44(10), 2081-2084. <https://doi.org/10.1002/esp.4637>
- The Jones Center at Ichauway. (2024). *Forest resources management*. <https://www.jonesctr.org/conservation/#forest-resources-management>
- Kameyama, S., & Sugiura, K. (2021). Effects of differences in structure from motion software on image processing of unmanned aerial vehicle photography and estimation of crown area and tree height in forests. *Remote Sensing*, 13(4), Article 626. <https://doi.org/10.3390/rs13040626>
- Katal, N., Rzanny, M., Mäder, P., & Wäldchen, J. (2022). Deep learning in plant phenological research: A systematic literature review. *Frontiers in Plant Science*, 13, Article 805738. <https://doi.org/10.3389/fpls.2022.805738>
- Leckie, D. G. (1990). Advances in remote sensing technologies for forest surveys and management. *Canadian Journal of Forest Research*, 20(4), 464-483. <https://doi.org/10.1139/x90-063>
- Lefsky, M. A., Cohen, W. B., Parker, G. G., & Harding, D. J. (2002). Lidar remote sensing for ecosystem studies. *BioScience*, 52(1), 19-30. [https://doi.org/10.1641/0006-3568\(2002\)052\[0019:LRSFES\]2.0.CO;2](https://doi.org/10.1641/0006-3568(2002)052[0019:LRSFES]2.0.CO;2)
- Lenhardt, J. (2022, October 26). *Use deep learning to assess palm tree health*. Esri. <https://learn.arcgis.com/en/projects/use-deep-learning-to-assess-palm-tree-health/>
- Li, W., & Hsu, C. Y. (2022). GeoAI for large-scale image analysis and machine vision: Recent progress of artificial intelligence in geography. *ISPRS International Journal of Geo-Information*, 11(7), Article 385. <https://doi.org/10.3390/ijgi11070385>

Lim, K., Treitz, P., Wulder, M., St-Onge, B., & Flood, M. (2003). LiDAR remote sensing of forest structure. *Progress in Physical Geography*, 27(1), 88-106.

The Longleaf Alliance. (2021). *Restoration through partnerships*.  
<https://longleafalliance.org/what-we-do/restoration-through-partnerships/>

The Longleaf Alliance [@longleaf\_alliance]. (2024, December 18). *The Longleaf Alliance is “moving the needle” thanks to the unwavering support of our members and partners! Here are just [Infographic]*. Instagram.  
<https://www.instagram.com/p/DDujh33trf1/>

Lord, L. (2022, October 20). *Bringing back longleaf: Forests for the future* [Symposium presentation]. The River Basin Center Third Wednesday Symposium, Athens, GA, United States.

Lund, H. G. (Ed.), Befort, W. A., Brickell, J. E., Ciesla, W. M., Collins, E. C., Czaplewski, R. L., Disperati, A. A., Douglass, R. W., Dull, C. W., Greer, J. D., Hershey, R. R., LaBou, V. J., Lachowski, H., Murtha, P. A., Nowak, D. J., Roberts, M. A., Schram, P., Shedha, M. D., Singh, A., & Winterberger, K. C. (1997). Chapter 11: Forestry. In W. R. Philipson (Ed.), *Manual of Photographic Interpretation* (2nd ed., pp. 399-440). American Society for Photogrammetry and Remote Sensing.  
[https://www.fs.usda.gov/rm/pubs\\_other/rmrs\\_1997\\_lund\\_h001.pdf](https://www.fs.usda.gov/rm/pubs_other/rmrs_1997_lund_h001.pdf)

Madden, M., Jordan, T., Bernardes, S., Goetcheus, C., Olson, K., & Cotten, D. (2019). Small unmanned aerial systems (sUAS) and structure from motion for identifying, documenting, and monitoring cultural and natural resources. In J.B. Sharma (Ed.), *Applications of small unmanned aircraft systems: Best practices and case studies* (pp. 179-209). CRC Press. <http://dx.doi.org/10.1201/9780429244117-9>

Madikyzy, I. [inkar.madikyzy]. (2024, August 7). *Welcome to our forum! Let's break this down into key parts. Float solution status means the rover receives corrections from [Comment on the online forum post Understanding RMS and other sources of error?]*. Emlid Community. <https://community.emlid.com/t/understanding-rms-and-other-sources-of-error/39241/8>

Maltamo, M., Næsset, E., & Vauhkonen, J. (Eds.). (2014). *Forestry applications of airborne laser scanning: Concepts and case studies*. Springer.

- Manfreda, S., McCabe, M. F., Miller, P. E., Lucas, R., Pajuelo Madrigal, V., Mallinis, G., Ben Dor, E., Helman, D., Estes, L., Ciraolo, G., Müllerová, J., Tauro, F., De Lima, M. I., De Lima, J. L. M. P., Maltese, A., Frances, F., Caylor, K., Kohv, M., Perks, M., Ruiz-Pérez, G., Su, Z., Vico, G., & Toth, B. (2018). On the use of unmanned aerial systems for environmental monitoring. *Remote Sensing*, 10(4), Article 641. <https://doi.org/10.3390/rs10040641>
- Markets and Markets. (2022, August). *LiDAR Drone Market*. <https://www.marketsandmarkets.com/Market-Reports/lidar-drone-market-128835365.html>
- Mathew, S., & Yadav, P. (2021, August 2). Performing feature extraction & classification using deep learning with ArcGIS Pro. *ArcGIS Blog*. <https://www.esri.com/arcgis-blog/products/arcgis-pro/imagery/performing-feature-extraction-classification-using-deep-learning-with-arcgis-pro>
- McManamon, P. F. (2019). *Lidar technologies and systems*. Society of Photo-Optical Instrumentation Engineers. <https://doi.org/10.1117/3.2518254>
- Means, D. B. (2006). Vertebrate faunal diversity of longleaf pine ecosystems. In S. Jose, E. J. Jokela, & D. L. Miller (Eds.), *The longleaf pine ecosystem: ecology, silviculture, and restoration* (pp. 157-213). Springer Series on Environmental Management. [https://doi.org/10.1007/978-0-387-30687-2\\_6](https://doi.org/10.1007/978-0-387-30687-2_6)
- Means, J. E., Acker, S. A., Harding, D. J., Blair, J. B., Lefsky, M. A., Cohen, W. B., Harmon, M. E., & McKee, W. A. (1999). Use of large-footprint scanning airborne lidar to estimate forest stand characteristics in the Western Cascades of Oregon. *Remote Sensing of Environment*, 67(3), 298-308. [https://doi.org/10.1016/S0034-4257\(98\)00091-1](https://doi.org/10.1016/S0034-4257(98)00091-1)
- Mielcarek, M., Kamińska, A., & Stereńczak, K. (2020). Digital aerial photogrammetry (DAP) and airborne laser scanning (ALS) as sources of information about tree height: Comparisons of the accuracy of remote sensing methods for tree height estimation. *Remote Sensing*, 12(11), Article 1808. <https://doi.org/10.3390/rs12111808>
- Miura, N., & Jones, S. D. (2010). Characterizing forest ecological structure using pulse types and heights of airborne laser scanning. *Remote Sensing of Environment*, 114(5), 1069-1076. <https://doi.org/10.1016/j.rse.2009.12.017>
- Mlambo, R., Woodhouse, I. H., Gerard, F., & Anderson, K. (2017). Structure from motion (SfM) photogrammetry with drone data: A low cost method for monitoring greenhouse gas emissions from forests in developing countries. *Forests*, 8(3), Article 68. <https://doi.org/10.3390/f8030068>

- Nelson, R., Krabill, W., & MacLean, G. (1984). Determining forest canopy characteristics using airborne laser data. *Remote Sensing of Environment*, 15(3), 201-212. [https://doi.org/10.1016/0034-4257\(84\)90031-2](https://doi.org/10.1016/0034-4257(84)90031-2)
- Ni, W., Sun, G., Pang, Y., Zhang, Z., Liu, J., Yang, A., Wang, Y., & Zhang, D. (2018). Mapping three-dimensional structures of forest canopy using UAV stereo imagery: Evaluating impacts of forward overlaps and image resolutions with LiDAR data as reference. *IEEE Journal of Selected Topics in Applied Earth Observations and Remote Sensing*, 11(10), 3578-3589. <https://doi.org/10.1109/JSTARS.2018.2867945>
- Nilsson, M. (1996). Estimation of tree heights and stand volume using an airborne lidar system. *Remote Sensing of Environment*, 56(1), 1-7. [https://doi.org/10.1016/0034-4257\(95\)00224-3](https://doi.org/10.1016/0034-4257(95)00224-3)
- Noss, R. F., LaRae, E. T., & Scott, J. M. (1995). *Endangered ecosystems of the United States: A preliminary assessment of loss and degradation* (Report No. 28). US Department of the Interior, National Biological Service. <https://digitalmedia.fws.gov/digital/collection/document/id/1720/>
- O'Brien, J. J., Hiers, J. K., Callaham, M. A., Mitchell, R. J., & Jack, S. B. (2008). Interactions among overstory structure, seedling life-history traits, and fire in frequently burned neotropical pine forests. *AMBIO: A Journal of the Human Environment*, 37(7), 542-547. <https://doi.org/10.1579/0044-7447-37.7.542>
- Over, J. R., Ritchie, A. C., Kranenburg, C. J., Brown, J. A., Buscombe, D., Noble, T., Sherwood, C. R., Warrick, J. A., & Wernette, P. A. (2021). *Processing coastal imagery with Agisoft Metashape Professional Edition, version 1.6—Structure from motion workflow documentation* (Open-File Report 2021-1039). United States Geological Survey. <https://doi.org/10.3133/ofr20211039>
- Peet, R. K., & Allard, D. J. (1993). Longleaf pine vegetation of the southern Atlantic and eastern Gulf Coast regions: A preliminary classification. *Proceedings of the Tall Timbers fire ecology conference*, 18, 45-81.
- Persson, Å., Holmgren, J., & Söderman, U. (2002). Detecting and measuring individual trees using an airborne laser scanner. *Photogrammetric Engineering and Remote Sensing*, 68(9), 925-932.
- Picos, J., Bastos, G., Míguez, D., Alonso, L., & Armesto, J. (2020). Individual tree detection in a eucalyptus plantation using unmanned aerial vehicle (UAV)-LiDAR. *Remote Sensing*, 12(5), Article 885. <https://doi.org/10.3390/rs12050885>

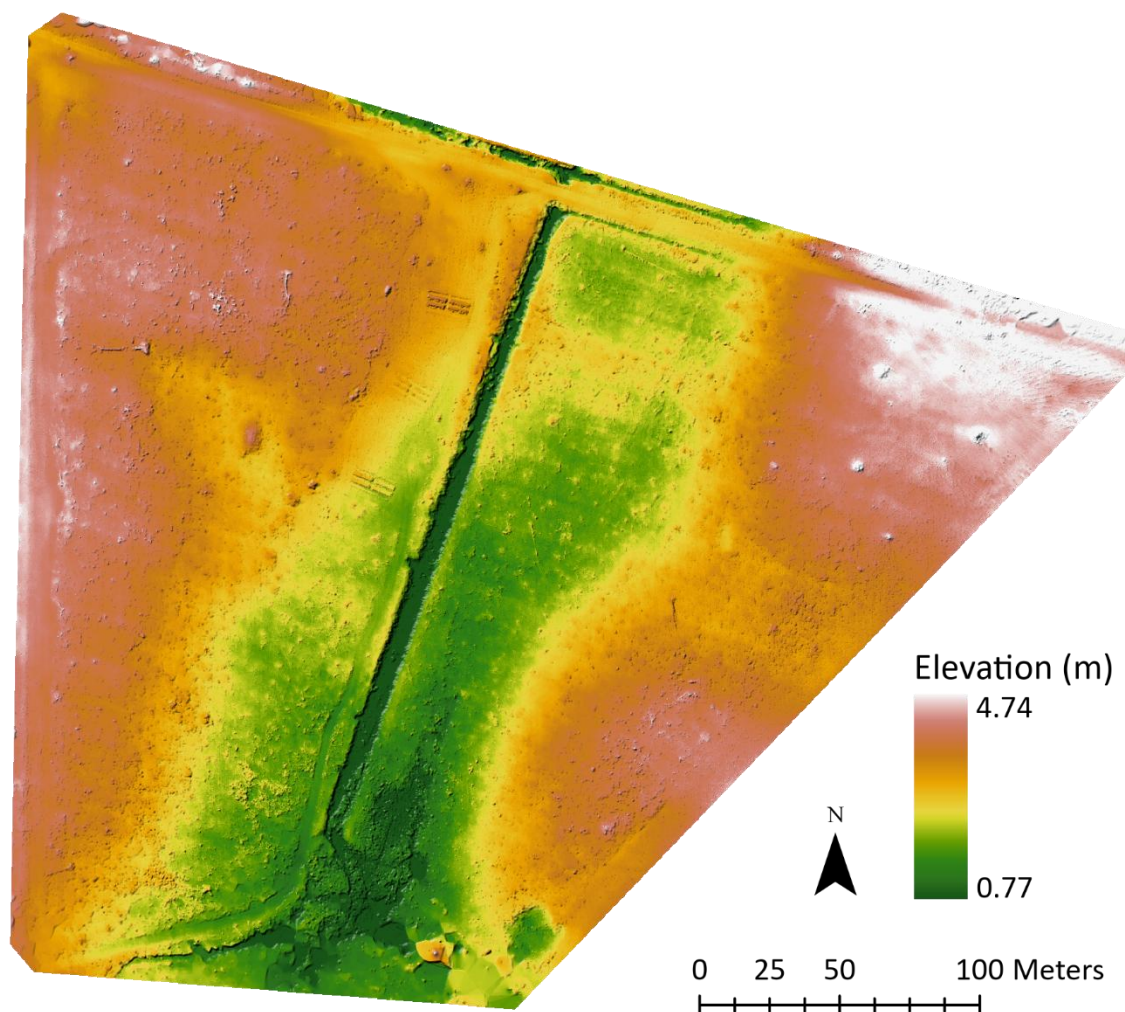


- Pirti, A. (2021). Evaluating the accuracy of post-processed kinematic (PPK) positioning technique. *Geodesy and Cartography*, 47(2), 66-70.  
<https://doi.org/10.3846/gac.2021.12269>
- Pratt-Sitaula, B., Beane, S., Krupnik, D., & Lynch, B. (2022, June 23). *Instructor guide for Emlid Reach RS2*. UNAVCO.  
[https://d32ogoqmya1dw8.cloudfront.net/files/gets/teaching\\_materials/high-precision/emlid-reachrs2-instructor-guide-reachview3.v4.pdf](https://d32ogoqmya1dw8.cloudfront.net/files/gets/teaching_materials/high-precision/emlid-reachrs2-instructor-guide-reachview3.v4.pdf)
- Ren, S., He, K., Girshick, R., & Sun, J. (2016). Faster R-CNN: Towards real-time object detection with region proposal networks. *IEEE Transactions on Pattern Analysis and Machine Intelligence*, 39(6), 1137-1149.  
<https://doi.org/10.1109/TPAMI.2016.2577031>
- Renslow, M. S. (Ed.). (2012). *Manual of airborne topographic lidar*. American Society for Photogrammetry and Remote Sensing.
- Rodríguez-Puerta, F., Gómez-García, E., Martín-García, S., Pérez-Rodríguez, F., & Prada, E. (2022). UAV-based LiDAR scanning for individual tree detection and height measurement in young forest permanent trials. *Remote Sensing*, 14(1), Article 170.  
<https://doi.org/10.3390/rs14010170>
- Roussel, J. R., & Auty, D. (2022). *lidR: Airborne LiDAR data manipulation and visualization for forestry applications* (Version 4.0.0) [R package]. <https://cran.r-project.org/package=lidR>
- Roussel, J. R., Auty, D., Coops, N. C., Tompalski, P., Goodbody, T. R. H., Sánchez Meador, A., Bourdon, J. F., De Boissieu, F., & Achim, A. (2020). lidR: An R package for analysis of Airborne Laser Scanning (ALS) data. *Remote Sensing of Environment*, 251, Article 112061. <https://doi.org/10.1016/j.rse.2020.112061>
- Sankey, T., Donager, J., McVay, J., & Sankey, J. B. (2017). UAV lidar and hyperspectral fusion for forest monitoring in the southwestern USA. *Remote Sensing of Environment*, 195, 30-43. <https://doi.org/10.1016/j.rse.2017.04.007>
- Sanz-Ablanedo, E., Chandler, J. H., Rodríguez-Pérez, J. R., & Ordóñez, C. (2018). Accuracy of unmanned aerial vehicle (UAV) and SfM photogrammetry survey as a function of the number and location of ground control points used. *Remote Sensing*, 10(10), Article 1606. <https://doi.org/10.3390/rs10101606>

- Sharma, J. B. (Ed.). (2019). *Applications of small unmanned aircraft systems: Best practices and case studies*. CRC Press. <https://doi.org/10.1201/9780429244117>
- Singh, K. K., & Frazier, A. E. (2018). A meta-analysis and review of unmanned aircraft system (UAS) imagery for terrestrial applications. *International Journal of Remote Sensing*, 39(15-16), 5078-5098. <https://doi.org/10.1080/01431161.2017.1420941>
- Snavely, N., Seitz, S. M., & Szeliski, R. (2008). Modeling the world from internet photo collections. *International Journal of Computer Vision*, 80, 189-210. <https://doi.org/10.1007/s11263-007-0107-3>
- Spurr, S. H. (1948). *Aerial photographs in forestry*. The Ronald Press Company. <https://www.cabidigitallibrary.org/doi/full/10.5555/19480602336>
- Swanson, D. A. (with Sutter, P. S.). (2012). *Remaking Wormsloe Plantation: The environmental history of a lowcountry landscape*. University of Georgia Press.
- Swayze, N. C., Tinkham, W. T., Vogeler, J. C., & Hudak, A. T. (2021). Influence of flight parameters on UAS-based monitoring of tree height, diameter, and density. *Remote Sensing of Environment*, 263, Article 112540. <https://doi.org/10.1016/j.rse.2021.112540>
- Tall Timbers. (2023a). *Land Conservancy of Tall Timbers*. <https://talltimbers.org/land-conservation/land-conservation-of-tall-timbers/>
- Tall Timbers. (2023b). *Where we conserve*. <https://talltimbers.org/land-conservation/land-conservation-where-we-conserve/>
- Tang, L., & Shao, G. (2015). Drone remote sensing for forestry research and practices. *Journal of Forestry Research*, 26(4), 791-797. <https://doi.org/10.1007/s11676-015-0088-y>
- Thelen, R. (1919). Aerial photography and national forest mapping. *Journal of Forestry*, 17(5), 515-522. <https://academic.oup.com/jof/article-abstract/17/5/515/4751932>
- Thorley, G. A. (Ed.). (1975). Forest lands: Inventory and assessment, chapter 17. In R. G. Reeves (Ed.), *Manual of remote sensing* (Vol. 2, pp. 1353-1426). American Society for Photogrammetry and Remote Sensing.

- Turner, D., Lucieer, A., & Watson, C. (2012). An automated technique for generating georectified mosaics from ultra-high resolution unmanned aerial vehicle (UAV) imagery, based on structure from motion (SfM) point clouds. *Remote Sensing*, 4(5), 1392-1410. <https://doi.org/10.3390/rs4051392>
- Ullah, S., Dees, M., Datta, P., Adler, P., & Koch, B. (2017). Comparing airborne laser scanning, and image-based point clouds by semi-global matching and enhanced automatic terrain extraction to estimate forest timber volume. *Forests*, 8(6), Article 215. <https://doi.org/10.3390/f8060215>
- Ullman, S. (1979). The interpretation of structure from motion. *Proceedings of the Royal Society of London. Series B. Biological Sciences*, 203(1153), 405-426. <https://doi.org/10.1098/rspb.1979.0006>
- United States Geological Survey. (2024, October 16). *Annual National Land Cover Database (NLCD) collection 1 land cover conterminous United States (2023)* [Data set]. United States Geological Survey. <https://www.mrlc.gov/data>
- Van Tassel, C. (2021, January 12). *Defining the true cost behind implementing lidar systems into your business*. Candrone. <https://candrone.com/blogs/news/the-real-cost-of-starting-a-lidar-drone-business>
- Véga, C., & Durrieu, S. (2011). Multi-level filtering segmentation to measure individual tree parameters based on lidar data: Application to a mountainous forest with heterogeneous stands. *International Journal of Applied Earth Observation and Geoinformation*, 13(4), 646-656. <https://doi.org/10.1016/j.jag.2011.04.002>
- Wade, D. D., & Lundsford, J. (1990). Fire as a forest management tool: Prescribed burning in the southern United States. *Unasylva*, 41(3), 28-38.
- Wang, G. G., Pile, L. S., Knapp, B. O., & Hu, H. (2016). Longleaf pine adaptation to fire: Is early height growth pattern critical to fire survival? In C. J. Schweitzer, W. K. Clatterbuck, & C. M. Oswalt (Eds.), *Proceedings of the 18th Biennial Southern Silvicultural Research Conference* (pp. 214-218). U.S. Department of Agriculture. [http://www.srs.fs.usda.gov/pubs/gtr/gtr\\_srs212.pdf#page=226](http://www.srs.fs.usda.gov/pubs/gtr/gtr_srs212.pdf#page=226)
- Westoby, M. J., Brasington, J., Glasser, N. F., Hambrey, M. J., & Reynolds, J. M. (2012). 'Structure-from-Motion' photogrammetry: A low-cost, effective tool for geoscience applications. *Geomorphology*, 179, 300-314. <https://doi.org/10.1016/j.geomorph.2012.08.021>

- Wu, D., Johansen, K., Phinn, S., Robson, A., & Tu, Y. H. (2020). Inter-comparison of remote sensing platforms for height estimation of mango and avocado tree crowns. *International Journal of Applied Earth Observation and Geoinformation*, 89, Article 102091. <https://doi.org/10.1016/j.jag.2020.102091>
- Wulder, M. A., White, J. C., Nelson, R. F., Næsset, E., Ørka, H. O., Coops, N. C., Hilker, T., Bater, C. W., & Gobakken, T. (2012). Lidar sampling for large-area forest characterization: A review. *Remote Sensing of Environment*, 121, 196-209. <https://doi.org/10.1016/j.rse.2012.02.001>
- Zarco-Tejada, P. J., Diaz-Varela, R., Angileri, V., & Loudjani, P. (2014). Tree height quantification using very high resolution imagery acquired from an unmanned aerial vehicle (UAV) and automatic 3D photo-reconstruction methods. *European Journal of Agronomy*, 55, 89-99. <https://doi.org/10.1016/j.eja.2014.01.004>
- Zhang, C., Zhou, J., Wang, H., Tan, T., Cui, M., Huang, Z., Wang, P., & Zhang, L. (2022). Multi-species individual tree segmentation and identification based on improved Mask R-CNN and UAV imagery in mixed forests. *Remote Sensing*, 14(4), Article 874. <https://doi.org/10.3390/rs14040874>

**APPENDIX A****2023 UAS LIDAR-DERIVED DEM FOR THE STUDY AREA**

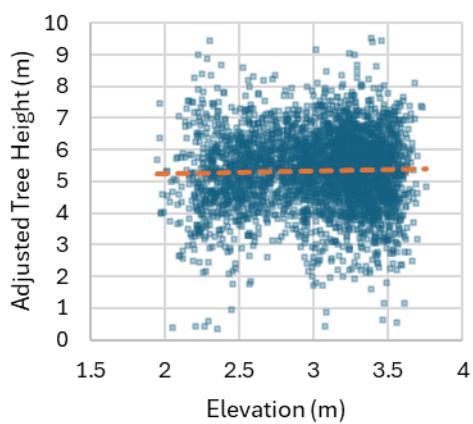
**APPENDIX B**

**RELATIONSHIPS BETWEEN INDIVIDUAL VARIABLES AND LONGLEAF PINE GROWTH**

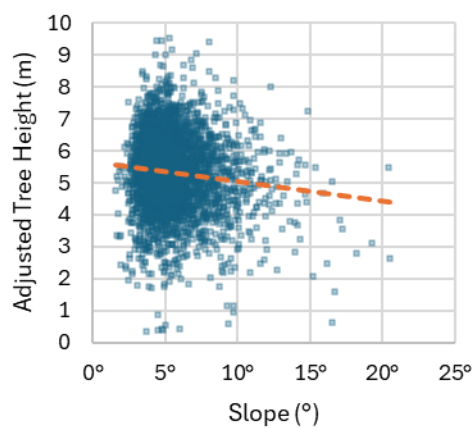
**AND SURVIVAL**

### Variable Correlations with Longleaf Pine Height

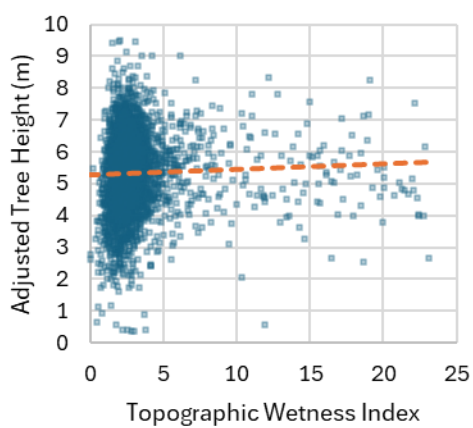
Elevation



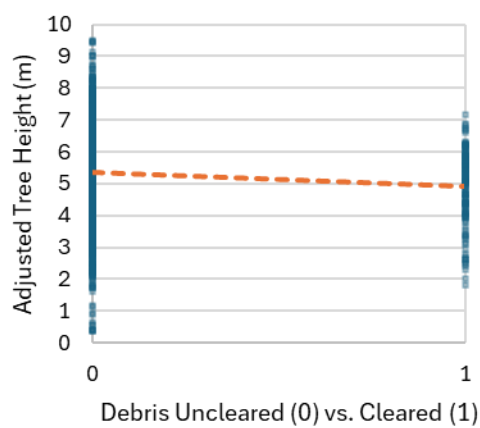
Slope



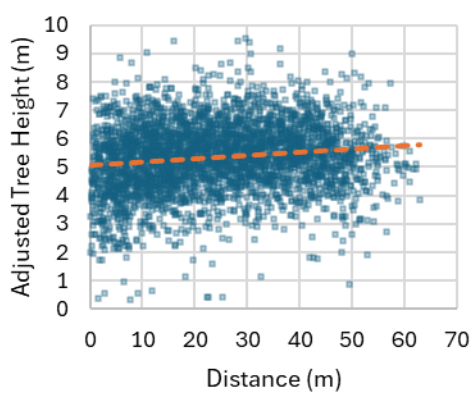
Topographic Wetness



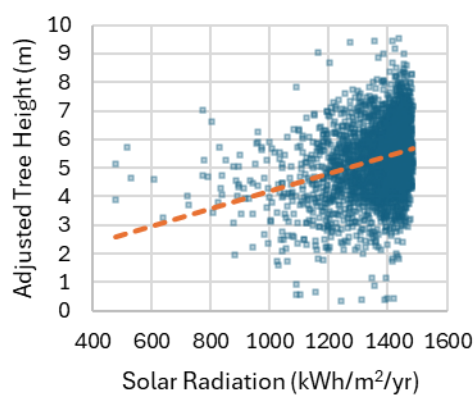
Site Preparation Methods



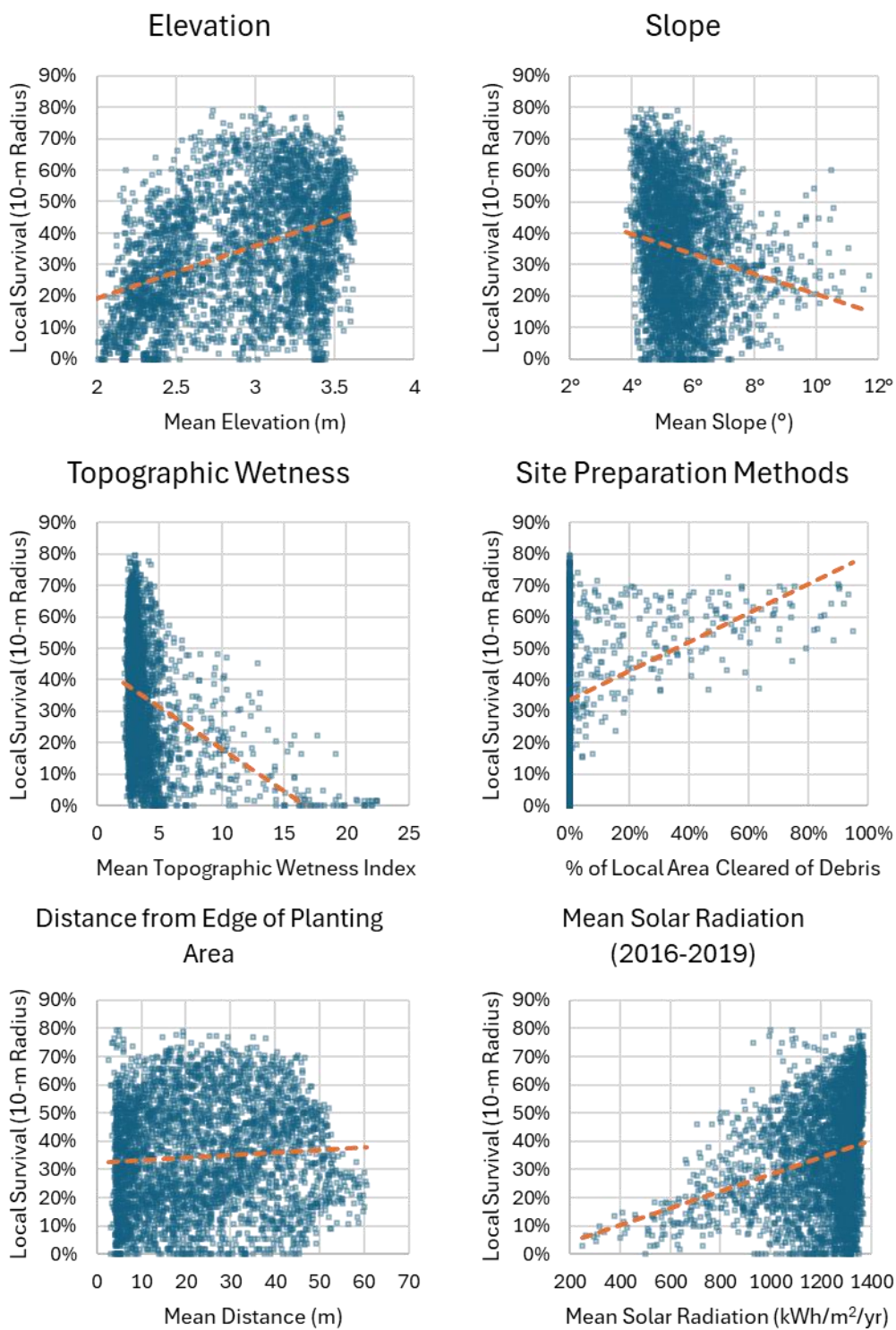
Distance from Edge of Planting Area



Mean Solar Radiation (2016-2019)



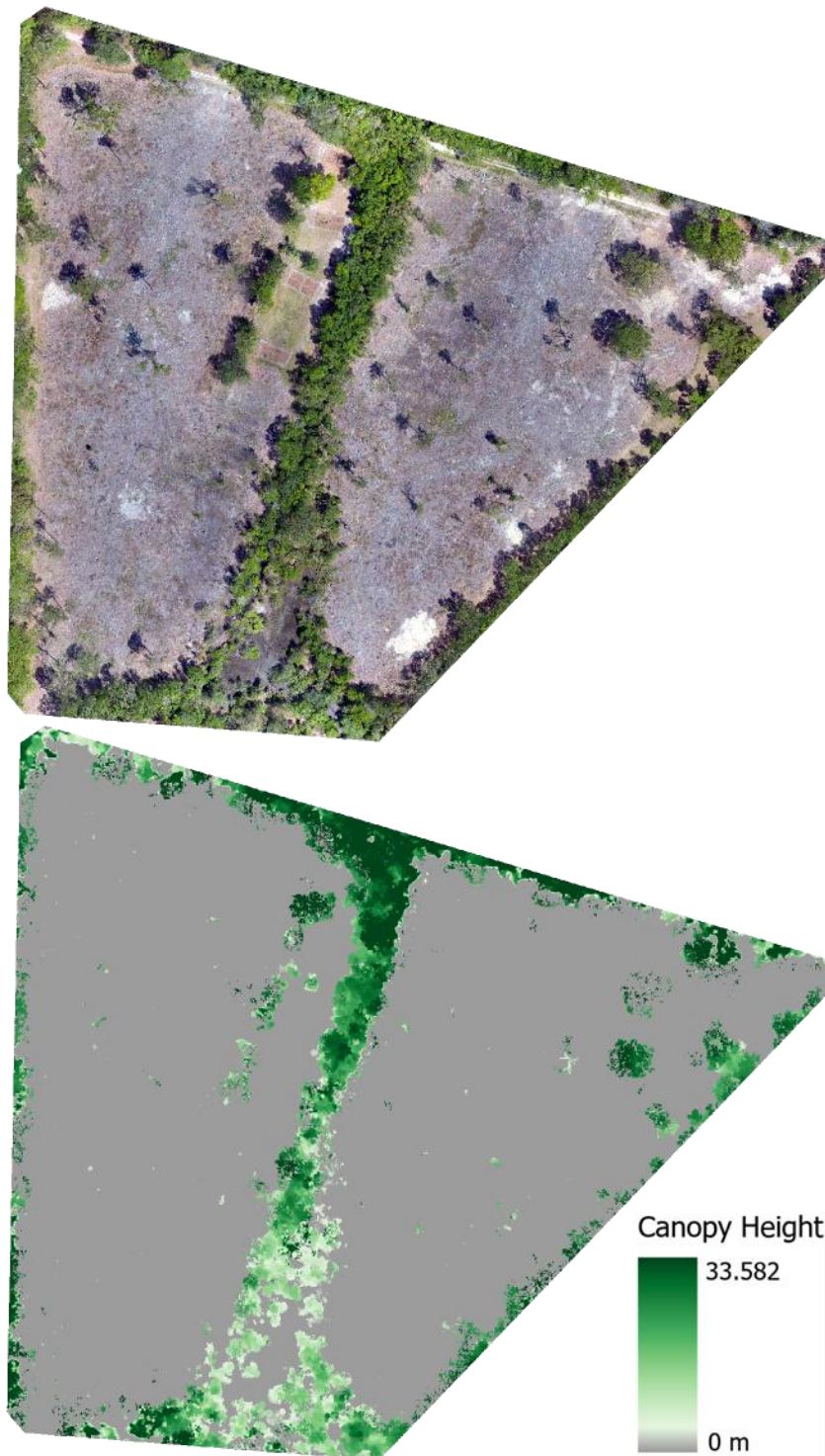
### Variable Correlations with Longleaf Pine Survival



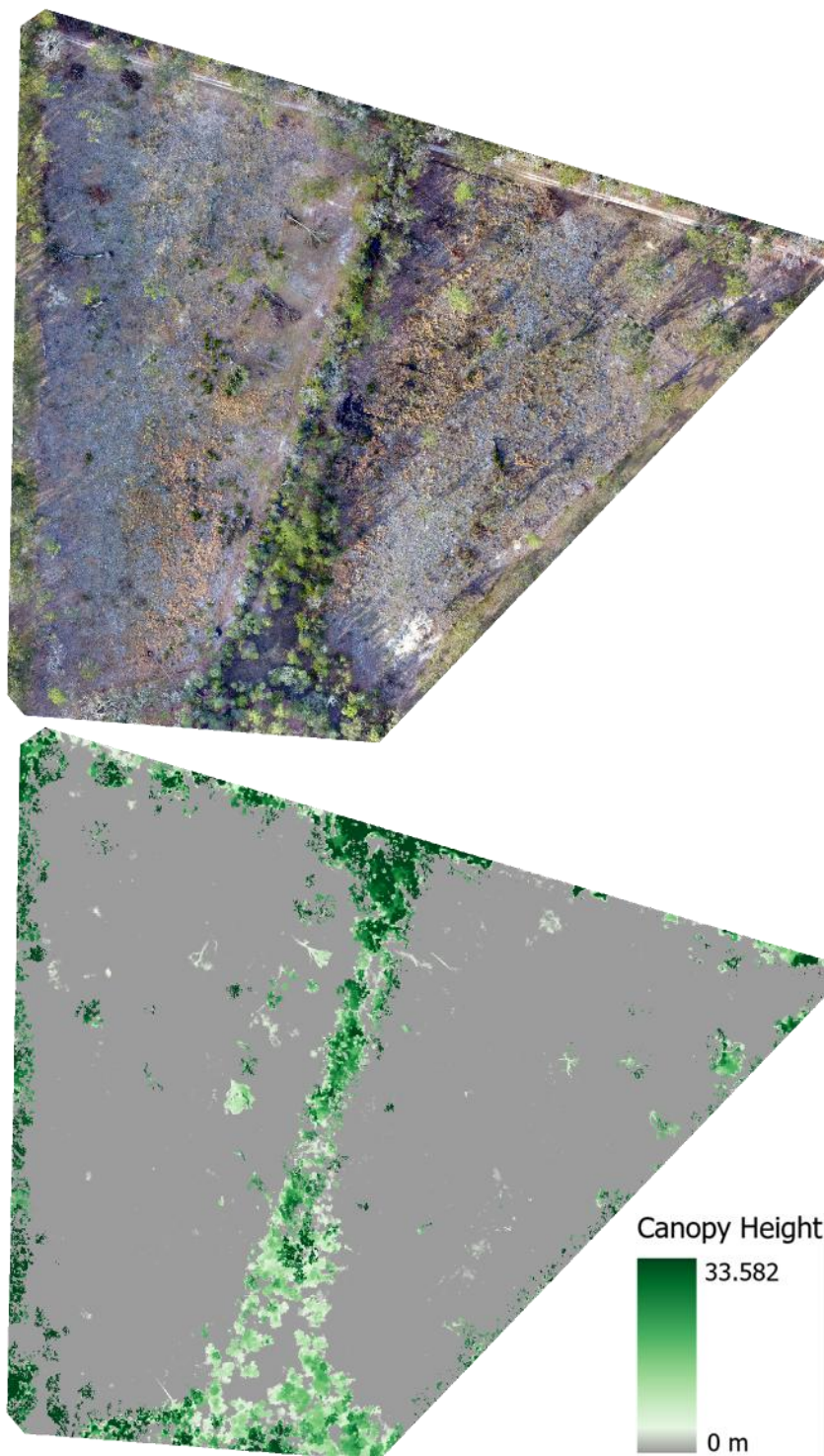


**APPENDIX C****UAS SFM TIME SERIES: FULL STUDY AREA**

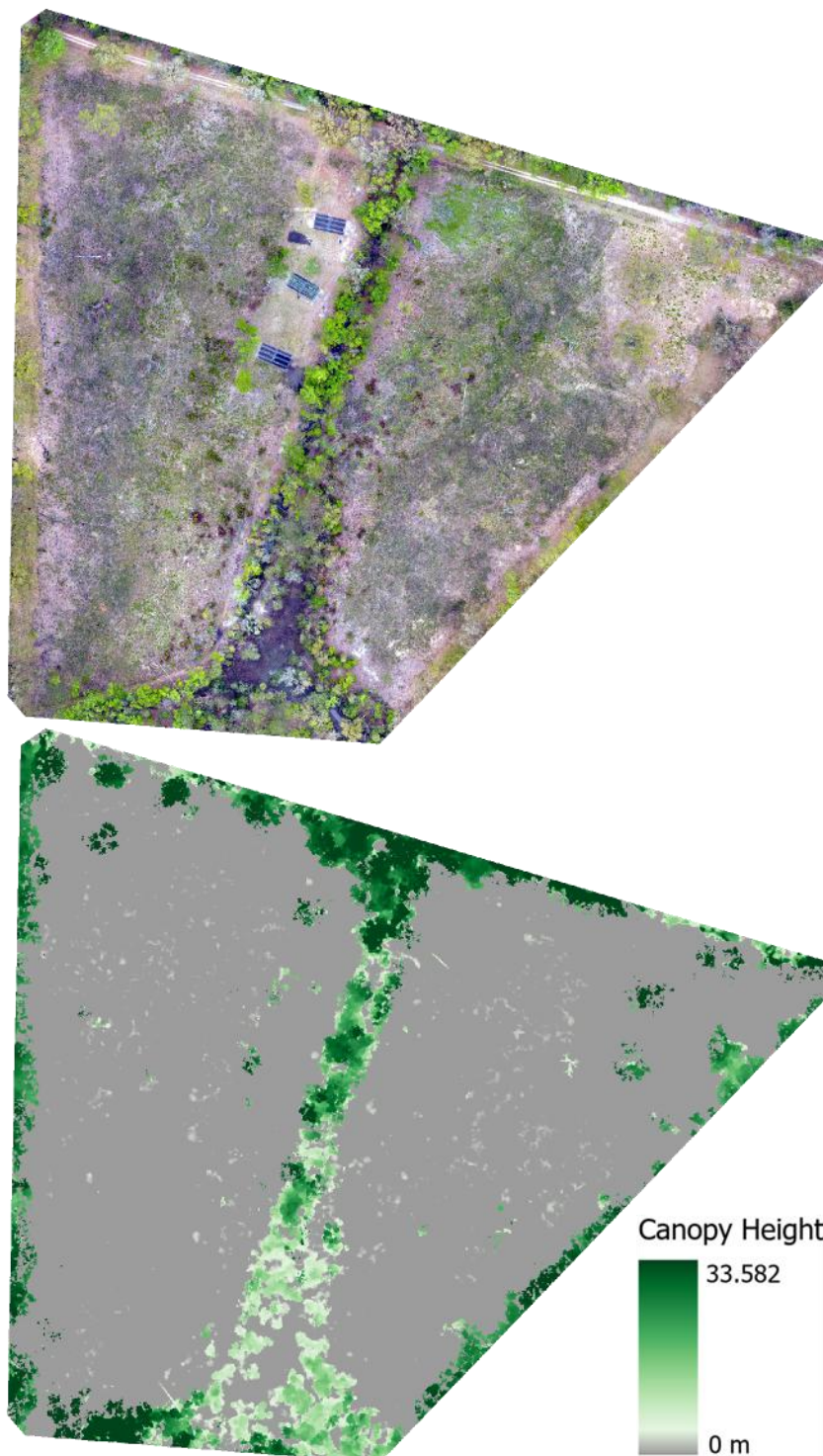
22 April 2016



15 January 2017

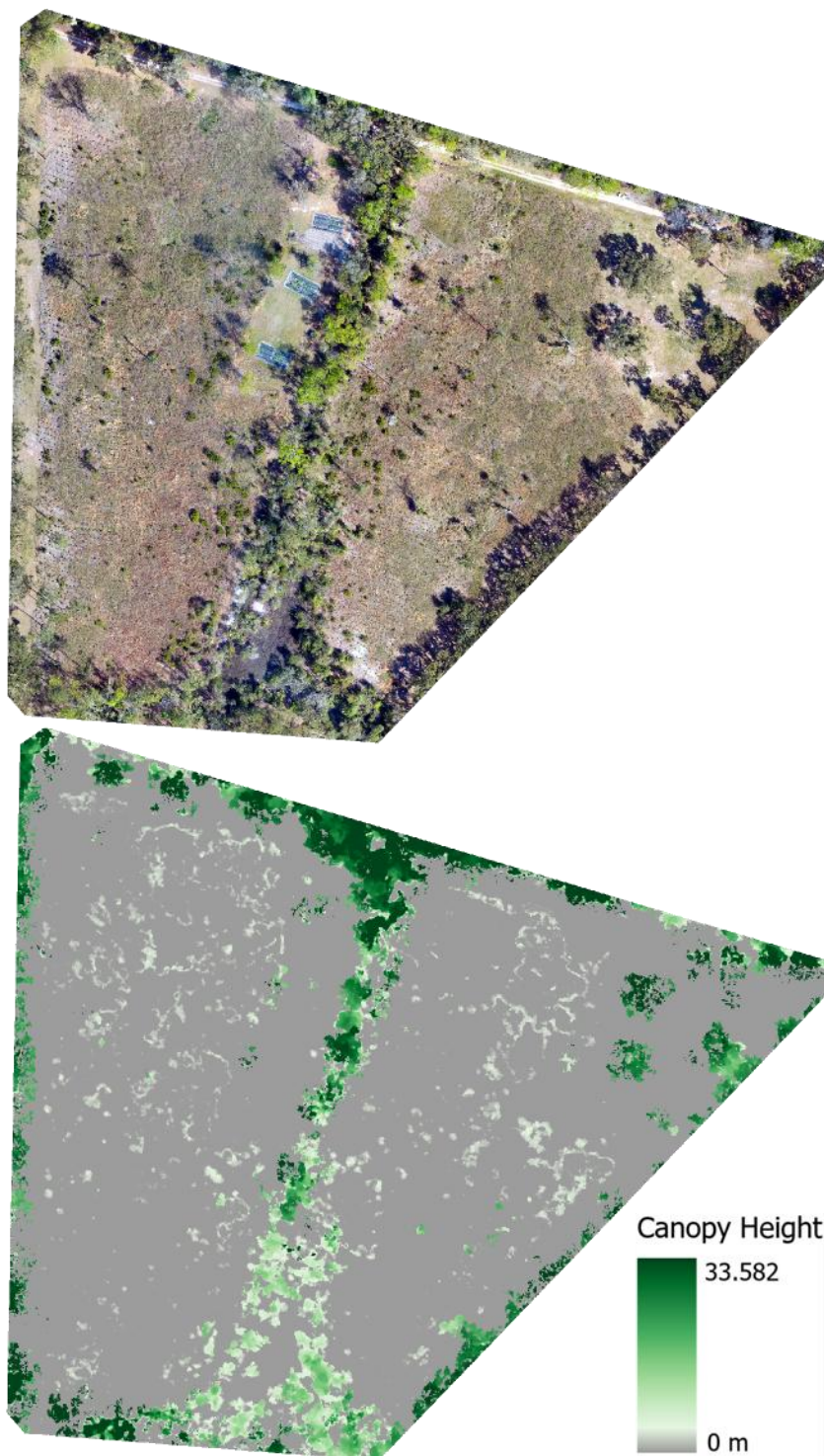


**4 April 2018**

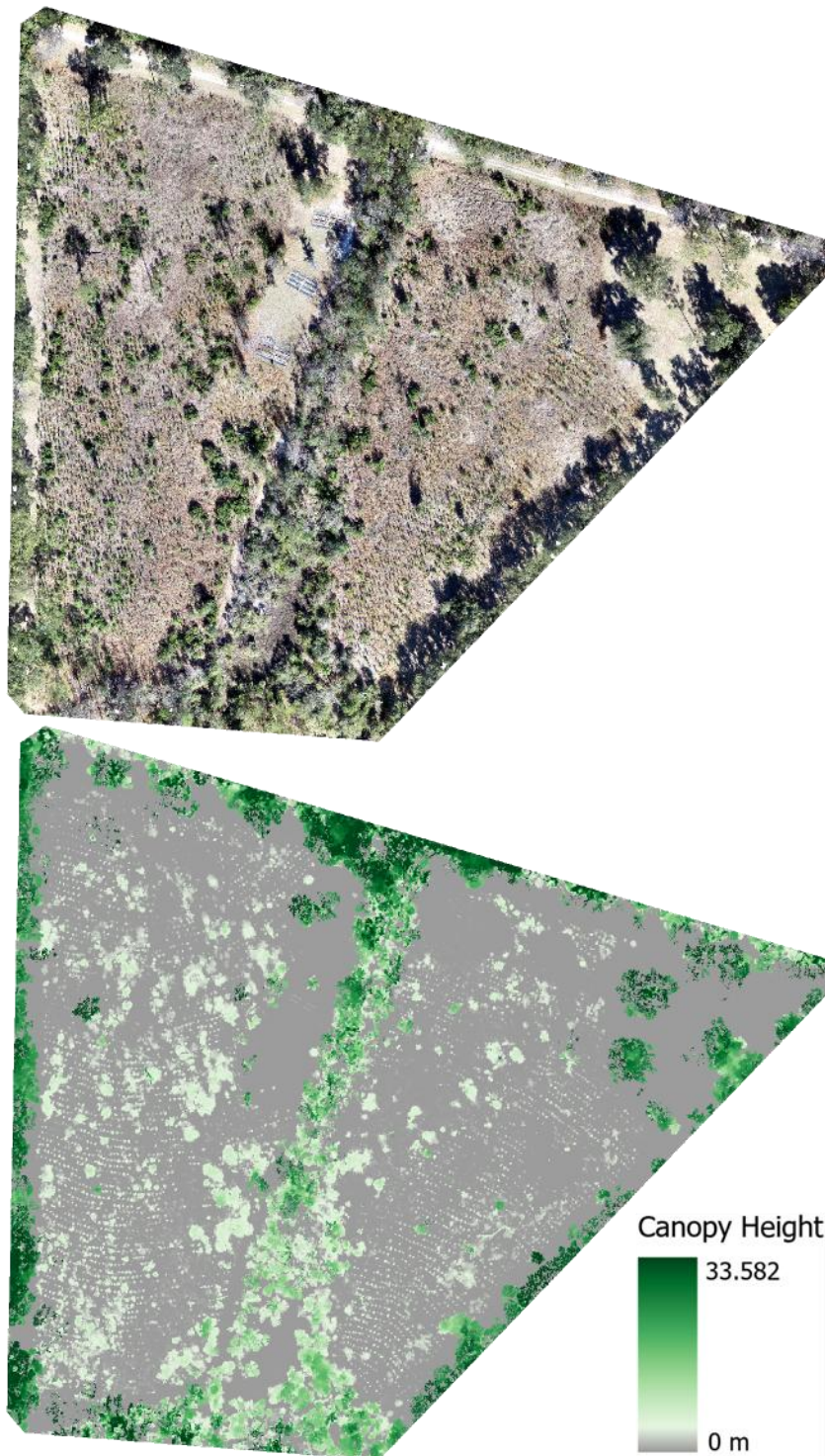




**24 March 2019**

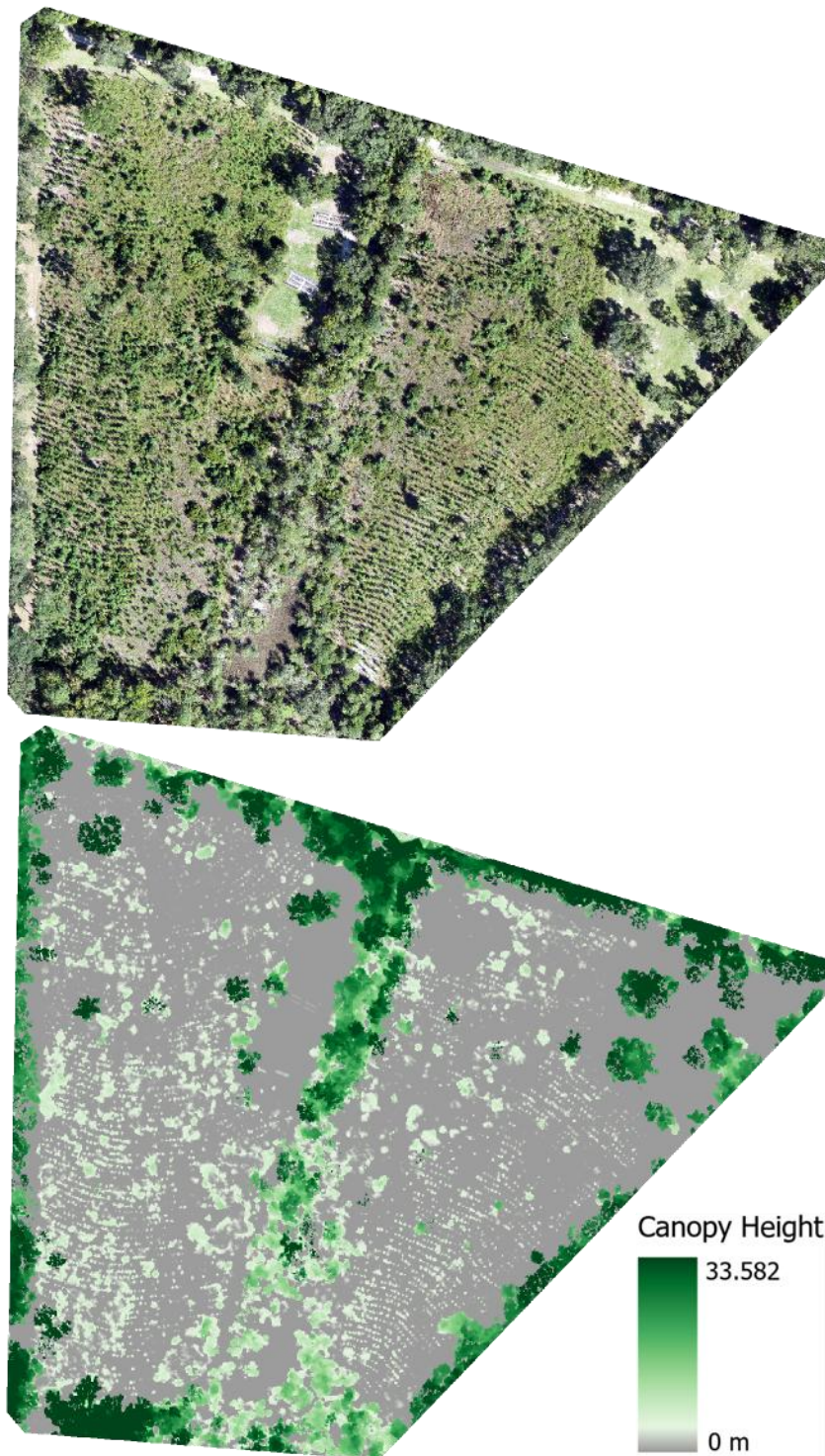


**3 February 2021**

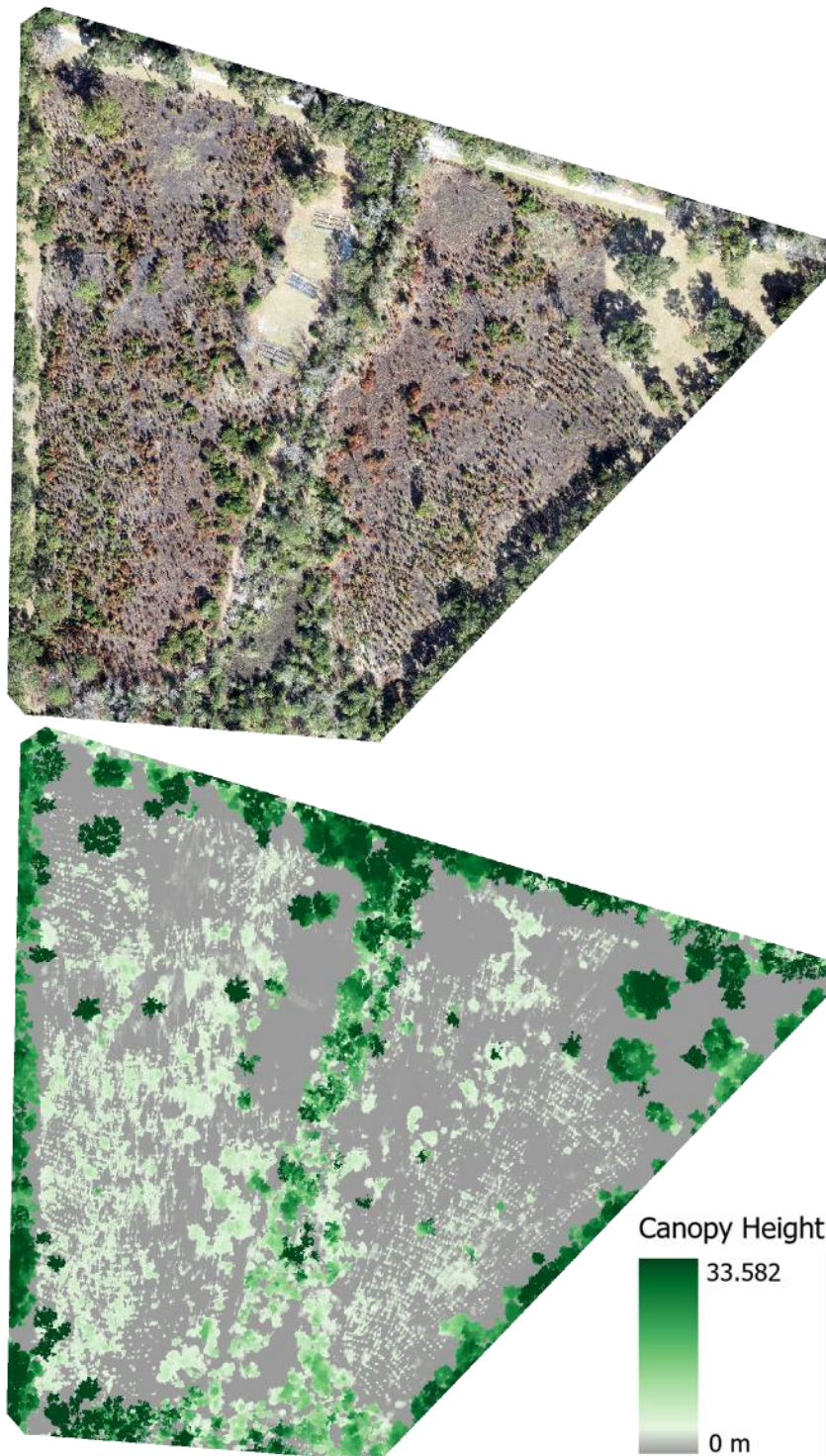




**26 September 2021**

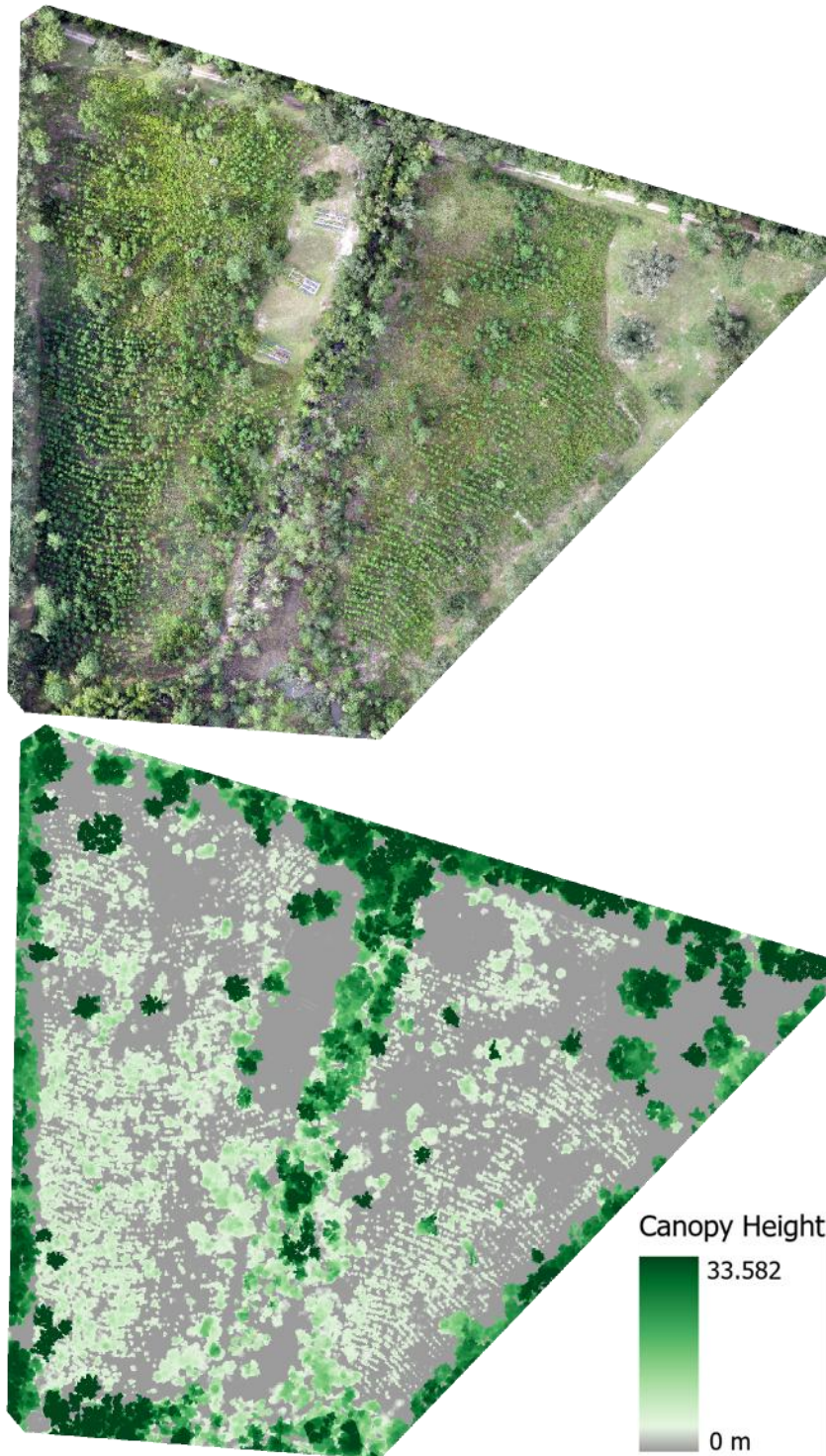


**23 February 2022**

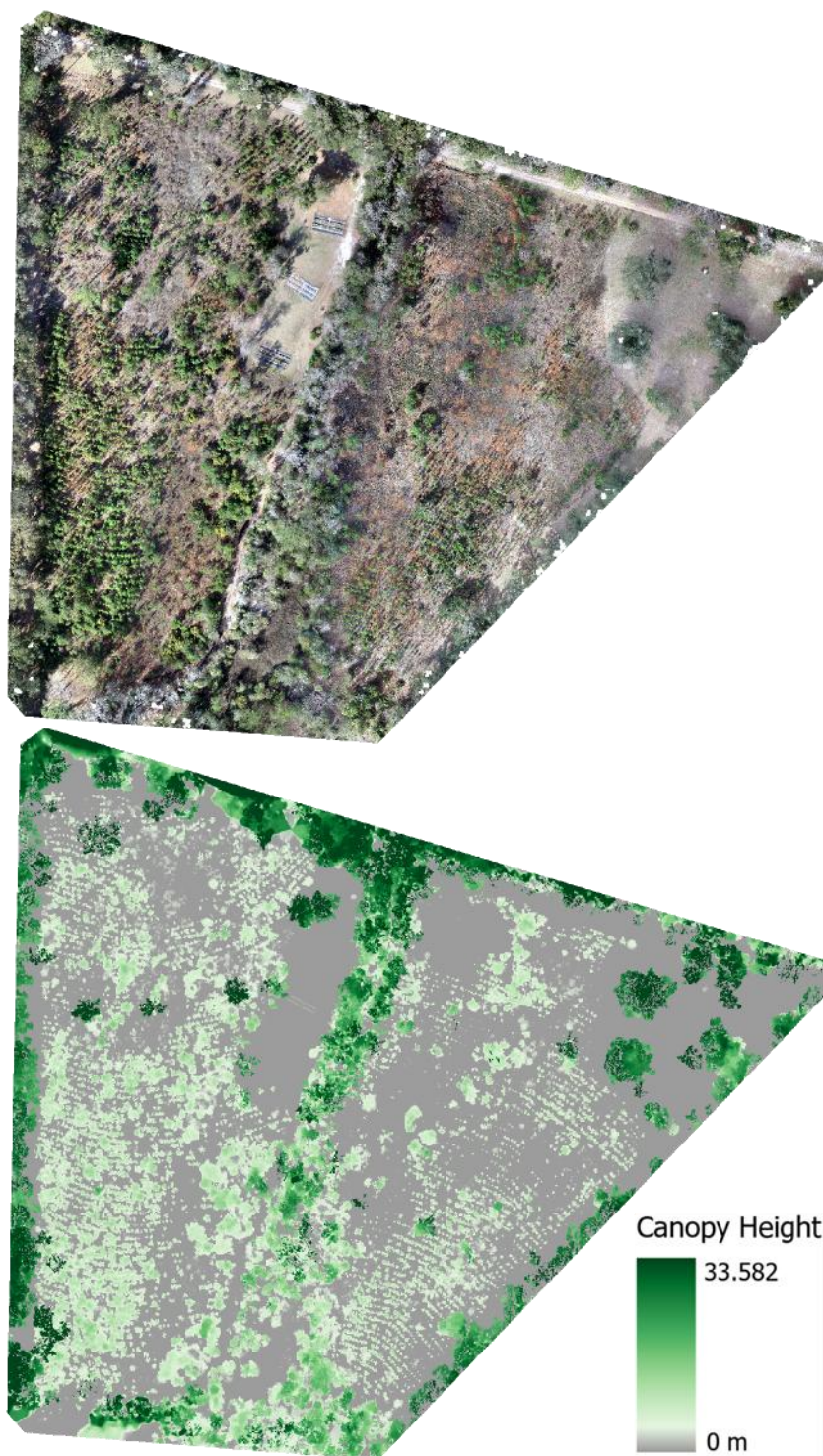




**7 September 2022**



**19 February 2023**



## APPENDIX D

### MEASURED HEIGHTS AND POSITIONAL DATA OF TREES USED FOR GROUND TRUTH

Tree Number	Tree Heights (m)		Positional Data		
	9/7/2022	2/15/2023	Latitude	Longitude	Orthometric Height (m)
1	3.95	4.06	31.96916172	-81.06654186	3.737
2	4.70	4.79	31.96920683	-81.06659270	3.485
3	4.47	4.64	31.96925710	-81.06664445	3.011
4	4.14	4.28	31.96931147	-81.06669626	3.180
5	5.93	6.57	31.96938276	-81.06671036	3.137
6	4.89	4.95	31.96945115	-81.06673291	2.685
7	5.16	5.62	31.96949874	-81.06676744	2.653
8	5.05	5.12	31.96950601	-81.06668477	2.668
9	6.12	6.40	31.96949171	-81.06664736	2.679
10	5.05	5.19	31.96944603	-81.06662708	2.714
11	6.39	6.25	31.96940864	-81.06662796	2.819
12	4.88	5.10	31.96934685	-81.06655405	2.977
13	4.73	4.99	31.96929896	-81.06650980	3.011
14	5.04	5.30	31.96926043	-81.06646098	3.149
15	5.74	5.85	31.96927881	-81.06638315	2.929
16	6.10	6.33	31.96932435	-81.06642210	2.912
17	5.41	5.72	31.96938762	-81.06645605	2.811
18	6.23	6.07	31.96942967	-81.06649950	2.800
19	4.13	4.33	31.96950377	-81.06655676	2.641
20	4.41	4.52	31.96954602	-81.06656827	2.675
21	4.63	4.64	31.96958043	-81.06656667	2.522
22	5.18	5.41	31.96963951	-81.06653932	2.558
23	3.49	3.66	31.96961511	-81.06649415	2.602
24	5.04	5.25	31.96955192	-81.06650933	2.454
25	6.09	6.00	31.96951408	-81.06646128	2.639
26	4.72	4.94	31.96941721	-81.06639858	2.788
27	4.77	4.85	31.96937286	-81.06634215	2.801
28	6.21	6.40	31.96936779	-81.06627827	2.809
29	5.87	5.79	31.96938151	-81.06629701	2.806
30	4.50	4.54	31.96952202	-81.06641749	2.475

Tree Number	Tree Heights (m)		Positional Data		
	9/7/2022	2/15/2023	Latitude	Longitude	Orthometric Height (m)
31	3.25	3.29	31.96957286	-81.06643441	2.575
32	3.34	3.58	31.96953535	-81.06638885	2.554
33	5.21	5.30	31.96948929	-81.06632823	2.579
34	3.00	3.23	31.96947459	-81.06635515	2.616
35	4.59	4.70	31.96942481	-81.06624564	1.628
36	5.58	5.69	31.96938939	-81.06625441	2.638